UNIVERSIDADE FEDERAL DO CEARÁ
CENTRO DE TECNOLOGIA
DEPARTAMENTO DE ENGENHARIA E CIÊNCIA DE MATERIAIS
PROGRAMA DE PÓS-GRADUAÇÃO EM ENGENHARIA E CIÊNCIA DE MATERIAIS

JOSÉ JOELSON PIRES OLIVEIRA

CHEMICAL SENSING USING CARBON QUANTUM DOTS FOR THE DETECTION OF COBALT AND CYANIDE IONS

FORTALEZA
2024

JOSÉ JOELSON PIRES OLIVEIRA

CHEMICAL SENSING USING CARBON QUANTUM DOTS FOR THE DETECTION OF COBALT AND CYANIDE IONS

Doctoral thesis submitted to the Programa de Pós-Graduação em Engenharia e Ciência de Materiais of the Universidade Federal do Ceará as a requeriment for the degree of doctor in engineering and materials sciences.
Concentration área: physical and mechanical properties of materials.

Supervisor: Prof. Dr. Pierre Basílio Almeida Fechine.
Co-supervisor: Dr. Rafael Melo Freire.

FORTALEZA
2024

Dados Internacionais de Catalogação na Publicação
Universidade Federal do Ceará
Sistema de Bibliotecas
Gerada automaticamente pelo módulo Catalog, mediante os dados fornecidos pelo(a) autor(a)

O47c Oliveira, José Joelson Pires.
Chemical sensing using carbon quantum dots for the detection of cobalt and cyanide ions / José Joelson Pires Oliveira. – 2024.
84 f. : il. color.

Tese (doutorado) – Universidade Federal do Ceará, Centro de Tecnologia, Programa de Pós-Graduação em Engenharia e Ciência de Materiais, Fortaleza, 2024.
Orientação: Prof. Dr. Pierre Basílio Almeida Fechine.
Coorientação: Prof. Dr. Rafael Melo Freire.

1. Carbon quantum dots. 2. Chemical sensing. 3. Fluorescence. I. Título.

CDD 620.11

JOSÉ JOELSON PIRES OLIVEIRA

CHEMICAL SENSING USING CARBON QUANTUM DOTS FOR THE DETECTION OF COBALT AND CYANIDE IONS

Tese apresentada ao Programa de Pós-Graduação em Engenharia e Ciência de Materiais da Universidade Federal do Ceará, como requisito parcial à obtenção do título de doutor em engenharia e ciência de materiais.
Área de concentração: propriedades físicas e mecânicas dos materiais.

Aprovada em: __/__/____.

BANCA EXAMINADORA

_____
Prof. Dr. Pierre Basílio Almeida Fechine (Orientador)
Universidade Federal do Ceará (UFC)

_____
Prof. Dr. Walney Silva Araújo
Universidade Federal do Ceará (UFC)

_____
Prof. Dr. Claudenilson da Silva Clemente
Universidade Federal do Ceará (UFC)

_____
Prof. Dr. Bruno Peixoto de Oliveira
Universidade Federal do Cariri (UFCA)

_____
Prof. Dr. Francisco de Assis Avelino de Figueredo Sobrinho
Instituto Federal do Ceará (IFCE)

_____
Prof. Dr. Claudio José Reis de Carvalho
Embrapa Agroindústria Trópica

I dedicate this work to God, to my parents, Francisca Teixeira Pires and José Agripino Oliveira, to the love of my life, Renata Melo de Sousa, and to my brothers, Maria Joelma Pires Oliveira and Carlos Joel Pires Oliveira.

ACKNOWLEDGMENTS

To God, for all the blessings granted to me;

To my parents and my brothers for all their encouragement and support throughout my career, giving me the opportunity to transform my social reality through study;

To my fiancee Renata Melo de Sousa, for being a faithful companion and always being by my side in good and bad times, supporting and understanding me;

To Professor Piere Basílio Almeida Fechine, for agreeing to guide me during doctor's degree. I was able to learn a lot from you. Your simplicity, your patience and your love for your work inspire me;

To my co-supervisor Rafael Melo Freire, for accepting the challenge of following me closely during my doctor's degree. Thank you for all the teaching and all the directions highlighted in this research;

To my friend Samuel Veloso Carneiro, for being with me at all times. You were the first friend I made when I arrived in Fortaleza in 2018. Since then, you have always motivated me in my academic career and have been an inspiration to me. I am grateful to God for having you as a friend;

To the Advanced Materials Chemistry Group (GQMat), where I learned a lot from my colleagues during group meetings and conversations in the laboratory. At GQMat, in addition to developing the experiments in this work, we share life experiences that contribute positively to our professional and personal development. I am very grateful to all my group colleagues who contributed directly or indirectly to this research, in particular I would like to mention Vivian, Sheyliane, Harisson and Marcos, who helped with the experiments presented in this research;

To Prof. Renato Antunes, from Universidade Federal do ABC, for making the XPS measurements available, essential for the development of the works presented in this thesis;

To Professors Adonay Rodrigues Loiola and Gisele Simone Lopes, who were part of my Qualification Exam, for all the suggestions that made this work even better;

To the Federal University of Ceará (UFC), for its entire structure and staff. UFC made my dream of becoming a master and now a doctor possible, contributing to my academic training;

To the Graduate Program in Engineering and Materials Science for all the infrastructure made available to carry out this work;

To the Graduate Program in Chemistry, for making its Analytical Center available for carrying out experiments;

To the Fundação Cearense de Apoio ao Desensvolvimento Científico e Tecnológico (Funcap), for granting the scholarship.

RESUMO

Pontos Quânticos de Carbono (CQDs) são nanopartículas fluorescentes, biocompatíveis, com baixa toxicidade e com estrutura repleta de grupos superficiais hidrofílicos que garantem sua boa dispersibilidade em água. Todas essas propriedades fazem deste nanomaterial um excelente candidato para aplicações em sensoriamento químico, utilizando sua fluorescência como sinal de resposta. Nesta tese, várias estratégias de sensoriamento são descritas tal como sensoriamento *turn-off*, onde a fluorescência dos CQDs é suprimida pela adição do analito Co^{2+}; sensor colorimétrico, baseado na absorbância dos CQDs/Co^{2+} a 315 nm; sensoriamento *turn-off/turn-on*, onde íons Fe^{3+} suprimem a fluorescência dos CQDs, mas o sinal é recuperado pela adição do analito CN^-; e sensor *array*, o qual utiliza algorítmos de análise multivariada (ferramentas quimiométricas), tal como análise de componentes principais (PCA) e análise linear discriminante (LDA), com intuito de discriminar sinais analíticos como em uma impressão digital. Os resultados apresentados neste trabalho demonstram a capacidade e a versatilidade dos CQDs ao funcionarem como nanosondas fluorescentes sensíveis, capazes de detectar íons Co^{2+} em amostra real de plasma sanguíneo com recuperação de sinal de 100,94%, íons CN^-em amostral real de água da torneira com recuperação de 94,8% e discrimanar com 100% de acurácia (baseado em LDA) diferentes espécies presentes em formulações de biscoito, incluindo glúten. Assim, esta pesquisa busca divulgar os CQDs como sensores químicos alternativos, contribuindo no estabelecimento de um método padrão para a detecção de ions Co^{2+} e no campo de segurança alimentar, quantificando íons CN^-e detectando glúten.

Palavras-chave: Pontos quânticos de carbono; sensoriamento químico; fluorescência.

ABSTRACT

Carbon Quantum Dots (CQDs) are fluorescent, biocompatible nanoparticles, with low toxicity and a structure full of hydrophilic surface groups that guarantee their good dispersibility in water. All these properties make this nanomaterial an excellent candidate for applications in chemical sensing, using its fluorescence as a response signal. In this thesis, several sensing strategies are described such as turn-off sensing, where the fluorescence of CQDs is quenched by the addition of the Co^{2+} analyte; colorimetric sensor, based on the absorbance of CQDs/Co^{2+} at 315 nm; turn-off/turn-on sensing, where Fe^{3+} ions quench the fluorescence of CQDs, but the signal is recovered by the addition of the CN^- analyte; and sensor array, which uses multivariate analysis algorithms (chemometric tools), such as principal component analysis (PCA) and linear discriminant analysis (LDA), in order to discriminate analytical signals as in a fingerprint. The results presented in this work report the capacity and versatility of CQDs by functioning as sensitive fluorescent nanoprobes, capable of detecting Co^{2+} ions in a real sample of blood plasma with recovery of 100.94%, CN^- ions in a real sample of tap water with recovery of 94.8% and discriminating with 100% of accuracy (based on LDA) different species present in biscuit formulations, including gluten. Thus, this research promotes CQDs as alternative chemical sensors, contributing to the establishment of a standard method for detecting Co^{2+} ions and in the field of food safety, quantifying CN^- and detecting gluten.

Keywords: Carbon quantum dots; chemical sensing; fluorescence.

LIST OF FIGURES

Figure 1 – State of the art for scientific production involving the term “carbon quantum dots”, performed on the ScienceDirect website on January 16, 2024..... 15

Figure 2 – Schematic representation of top-down and bottom-up approaches for the synthesis of CQDs..... 17

Figure 3 – Reaction scheme for the N-CD-Ch synthesis..... 27

Figure 4 – (a) Topography image of N-CD-Ch confirms the formation of nanoparticles of regular size; (b) Section height profile associated with the red line on the topography image; (c) TEM and (d) size distributions images of N-CD-Ch; (e) Raman spectrum and (f) FTIR spectra of N-CD-Ch..... 31

Figure 5 – (a) XPS survey spectrum and high-resolution XPS spectra of (b) C1s and (c) N1s; (d) chemical structure of N-CD-Ch..... 32

Figure 6 – (a) The UV-Vis absorption and fluorescence spectra of N-CD-Ch. Inset: photograph of N-CD-Ch water suspension under visible light (left) and UV light (right); (b) Fluorescence spectra of N-CD-Ch sample under different excitation wavelengths..... 33

Figure 7 – Photostability experiment for 40 min..... 34

Figure 8 – (a) Fluorescence spectra of N-CD-Ch at different concentrations. Inset: the linear relationship between fluorescence intensity and N-CD-Ch concentration at 465 nm; (b) pH-response fluorescence at 465 nm; (c) fluorescence intensity after the addition of different concentrations of Co^{2+}. In the range of 0 to 50 µmol L^{-1} the increment was 5 µmol L^{-1}, while in the range of 50 to 500 µmol L^{-1} the increment was 50 µmol L^{-1}. Inset: photograph of the aqueous solution of N-CD-Ch under UV light at different concentrations of Co^{2+}, ranging from 0 to 500 µmol L^{-1} with an increment of 50 from left to right; (d) UV-Vis absorption as a function of Co^{2+} concentration. Inset: photograph of the aqueous solution of N-CD-Ch from 0 (left) to 500 µmol L^{-1} of Co^{2+} (right) with an increment of 50. 35

All average and standard deviation values were calculated based on triplicate experiments.....

Figure 9 – The linear relationship between the normalized photoluminescence at 465 nm and Co^{2+} concentration. All average and standard deviation values were calculated based on triplicate experiments..... 37

Figure 10 – Absorption spectra of N-CD-Ch (blue line) and N-CD-Ch with Co^{2+} ion (yellow line) in the concentration of 250 µmol L^{-1}..... 37

Figure 11 – Titration curves at (a) 298.75 K (b) 308.15 K and (c) 318.15 K. The inset shows the fit to Stern-Volmer Equation. All measurements were recorded at 465 nm of the emission spectrum. (d) Graph obtained from the Van't Hoff equation for determination of thermodynamic parameters. All average and standard deviation values were calculated based on triplicate experiments..... 39

Figure 12 – Schematic representation of the complexation mechanism between N-CD-Ch and Co^{2+} ions..... 40

Figure 13 – Overlapping of absorbance of quencher (yellow dots) with excitation (red line) and emission spectra (blue line) of N-CD-Ch..... 40

Figure 14 – (a) Real blood plasma sample; (b) decomposition of the organic matrix at 88 ° C with the addition of HNO_3 and H_2O_2; (c) treated and diluted real sample; (d) addition of different concentration of Co^{2+} ions to the real sample..... 42

Figure 15 – (a) Titration curve of Co^{2+} in the real sample of human blood in PBS buffer pH 7.4. (b) Fluorescence response of the N-CD-Ch aqueous solution in the presence of different ions with Co^{2+} (brown bars) and without Co^{2+} (blue bars). (c) Canonical score plot obtained from the LDA after PCA of real sample titration. (d) Canonical score plot obtained from the LDA after PCA of different ions with Co^{2+}. (e) Color comparison of N-CD-Ch solution after addition of different ions at 250 µmol L^{-1}. Average and standard deviation values of (a) and (b) were calculated based on three replicates, while (c) and (d) classifications were obtained based on six replicates and 95% confidence level..... 43

Figure 16 – The linear relationship between fluorescence at 465 nm and Co^{2+} concentration present in the real sample. All average and standard deviation values were calculated based on triplicate experiments..... 44

Figure 17 – AFM results of CD-90: (a) topography image and AFM section height profile of the particles (inset); (b) phase image. The AFM scanning was performed over a 4 µm x 4 µm region..... 51

Figure 18 – Confocal microscopy analysis of CD-90 dried film with emission at: (a) 405nm; (b) 488nm; (c) 561 nm and (d) the merge of the channels..... 52

Figure 19 – FTIR spectra of CD-90 and their precursors (mix of citric acid and ethylenediamine) 53

Figure 20 – (a) XPS survey; high-resolution spectra: (b) C1s; (c) N1s and description of N rings present in carbon lattice (inset); (d) O1s……... 54

Figure 21 – Results of spectroscopic characterizations: (a) UV-Vis, excitation and emission spectra of CD-90; (b) Photoluminescence spectra with different excitation wavelengths (300 to 400 nm) of CD-90. Inset: CD-90 under UV lamp…….. 55

Figure 22 – Fluorescence-response evaluation of CD-90 at different experimental conditions: (a) concentration effect of CD-90 on fluorescence; (b) PL intensity as a function of concentration; (c) effect of pH in the CD-90 fluorescence intensity; (d) fluorescence intensity in the presence of species presents in cookies formulations at concentration of 25 ppm. All average and standard deviation values were calculated based on triplicate experiments..... 57

Figure 23 – UV-Vis absorption spectrum (Abs Fe^{3+}) and excitation spectrum of CD-90 for evaluation of spectral overlap and confirmation of IFE..... 58

Figure 24 – 3D-Canonical score plot for the fluorescence patterns obtained from LDA: (a) analytical standards; (b) real sample of cookies. The species were detected at concentration of 25 ppm in CD-90 suspension under neutral pH. All measurements were based on experiments with six replicates..... 59

Figure 25 – Sensing tests for the detection of $Fe3^{+}/CN^{-}$: (a) turn-off sensing with fluorescence quenching of the CD-90 fluorescence spectrum; (b) variation in fluorescence intensity with Fe^{3+} concentration at wavelength 440 nm; (c) turn-on sensing with fluorescence recovery of the CD-90 fluorescence spectrum; (d) variation in fluorescence intensity with CN^{-} concentration at wavelength 440 nm. All average and standard deviation values were calculated based on triplicate experiments..... 60

LIST OF TABLES

Table 1 – Comparison of the proposed method with earlier reported literature for the detection of Co^{2+}..... 38

Table 2 – The Stern-Volmer constant, bimolecular rate constant and thermodynamic parameters as a function of the temperature..... 41

Table 3 – Linear adjustment for quenched and recovery of CD-90 fluorescence..... 61

Table 4 – Comparison of the proposed method with earlier reported literature for the detection of CN^-..... 61

Table 5 – Determination results of CN^- ions in real sample of tap water under optimal conditions (N=3)..... 62

LIST OF ACRONYMS AND ABBREVIATIONS

AFM	Atomic Force Microscopy
bPEI	branched Poly(ethyleneimine)
CD-90	CQDs obtained from citric acid and ethylenediamine
ChCl	Choline chloride
CQDs	Carbon Quantum Dots
FLIM	Fluorescence Lifetime Imaging Microscopy
FTIR	Fourier Transform Infrared Spectroscopy
G-CQDs	Carbon quantum dots with emission of green light
HCA	Hierarchical Clustering Analysis
HPLC	High-Performance Liquid Chromatography
HRTEM	High Resolution Transmission Electron Microscopy
ICP-MS	Inductively Coupled Plasma Mass Spectrometry
IFE	Inner Filter Effect
LDA	Linear Discriminant Analysis
LOD	Limit Of Detection
LSCM	Laser Scanning Confocal Microscopy
N-CD-Ch	CQDs obtained from choline chloride and branched Poly(ethyleneimine)
PBS	Phosphate Buffer Saline
PCA	Principal Component Analysis
PCs	Principal Components
PL	Photoluminescence
QY	Qauntum Yiel fluorescent
R-CQDs	Carbon quantum dots with emission of green red
RSD	Relative Standard Deviation
TEM	Transmission Electron Microscopy
UV-Vis	Ultraviolet-Visible
WADA	World Anti-Doping Agency
WHO	World Health Organization
XPS	X-ray Photoelecton Spectroscopy

SUMMARY

1 INTRODUCTION AND OBJECTIVES 14
1.1 Introduction 14
1.2 Objectives 16
1.2.1 General 16
1.2.2 Specifics 16
2 LITERATURE REVIEW: CARBON QUANTUM DOTS AS NANOPROBES FOR DETECTION SYSTEMS 17
2.1 Synthesis of CQDs 17
2.1.1 Top-down methods 18
2.1.2 Bottom-up methods 19
2.2 Characterization of CQDs 20
2.3 Sensing strategies from CQDs 21
2.3.1 Turn-off sensor 21
2.3.2 Turn-off/turn-on sensor 21
2.3.3 Colorimetric sensor 22
2.3.4 Sensor array 22
3 DETERMINATION OF CO^{2+} IONS IN BLOOD SAMPLES: A MULTI-WAY SENSING BASED ON NH_2-RICH CARBON QUANTUM DOTS 23
3.1 Introduction 24
3.2 Material and methods 26
3.2.1 Material and Reagents 26
3.2.2 N-CD-Ch synthesis 26
3.2.3 Instrumentation and characterization 27
3.2.4 Fluorescent quantum yield 27
3.2.5 Sensing strategy 28
3.2.6 Thermodynamics properties 29
3.3 Results and discussion 30
3.3.1 N-CD-Ch characterization 30
3.3.2 Sensing tests 34
3.3.3 Thermodynamic and interaction mechanism 38
3.3.4 Co^{2+} sensing in real samples and interferents investigation 41
3.4 Conclusions 45
4 CARBON QUANTUM DOTS WITH ULTRA-HIGH QUANTUM YIELD FOR VERSATILE TURN-ON SENSOR OF GLUTEN AND CYANIDE IONS 46
4.1 Introduction 47

4.2 Experimental section 48
4.2.1 Material and reagents 48
4.2.2 Synthesis of CQDs 49
4.2.3 Instrumentation and characterization of CQDs 49
4.2.4 Sensing experiments 50
4.3 Results and discussion 51
4.3.1 Characterization of CD-90 51
4.3.2 Optimization of experimental conditions for sensing of CN^- 55
4.3.3 Development of sensor array for gluten detection and turn-off/turn-on sensing for CN^- *detection* 58
4.4 Conclusion 62
5 GENERAL CONCLUSIONS 63
REFERENCES 68

CHAPTER I

1 INTRODUCTION AND OBJECTIVES

1.1 Introduction

Nanotechnology was treated for many years as a futuristic topic, but currently it is increasingly present in various fields of knowledge, such as chemistry, physics and biology. Briefly, a nanomaterial can be defined as a material that has a size between 1 and 100 nm in at least one of its dimensions (FECHINE, 2020). A nanomaterial has unique properties when compared to the bulk material. The surface area increases significantly at the nanoscale and as a consequence the atoms have more contact with the external environment, causing changes in the mechanical, thermal, magnetic, optical and electronic properties of the material (KHAN *et al.*, 2022). The exploration of these properties leads to several research fields such as energy storage, advanced materials design and sensing, in which the latter is the object of study of this thesis (PATIL *et al.*, 2024).

A sensor can be understood as a device that responds to physical stimuli by transmitting a measurable and corresponding impulse. In this way, a chemical sensor is capable of measuring the content of an analyte through a signal proportional to its concentration (CARNEIRO *et al.*, 2023). For example, a colorimetric chemical sensor explores the phenomenon of light absorption at a given wavelength (ALORABI, 2021), while a fluorescent chemical sensor is based on the phenomenon of light emission, where the emission intensity is used as the sensor response signal (OZMEN; DEMIR; KARAGOZ, 2021).

In the field of chemical sensing, various materials can be used, such as modified electrodes (JANG *et al.*, 2021), thin films (NAJLAOUI *et al.*, 2021) and semiconductor quantum dots (GALSTYAN, 2021). Semiconductor quantum dots are fluorescent materials formed by heavy metal or inorganic material ranging in size from 2 to 10 nm (GIDWANI *et al.*, 2021). However, due to the presence of these types of chemical entities, inorganic quantum dots present toxicity problems, which compromise their application in many clinical studies (NAIR *et al.*, 2020). In this sense, the carbon quantum dots (CQDs) have stood out as an alternative material to inorganic quantum dots.

CQDs are fluorescent nanoparticles discovered accidentally in 2004 after some steps of purifying carbon nanotubes (XU, X. *et al.*, 2004). This nanomaterial has a quasi-spherical shape with an average diameter from 2-10 nm (NAZRI *et al.*, 2021) and its structure

consists of a core of sp^2-sp^3 hybridized carbons with the surface of the nanoparticle being adorned by functional groups containing heteroatoms, such as oxygen, nitrogen, phosphorus and sulfur (WANG, HANG *et al.*, 2024). CQDs exhibit excellent photoluminescence, are biocompatible (GUO *et al.*, 2021), have low toxicity (CARNEIRO *et al.*, 2019), excellent chemical stability and have a high area-to-volume ratio, which facilitates the surface functionalization of these nanoparticles. (SAADH *et al.*, 2024).

In general, CQDs can be used in several areas, such as photocatalysis (ZHANG, L. Y. *et al.*, 2021), bioimaging (LUO *et al.*, 2021), WLEDs manufacturing (PARK, S. J.; YANG; MOON, 2021), energy storage, solar cells and sensors (ARIAS VELASCO *et al.*, 2023). Given this highlight, a search was carried out in the scientific database ScienceDirect (http://www.sciencedirect.com) for the term "carbon quantum dots", as shown in Figure 1. The result reveals an exponential growth in the number of works published in the last decade, indicating the relevance of this nanomaterial in the scientific world.

Fig. 1. State of the art for scientific production involving the term "carbon quantum dots", performed on the ScienceDirect website on March 28, 2024.

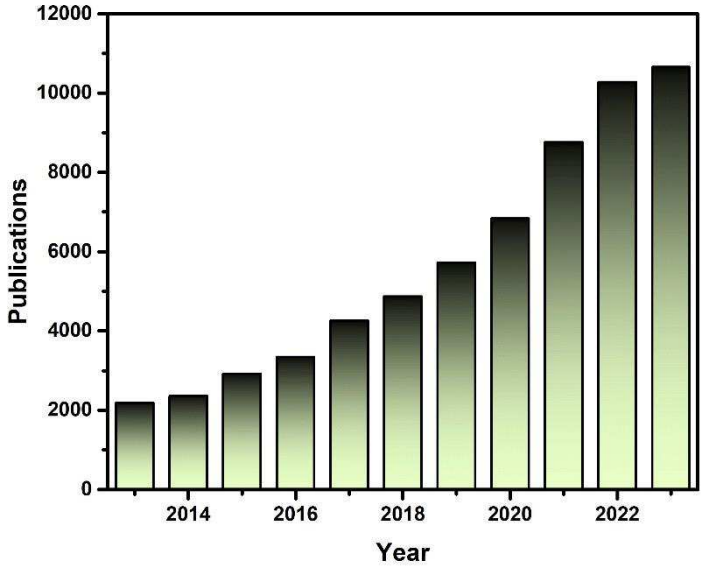

Source: Author.

In this work, carbon quantum dots (CQDs) were used in the development of sensing platforms to quantify cobalt and cyanide ions. Co^{2+} ions, when administered to athletes, cause an increase in the content of erythroproietin, which is responsible for controlling red blood cells (GALAY; DOROGIN; TEMERDASHEV, 2021). Thus, athletes with excess Co^{2+} have undue advantages in anaerobic exercises and that is why the World Anti-Doping Agency (WADA)

added cobalt to its list of restrictions, which sparked interest in cobalt sensing. On the other hand, CN^- is one of the most toxic ions that can be found in food. It can complex with the ferric ions present in the cytochrome oxidase enzyme, leading to hypoxia in the body, which can be fatal to the consumer who ingests food or water contaminated with this species (DONG *et al.*, 2013).

1.2 Objectives

1.2.1 General

To develop sensing strategies based on CQDs fluorescence for applications in anti-doping tests and food safety.

1.2.2 Specifics

a) To synthesize CQDs and study their morphological, structural and optical properties;
b) To develop a turn-off sensor based on the fluorescence quenching caused by Co^{2+} ions;
c) To develop a colorimetric sensor based on the interaction of the CQDs with Co^{2+} ions;
d) To use chemometric tools to discriminate different concentrations of Co^{2+} ions and interfering ions;
e) To quantify Co^{2+} ions in real blood plasma sample;
f) To synthesize CQDs with ultra-high quantum yield fluorescence;
g) To develop a turn-off/turn-on sensor for CN^- detection;
h) To use chemometric tools to develop a sensor array for gluten detection;
i) To quantify CN^- in real samples of tap water.

CHAPTER II

2 LITERATURE REVIEW: CARBON QUANTUM DOTS AS NANOPROBES FOR DETECTION SYSTEMS

2.1 Synthesis of CQDs

CQDs can be obtained by two distinct approaches, top-down and bottom-up, as illustrated in Figure 2. In the top-down approach, the bulk material reaches the nanometric scale through methods such as laser ablation, arc discharge and electrochemical method. This synthetic route generates CQDs with defined optical activity and various quantum yields (QY). However, this approach requires high temperatures, high energy and an acidic medium, making the synthesis processes expensive, dangerous and environmentally unfriendly (EMAM, 2024). On the other hand, in the bottom-up approach, CQDs are obtained from small molecules that polymerize to form these nanoparticles. In this approach, solvothermal/ hydrothermal synthesis and microwave irradiation are often used. This synthetic route has several advantages such as controlling the size of CQDs and functionalizing their surface, the synthesis methods are simpler and environmentally friendly and renewable resources rich in biomolecules can be carbonized to produce green CQDs (KUMAR; RHIM, 2024).

Fig. 2. Schematic representation of top-down and bottom-up approaches for the synthesis of CQDs.

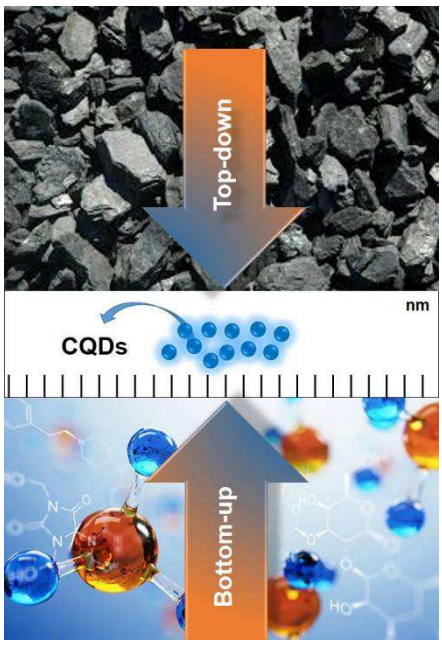

Source: Author.

2.1.1 Top-down methods

The laser ablation method consists of irradiating a laser onto a carbon target. Basically, there are two parameters that can be adjusted to control the properties of the generated CQDs, laser turning and multi-target precursors (BAO *et al.*, 2023). The literature reports a conventional method in which it was used 0.02 g of nano-carbon material dispersed in 50 mL of solvent (water, ethanol, ketone) to prepare the carbon target. After ultrasonication, 4 mL of the suspension was added into a glass cell for laser irradiation, which occurred using an Nd:YAG pulsed laser with a second harmonic wavelength of 532 nm. Then, the solution was centrifuged at 6000 rpm for 30 min and the supernatant was used for spectrofluorophotometer assays. The authors observed that the fluorescent nanomaterial (size 50 nm) presented an photoluminescence (PL) dependent on the excitation wavelength and that the PL intensity decreased by only 4.5% after 4 h, indicating the excellent stability of the nanomaterial (LI, XIANGYOU *et al.*, 2010).

Arc discharge consists of a reorganization of carbon atoms from bulk precursor material. In a reactor, when electric current is applied, the temperature reaches 4000 K and plasma is generated at the anode. Subsequently, carbon vapor is deposited on the cathode, forming CQDs (KUMAR; RHIM, 2024). In a typical experiment, 20 mL of benzene is introduced into the arc discharge reactor and helium is used as the cavitation gas to purge the system. Then, ac power is activated and the discharge is maintained for 5 min. Instantly, it is observed that the plasma-treated benzene turns black, indicating the formation of the nanomaterial. The final product is then removed from the reactor and placed in a bottle with ethylenediamine for subsequent washing and separation of the nanoparticles (JIANG *et al.*, 2010). This synthesis method produces CQDs with good dispersibility in water, however, the high temperatures required and the subsequent purification steps limit the use of this technique (PERUMAL *et al.*, 2021).

Electrochemical method produces CQDs from the carbonization of organic material using electric current. The literature reports a methodology in which the size could be adjusted according to the applied potential (DENG, J. *et al.*, 2014). The authors set up a system with three electrodes, where platinum sheets were used as a working electrode and an auxiliary electrode, while a calomel electrode was used as a reference. The electrolytic bath consisted of NaOH/ethanol and the applied potential varied from 3-9 V with an reaction time of 3-4 h. CQDs with sizes ranging from 2.1 to 4.2 nm were obtained, with the observation that the nanoparticle size increases with the applied potential (DENG, J. *et al.*, 2014).

2.1.2 Bottom-up methods

Solvothermal or hydrothermal synthesis occurs in an autoclave reactor under high temperature and pressure conditions. The method's main advantage is the use of several precursor sources to produce CQDs. Organic materials such as saccharides, organic acids and even food waste can be mixed with various solvents (including water) to be used as a carbon source (KARAGIANNI *et al.*, 2023). For example, Pu *et al* (2023), synthesized CQDs by mixing 0.2 g of p-phenylenediamine, 50 µL of diethylenetriamine and 20 mL of anhydrous ethanol. The solvothermal synthesis was processed at 180 ºC for about 10 h and further purification steps were required, such as filtration, centrifugation and dialysis (PU *et al.*, 2023). In another work, Yang *et al* (2023) obtained CQDs by mixing 510 mg L^- GSH and 15 mL formamide homogeneously. The synthesis occurred in a 50 mL autoclave reactor at 160 ºC for 1 h. Then, the reaction product was cooled to room temperature and the supernatant was collected after centrifugation (4000 rpm, 20 min). A 0.22 µm filter membrane was applied to filter the supernatant. The purification was then completed through dialysis with a dialysis membrane (MW 3000 – 5000) for 3 days (YANG, JING *et al.*, 2023).

The purification of CQDs after synthesis is not exclusive to the solvothermal method. In fact, in hydrothermal synthesis this also happens because the excess reactants are normally not photoluminescent and cause a decrease in the QY of the CQDs. In the sense, Onat *et al* (2024) synthesized CQDs using the hydrothermal method, mixing a certain amount of caffeine and pure water. The mixture was heated at 180 ºC for 8 h. The produced CQDs was passed through a 0.45 µm filter by pressure filtration to remove impurities. The filtered CQD was centrifuged at 10,000 rpm for 60 min (ONAT *et al.*, 2024).

Another synthetic route for the synthesis of CQDs is the microwave irradiation method. In this type of synthesis, electromagnetic waves with a wavelength of 1 mm to 100 cm are irradiated on the precursors, forming CQDs of way fast and inexpensive (POURMADADI *et al.*, 2023). A recent example, CQDs with emission of green light (G-CQDs) and red light (R-CQDs) were produced using microwave irradiation at 180 ºC for 10 min. The difference in the emission regions was due to the differences in the selected precursors, where the G-CQDs were produced from citric acid and urea dissolved in water and the R-CQDs were obtained from o-phenylenediamine dissolved in water with HCl. Both CQDs obtained in this work also underwent purification processes such as centrifugation, filtration and dialysis. (NGUYEN *et al.*, 2023).

2.2 Characterization of CQDs

Various structural characterization techniques can be employed in the characterization of CQDs. Molaei (2023) used atomic force microscopy (AFM Park Scientific Instruments) to investigate the morphology and size of CQDs. The author found a spherical shape for the nanoparticles and an average size smaller than 8 nm (MOLAEI, 2023). However, high-resolution transmission electron microscopy (HRTEM) is a more robust technique for determining the size of nanoparticles, and is even capable of determining the interplanar spacing of the nanomaterial. For example, in the same work mentioned above, Molaei (2023) was able to verify a spacing in the lattice plane equal to 0.208 nm, which according to the author is similar to the 100 facet of graphite (MOLAEI, 2023).

Spectroscopic techniques combined with microscopy provide a more complete view of the structure of CQDs. Fourier Transform Infrared Spectroscopy (FTIR), Raman and X-ray Photoelecton Spectroscopy (XPS) are frequently present in works published in the literature. Mokhine *et al* (2024), obtained CQDs rich in hydrophilic surface groups such as -COOH and N related groups. The authors performed FTIR and observed modes centered at 3042 cm^{-1}, 1661 cm^{-1} and 1398 cm^{-1}, which were attributed to N-H, C=O and -COOH stretching vibration, respectively (MOKHINE *et al.*, 2024). Using Raman spectroscopy, CQDs can be characterized by the presence of two characteristic bands, one associated with sp^3-hybridized carbons (D band) and the other associated with sp^2-hybridized carbons (G band). For example, Kasinathan *et al* (2022) observed the D band at 1335 cm^{-1} and the G band at 1595 cm^{-1}. The authors find that the intensity of the I_D/I_G ratio was 0.84, demonstrating the partial amorphous nature of the nanomaterial (KASINATHAN *et al.*, 2022). Another frequently used spectroscopic analysis is XPS, which makes it possible to elucidate the composition of CQDs. Bulat *et al* (2024) obtained CQDs formed by 77.6% carbon, 19% oxygen and 3.4% nitrogen according to survey XPS spectrum. Furthermore, the high-resolution C1s spectrum showed peaks at 284.8, 286.0, 288.1 and 288.8 attributed to the C-C/C-H, C-O/C-OH/C-O-C, C=O/O-C-O e O=C-O bonds, respectively (BULAT *et al.*, 2024).

The optical characterization of CQDs is based on UV-Vis absorption spectrum and fluorescence spectra. Surendran *et al* (2024) obtained CQDs that presented two absorption peaks, one around 272 nm and the other at 304 nm, which are ascribed to the π-π^* and n-π^* transitions (SURENDRAN *et al.*, 2024). These two peaks frequently appear in published work on CQDs (AZIZI *et al.*, 2024; SPESSATO *et al.*, 2024). In the spectrofluorometer, the emission band of CQDs can be investigated and the study can be done based on the absorption observed

in UV-Vis. For example, in the work of Surendran *et al* (2024) the authors varied the excitation wavelength from 270 to 370 nm (within the region where CQDs showed absorption peaks in UV-Vis) and observed an emission maximum at 416 nm when the sample was excited at 330 nm (SURENDRAN *et al.*, 2024).

2.3 Sensing strategies from CQDs

CQDs have many advantages that make them promising materials for sensing applications. Biocompatibility, low toxicity, easy surface functionalization and excellent photoluminescence enhance its use in practical applications, especially in sensors, where the emission intensity can be used as a response signal when interacting with an analyte of interest.

2.3.1 Turn-off sensor

The direct interaction of an analyte (quencher) with CQDs (fluorophore) can cause a decrease in the fluorescence intensity of this nanomaterial and a turn-off sensor can be developed. In a recent example, Pu *et al* (2023) obtained CQDs via a one-step solvothermal process. After structural and optical characterizations, the authors used CQDs to quantify Fe^{3+} and Co^{2+} ions. For both analytes, when the concentration increased the emission intensity of the CQDs at 500 nm decreased and thus a turn-off sensing strategy for detection of Fe^{3+} and Co^{2+} could be developed. An often useful figure of merit in this type of work is the limit of detection (LOD), which is estimated from a linear regression, where the PL intensity is plotted as a function of the quencher concentration. In this specific work, the LOD for the detection of Fe^{3+} was 0.88 μM while the LOD for the detection of Co^{2+} was 0.95 μM (PU *et al.*, 2023).

2.3.2 Turn-off/turn-on sensor

Another sensing strategy that can be adopted using CQDs is turn-off/turn-on sensing. In this case, the CQDs have their fluorescence quenched by a quencher and then the fluorescence of the CQDs is recovered as the analyte is added to the mixture. Generally, Fe^{3+} ions are excellent fluorescence quenchers and can be used in these nanoprobes. Hamid *et al* (2023) synthesized fluorescent CQDs via microwave irradiation method and used Fe^{3+} ions to form a non-fluorescent complex with the CQDs. Then the authors were able to quantify ascorbic acid by adding this analyte to the CQDs/Fe^{3+} complex. The reducing property of ascobic acid

converted the Fe^{3+} ions to Fe^{2+} ions and then the non-fluorescent complex was undone. Thus, the fluorescence of CQDs was restored and increased linearly with analyte concentration. This turn-off/turn-on method of ascorbic acid detection had a linear behavior in the concentration range 2.0-100 µg/mL with a LOD of 0.6 µg/mL (AHMED ABDEL HAMID *et al.*, 2023).

2.3.3 Colorimetric sensor

In addition to the fluorescent methods mentioned in the previous subsections, CQDs can be used as nanoprobes in colorimetric sensors, where the response signal is the absorption intensity at a given wavelength. For example, Chen *et al* (2024) obtained green emissive CQDs with strong UV absorption at 451 nm. The authors noticed that mixing ClO^- with CQDs changed the color of the solution from light yellow to colorless by naked eye. Then, a colorimetric sensor could be built based on UV absorption at 451 nm. Increasing the concentration of ClO^- in the range of 0 to 160 µM proportionally decreased the absorption intensity, making it possible to detect the studied analyte. Finally, the LOD of the nanoprobe was calculated in the linear range to be 1.28 µM (CHEN *et al.*, 2024).

2.3.4 Sensor array

The interaction of CQDs with the analyte can be explored by analyzing the fluorescence spectrum integrally, i.e. considering the emission intensity at each wavelength present in the spectrum. This multivariate method of analysis generates a large amount of data, which is used as a "fingerprint" that characterizes a particular interaction of CQDs with the analyte. Zhu *et al* (2023) successfully discriminated six biothiols using the linear discriminant analysis (LDA) and hierarchical clustering analysis (HCA) chemometric tools. The authors developed a fluorescence response matrix consisting of 3 paper chips $\times$ 6 biothiols $\times$ 5 replicates. LDA and HCA convert complex multidimensional data into simple visualization patterns, grouping the data into six different groups without any overlap. The authors also investigated the possibility of identifying different concentrations (5-100 µM) of biothiols individually and in binary and ternary mixtures and again the sensor array was successful in discriminating the groups, indicating its good resolution of biothiols (ZHU *et al.*, 2023).

CHAPTER III[1]

3 DETERMINATION OF CO^{2+} IONS IN BLOOD SAMPLES: A MULTI-WAY SENSING BASED ON NH_2-RICH CARBON QUANTUM DOTS

Abstract

Multiple forms of detecting Co^{2+} are reported in this work to quantify these ions in real blood plasma samples. Carbon Quantum Dots (CQDs) were used as a fluorescent nanoprobe. The CQDs were obtained from a bottom-up approach using a hydrothermal method and choline chloride and branched poly(ethyleneimine) as precursor molecules. Several spectroscopic and structural characterizations were performed. The efficient fluorescence quenching of CQDs related to the Co^{2+} ion was used for the detection of the analyte, generating a sensing strategy with a limit of detection (LOD) of 0.98 μmol L^{-1}. Furthermore, the interaction between the Co^{2+} ion with the CQDs resulted in the color change of the solution from colorless to pale yellow. Thus, a colorimetric Co^{2+} sensor was also developed, since there was an absorption band at 315 nm attributed to the formation of the complex CQD + Co^{2+}. The colorimetric method showed an excellent sensitivity to Co^{2+}, with a LOD of 3.01 μmol L^{-1}. In addition, Principal Component Analysis (PCA) together with Linear Discriminant Analysis (LDA) were used successfully to distinguish different concentrations of Co^{2+} and different interfering ions present in the solution. Finally, a real sample of blood plasma was properly treated and doped with different concentrations of Co^{2+}, which was successfully quantified *via* fluorescent method. Therefore, the CQDs obtained in this work are a powerful and versatile Co^{2+} detection tool.

Keywords: Carbon Quantum Dots; Cobalt sensing; Colorimetric sensor; Chemometric tools.

OLIVEIRA, J. J. P. *et al.* Determination of Co2+ ions in blood samples: A multi-way sensing based on NH2-rich carbon quantum dots. **Dyes and Pigments**, v. 215, p. 111253, 1 jul. 2023.

[1] This chapter is the results of the research paper entitled "Determination of Co^{2+} ions in blood samples: a multi-way sensing based on NH_2-rich carbon quantum dots", published in the Dyes and Pigments.

3.1 Introduction

The good performance of a high-performance athlete is strictly related to the personal diet and intake of minerals, vitamins, and trace elements. In this regard, cobalt is an essential trace element, since its deficiency in the human body can lead to pathological conditions (SHAO *et al.*, 2021). However, cobalt is also known to cause effects similar to hypoxic training, when administered to athletes (SKALNY *et al.*, 2019). Commonly consumed in the chloride-form, cobalt increases an athlete's performance in anaerobic exercises, as it causes an increase in the content of erythropoietin, responsible for controlling the production of red blood cells (GALAY; DOROGIN; TEMERDASHEV, 2021).

Based on this reason, the World Anti-Doping Agency (WADA) added cobalt to its list of restrictions, and since then, cobalt sensing has attracted more attention. WADA does not specify the maximum concentration of cobalt in blood plasma, but it is known that concentrations below 300 μg L^{-1} of cobalt in the blood do not cause adverse health effects (SKALNY *et al.*, 2019). However, the World Health Organization (WHO) recommends a maximum value of $1.7x10^{-3}$ mol L^{-1} of Co^{2+} ions in drinking water (JAMES H. KIM, HERMAN J. GIBB, 2006). Hitherto, Co^{2+} ions have been detected mainly through Inductively Coupled Plasma Mass Spectrometry (ICP-MS) (MAYNAR, M. *et al.*, 2019) and High-Performance Liquid Chromatography (HPLC), commonly using the spectrophotometric detection method (SONG *et al.*, 2020). However, these techniques require trained analysts, expensive equipment and several sample pretreatment steps, limiting cobalt sensing. Given these difficulties, new sensing strategies are required and, as a result, chemical sensors have gained prominence, whether by electrochemical (CUARTERO, 2021), colorimetric (ALAMGIR *et al.*, 2020) or fluorescent methods (ZHAO, X. *et al.*, 2021).

A colorimetric chemical sensor explores the phenomenon of light absorption at a given wavelength (ALORABI, 2021), while a fluorescent chemical sensor is based on the phenomenon of light emission, where the emission intensity is used as the sensor response signal (OZMEN; DEMIR; KARAGOZ, 2021). Multivariate data analysis techniques can be integrated into these sensing strategies, performing pattern recognition and generating characteristic fingerprints, based on the response signals obtained (GEANĂ; ARTEM; APETREI, 2021). Among the main multivariate analysis techniques, Principal Component Analysis (PCA) and Linear Discriminant Analysis (LDA) are highlighted. PCA is an unsupervised pattern recognition tool that reduces the size of the data, while keeping significant information (CRUZ *et al.*, 2021). On the other hand, LDA is a supervised pattern recognition

method that can be understood as a data classification technique, tracing a relationship between objects and classes through a mathematical model (BASRI *et al.*, 2022).

In the field of chemical sensing, various materials can be used, such as modified electrodes (JANG *et al.*, 2021), thin films (NAJLAOUI *et al.*, 2021) and semiconductor quantum dots (GALSTYAN, 2021). Semiconductor quantum dots are fluorescent materials formed by heavy metal or inorganic material ranging in size from 2 to 10 nm (GIDWANI *et al.*, 2021). However, due to the presence of these types of chemical entities, inorganic quantum dots present toxicity problems, which compromise their application in many clinical studies (NAIR *et al.*, 2020). In this sense, the carbon quantum dots (CQDs) have stood out as an alternative material to inorganic quantum dots. CQDs are quasi-spherical nanoparticles ranging in size from 2-10 nm being considered a zero-dimensional material (NAZRI *et al.*, 2021), are biocompatible (GUO *et al.*, 2021), have different precursor sources (CARNEIRO *et al.*, 2021), low toxicity and are photoluminescent (CARNEIRO *et al.*, 2019).

In general, CQDs can be used in several areas, such as photocatalysis (ZHANG, L. Y. *et al.*, 2021), bioimaging (LUO *et al.*, 2021; WU, F. *et al.*, 2016, 2017), WLEDs manufacturing (PARK, S. J.; YANG; MOON, 2021) and also chemical sensing (JAYAN *et al.*, 2020), where its application in Co^{2+} ion detection systems is already reported in the literature (JING *et al.*, 2019; LIAO, S. *et al.*, 2018; SUN *et al.*, 2021; ZHAO, C. *et al.*, 2019). In this work, N-CD-Ch were produced from hydrothermal synthesis using precursors branched poly(ethyleneimine) (bPEI) and choline chloride (ChCl) in aqueous medium. Several spectroscopic characterizations have been carried out and the CQDs have shown promise in the sensitive and selective sensing of Co^{2+} ions present in a real serum sample with a recovery of 100.94%. In addition, it was possible to develop a multiple sensing of Co^{2+} by colorimetric and fluorescent channel and multivariate analysis, using the chemometric tools PCA and LDA. Moreover, the PCA and LDA model showed capability of distinguishing different interfering ions, demonstrating the versatility of the sensing platform in relation to the detection of different ions.

3.2 Material and methods

3.2.1 Material and Reagents

Sodium sulfate anhydrous (Na_2SO_4, 99.0-101.0%), sodium sulfite anhydrous (Na_2SO_3, ≥ 96.0%), monobasic sodium phosphate (NaH_2PO_4, 99.0%), dibasic sodium phosphate ($Na_2HPO_4{\cdot}12H_2O$, 99.0%), potassium nitrate (KNO_3, 99.0%), hydrogen peroxide (H_2O_2, 30%), sodium chloride (NaCl, 99.0%), manganese chloride ($MnCl_2{\cdot}4H_2O$, 98.0%), potassium chloride (KCl, 99.0%), calcium chloride ($CaCl_2{\cdot}2H_2O$, 74.0-78.0%), magnesium chloride ($MgCl_2{\cdot}6H_2O$, 98.0%), aluminum chloride ($AlCl_3{\cdot}6H_2O$, 99.0%) and cadmium chloride ($CdCl_2{\cdot}H_2O$, 99.0%) were purchased from Vetec. Cobalt chloride ($CoCl_2{\cdot}6H_2O$, 98.0%), zinc chloride ($ZnCl_2$, 97.0%), sodium hydroxide (NaOH, 98.0%), sodium nitrate ($NaNO_3$, 99.0%) and nitric acid (HNO_3, 65%) were purchased from Dinamica. Hydrochloric acid (HCl, 36.5-38.0%) and sodium carbonate (Na_2CO_3, 99.0%) were purchased from Synth. Choline chloride pure ($C_5H_{14}ClNO$) was purchased from Orion Cientific and *branched* poly(ethyleneimine) (*b*PEI, 25,000 g mol^{-1}) was purchased from Sigma-Aldrich. The real blood plasma sample was purchased from Seronorm™ Trace Elements Serum. All chemicals were used without previous treatment, except the real blood plasma sample.

3.2.2 N-CD-Ch synthesis

N-CD-Ch was synthesized by using a conventional hydrothermal method with slight adjustments (JI, Z. *et al.*, 2021; SU *et al.*, 2018; YUE *et al.*, 2020). First, *b*PEI (0.04 mmol) was dispersed in water (10 mL) and then choline chloride (3.58 mmol) was added to the mixture. Both precursor molecules act as a carbon source and are rich in nitrogen, which acts as a heteroatom and ensures different surface states in the formed CQDs (ZHANG, W. *et al.*, 2022). Then, the aqueous mixture was transferred into a 50 mL Teflon-lined autoclave and heated at 200 ºC using an 8-hour reaction time, as shown in Figure 3. After synthesis, the material was cooled down to room temperature and then diluted five times in water. In addition, the nanomaterial was purified via dialysis using a cellulose membrane Spectra/Por®6 of 1 kDa MWCO.

Fig. 3. Reaction scheme for the N-CD-Ch synthesis.

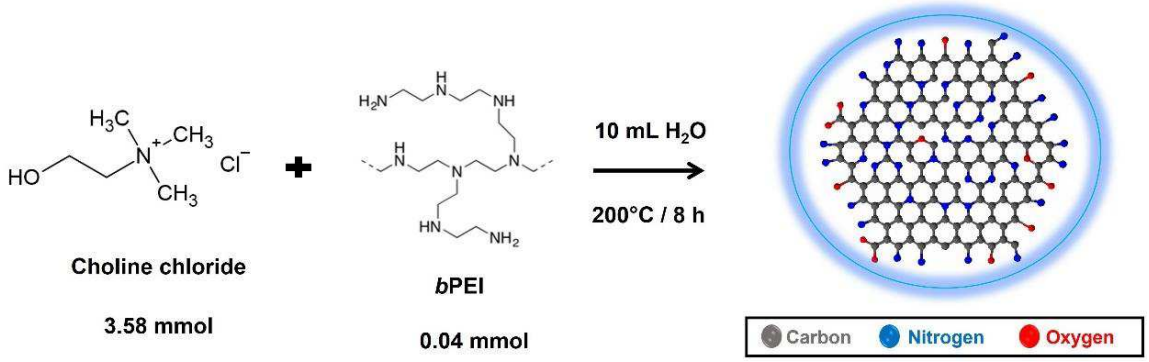

Source: (OLIVEIRA *et al*, 2023)

3.2.3 Instrumentation and characterization

Atomic force microscopy (AFM) images were obtained using an Asylum MFP-3D (Oxford instruments) operating in non-contact mode with a NCHR-50 silicon tip (Nano World, less than 8 nm of tip radius, 42 N/m of force constant, 320 kHz of resonance frequency), with a scan rate of 0.20 Hz. Transmission electron microscopy (TEM) images of nanoparticles were obtained using a Hitachi® HT7700 TEM system operating at an accelerating voltage of 120 kV. Raman spectroscopy was performed in a range of 500 to 2500 cm^{-1}, using a Horiba Raman spectrometer. The Fourier transform infrared (FTIR) spectrum was recorded by using a scanning range of 400 to 4000 cm^{-1}. X-ray photoelectron spectroscopy (XPS) was performed using a ThermoFisher Scientific model K-alpha+, applying monochrome radiation from Al-kα with a pass energy of 200 eV for the survey and 50 eV for high-resolution scanning spectra. The absorption spectra were recorded in the spectrophotometer UV-Vis Shimadzu UV-2600. The fluorescence spectra were obtained in the Shimadzu RF-6000 spectrofluorophotometer. Fluorescence Lifetime Imaging Microscopy (FLIM) was used to determine the fluorescence lifetime of N-CD-Ch.

3.2.4 Fluorescent quantum yield

The quantum yield (*QY*) of the N-CD-Ch was determined based on a method described previously, in which quinine sulfate in H_2SO_4 0.1 mol L^{-1} (QY_R of 54%) was used as a standard (SALJOUGHI; KHAKBAZ; MAHANI, 2020). The absorption values of the N-CD-Ch were kept below 0.05 to ensure that the re-absorption effect did not occur (LIU *et al.*, 2019). Equation 1 was used to calculate the *QY* of the N-CD-Ch:

$$QY = QY_S \times \frac{I}{I_S} \times \frac{A_S}{A} \times \frac{n^2}{n_S^2} \quad \textbf{(1)}$$

Where QY is the quantum yield of the N-CD-Ch, I is integrated emission intensity, A and n are, respectively, the absorbance and the refractive index. The s subscript is related to the standard.

3.2.5 Sensing strategy

Initially, some experimental parameters of the sensing platform were optimized, such as excitation wavelength (300-450 nm), N-CD-Ch concentration (0.01-1.50 mg mL^{-1}) and pH effect (1.81-9.18), which was adjusted from the addition of 0.1 mol L^{-1} NaOH and HCl solutions. Another factor investigated is related to the selectivity of the nanoprobe, which was tested by adding different interfering ions to the detection system. All ion solutions were added with a final concentration of 250 µmol L^{-1}. The sensing strategy is based on the turn-off fluorescence detection (LATIEF *et al.*, 2021) and colorimetric detection method (DEVI *et al.*, 2021). In short, 500 µL of N-CD-Ch (1.0 mg mL^{-1}) were transferred to a quartz cuvette, and then different concentrations of Co^{2+} were added, followed by PBS solution at pH 7.4 addition, up to final volume of 2.0 mL. For the fluorescence detection method, the emission spectra were recorded at the excitation wavelength of 340 nm, with a N-CD-Ch concentration of 0.25 mg mL^{-1}, and the PL intensity at 465 nm was used for Co^{2+} ion quantification. For the colorimetric method, the absorbance at 315 nm was used for Co^{2+} ion quantification. The limit of detection (*LOD*) of both methods was calculated from Equation 2:

$$LOD = \frac{3.3s}{b} \quad \textbf{(2)}$$

where *s* is the standard deviation of the fluorescence/absorbance measurements and *b* is the average values of the slope of the calibration curve (ZHANG, W. J. *et al.*, 2019). Co^{2+} ion detection in a real sample occurred using the fluorescent method. First, a vial of certified blood plasma sample (Seronorm™ Trace Elements Serum) was opened, a volume of sterile deionized water was filled as stated in the label of the vial, and the content was completely solubilized. The reconstituted serum was treated with nitric acid and hydrogen peroxide according to the methodology proposed by Maynar *et al* (MAYNAR, MARCOS *et al.*, 2018). Then, the sample was diluted 10^{-7} folds with ultrapure water and doped with different

concentrations of Co^{2+} (0-250 µmol L^{-1}). In addition, a calibration curve was constructed from the titration performed at 298.75 K and the recovery of the sensing platform was determined in the concentrations of 100 and 200 µmol L^{-1}.

3.2.6 Thermodynamics properties

Co^{2+} ions solution titrations were performed in a medium PBS buffer at a pH value of 7.4 at three different temperatures (298.75, 308.15 and 318.15 K). The fluorescence intensity at 465 nm was taken to construct an analytical curve and the data was described using a Stern-Volmer model, according to equations 3 and 4.

$$\frac{I_0}{I} = 1 + K_{SV}[Q] \quad \textbf{(3)}$$

$$k_q = \frac{K_{SV}}{\tau_0} \quad \textbf{(4)}$$

where I_0 and I are the fluorescence intensity in the absence and presence of the quencher, respectively; K_{SV} is the Stern-Volmer constant, k_q is the bimolecular rate constant of the fluorescence quenching process and τ_0 is the fluorescence lifetime; $[Q]$ is the concentration of the quencher (GEHLEN, 2020). Thermodynamic properties were also determined following a well-established method, using the Van't Hoff equation (VASHISHT *et al.*, 2020; ZHANG, S. R. *et al.*, 2021). The τ_0 was initially calculated through FLIM measurements. Subsequently, this value was used to find k_q, using the equation 4. The Van't Hoff graph was used to linearize the k_q values obtained at three different temperatures. Then, ΔH and ΔS were calculated according to equation 5 and ΔG was calculated from the equation 6:

$$lnk_q = -\frac{\Delta H}{R}\left(\frac{1}{T}\right) + \frac{\Delta S}{R} \quad \textbf{(5)}$$

$$\Delta G = -RTlnk_q \quad \textbf{(6)}$$

where k_q is the bimolecular rate constant, ΔH is the enthalpy variation, ΔS is the entropy variation, T is the temperature and R is the universal gas constant.

3.3 Results and discussion

3.3.1 N-CD-Ch characterization

Initially, the morphological properties of the N-CD-Ch were investigated. In this sense, AFM and TEM images were acquired and the results are displayed in Figure 4. The successful formation of nanoparticles was confirmed by performing AFM tapping mode analysis. Figure 4 (a) shows the topography image in which it is possible to identify the formation of nanoparticles with sizes of the order of 3.0 nm, as shown by the section profile (Figure 4 (b)) associated with the red line in Figure 4 (a). Furthermore, TEM images of the N-CD-Ch nanoparticles were obtained and an approximately round shape can be seen in Figure 4 (c). Figure 4 (d) shows the size distribution performed from the TEM images, demonstrating an average size 4.51 nm, value close to that estimated by AFM and is in agreement with the ones found in the literature (DSOUZA *et al.*, 2021; WANG, Z. *et al.*, 2021).

Raman spectroscopy measurements were performed to investigate the surface chemistry of the nanoparticles. Figure 4 (e) illustrates the deconvolution of the Raman spectrum, where four bands were observed and the two most intense are located at 1390 and 1517 cm^{-1} attributed to the D and G bands, respectively (LI, XUE *et al.*, 2020). The D band represents the degree of disorder in graphene structure due to the presence of sp^3 carbon, while the G band is related to the highly ordered graphene with domains of sp^2 carbon (LI, N. *et al.*, 2021). The ratio between the intensity of the D and G bands (I_D/I_G = 0.86) shows similarity between N-CD-Ch and graphene structure with the predominance of sp^2 carbon.

FTIR spectroscopy was used to elucidate the functional groups present in N-CD-Ch. The spectra presented in Figure 4 (f) indicate the presence of bands in the region of 3420 cm^{-1}, which can be attributed to the stretching vibration of O-H and N-H bonds (ZOU *et al.*, 2022). These bonds which are also present in both precursors. Additionally, the absorption bands at 2935 cm^{-1} can be assigned to the C-H stretching vibration (DHANDAPANI *et al.*, 2021), which is also present in the spectrum of precursor molecules. The strong bands at 1644 cm^{-1} and 1137 cm^{-1} confirmed the presence of C=O and C-O bonds (JOSEPH; THOMAS, 2022), respectively, while the bands at 1462 and 1313 cm^{-1} were assigned to the stretching vibration of C=C and C-N bonds (DING *et al.*, 2018; YANG, H. *et al.*, 2019). According to FTIR data, the N-CD-Ch structure contains carboxyl, hydroxyl and amino groups, causing electrostatic repulsion that contributes to the good solubility of this nanomaterial in water (RAIKWAR, 2022). Furthermore, the remarkable changes in the spectrum of N-CD-Ch in

relation to the spectra of its precursors, such as the appearance of the bands at 1644 and 1137 cm^{-1}, confirm that there was a chemical reaction that produced the CQDs.

Fig. 4. **(a)** Topography image of N-CD-Ch confirms the formation of nanoparticles of regular size; **(b)** Section height profile associated with the red line on the topography image; **(c)** TEM and **(d)** size distributions images of N-CD-Ch; **(e)** Raman spectrum and **(f)** FTIR spectra of N-CD-Ch.

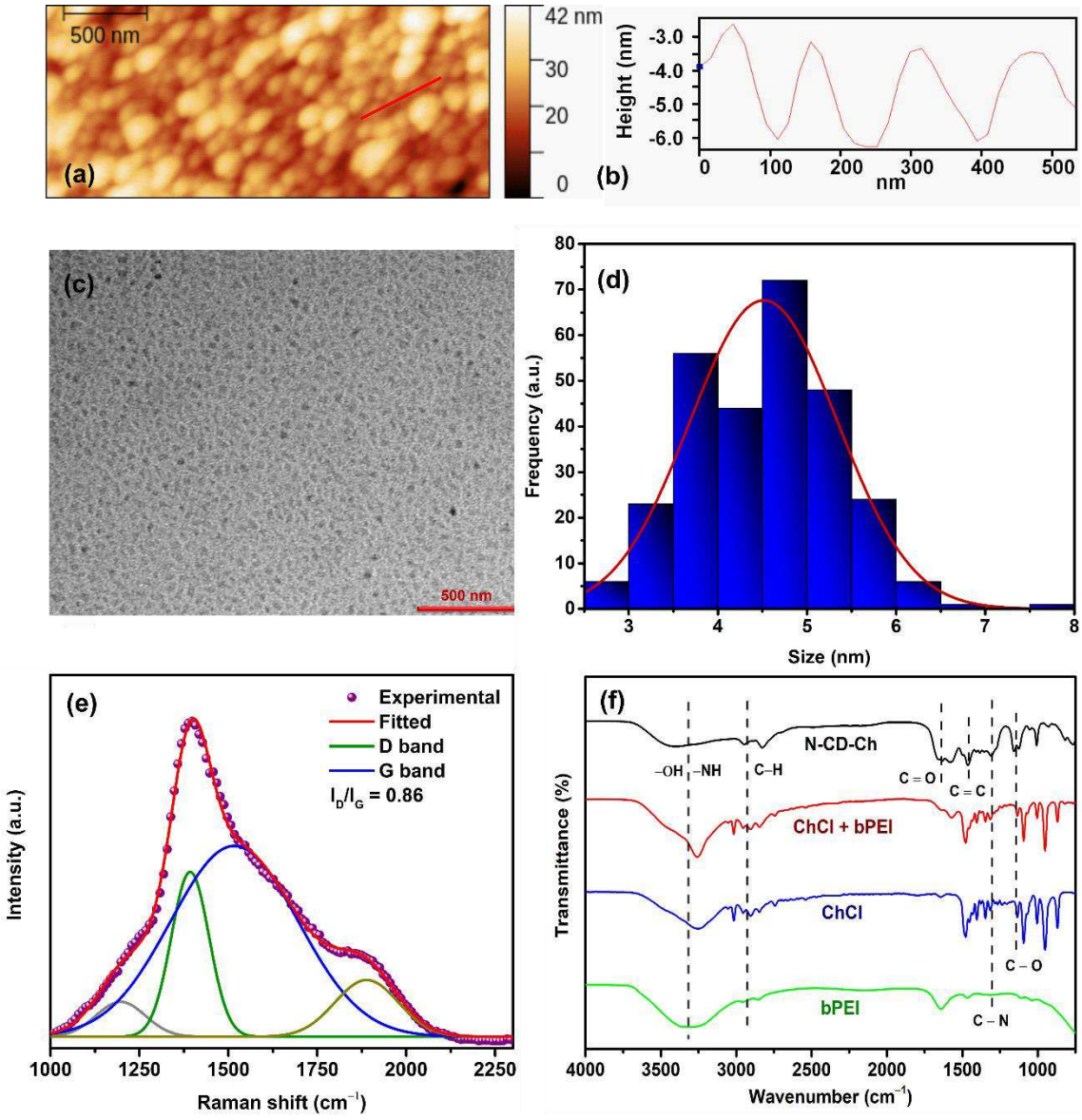

Source: (OLIVEIRA *et al*, 2023)

XPS analysis was conducted to deepen the study of the surface composition and chemical environment of the N-CD-Ch. The XPS survey spectrum shown in Figure 5 (a) detected signals at 285.35, 399.05 and 532.04 eV, corresponding to C1s, N1s and O1s, respectively. Therefore, N-CD-Ch is composed mainly of carbon (67.83%), nitrogen (24.18%)

and oxygen (7.99%). The deconvolution of the C1s spectrum in Figure 5 (b) shows two bands at 284.78 and 285.58 eV, which are assigned to C=C and C-C groups, respectively (MU *et al.*, 2021). The N1s spectrum in Figure 5 (c) shows two bands at 398.98 and 399.68 eV, which are related to the N-C and N-H groups, respectively (YANG, M. *et al.*, 2021). XPS, FTIR and Raman spectroscopy results showed a similar chemical structure profile regarding functional groups of N-CD-Ch (Figure 5 (d)). Herein, it would be able to propose a mechanism for quenching and further understanding the sensing platform in depth.

Fig. 5. (a) XPS survey spectrum and high-resolution XPS spectra of **(b)** C1s and **(c)** N1s; **(d)** chemical structure of N-CD-Ch.

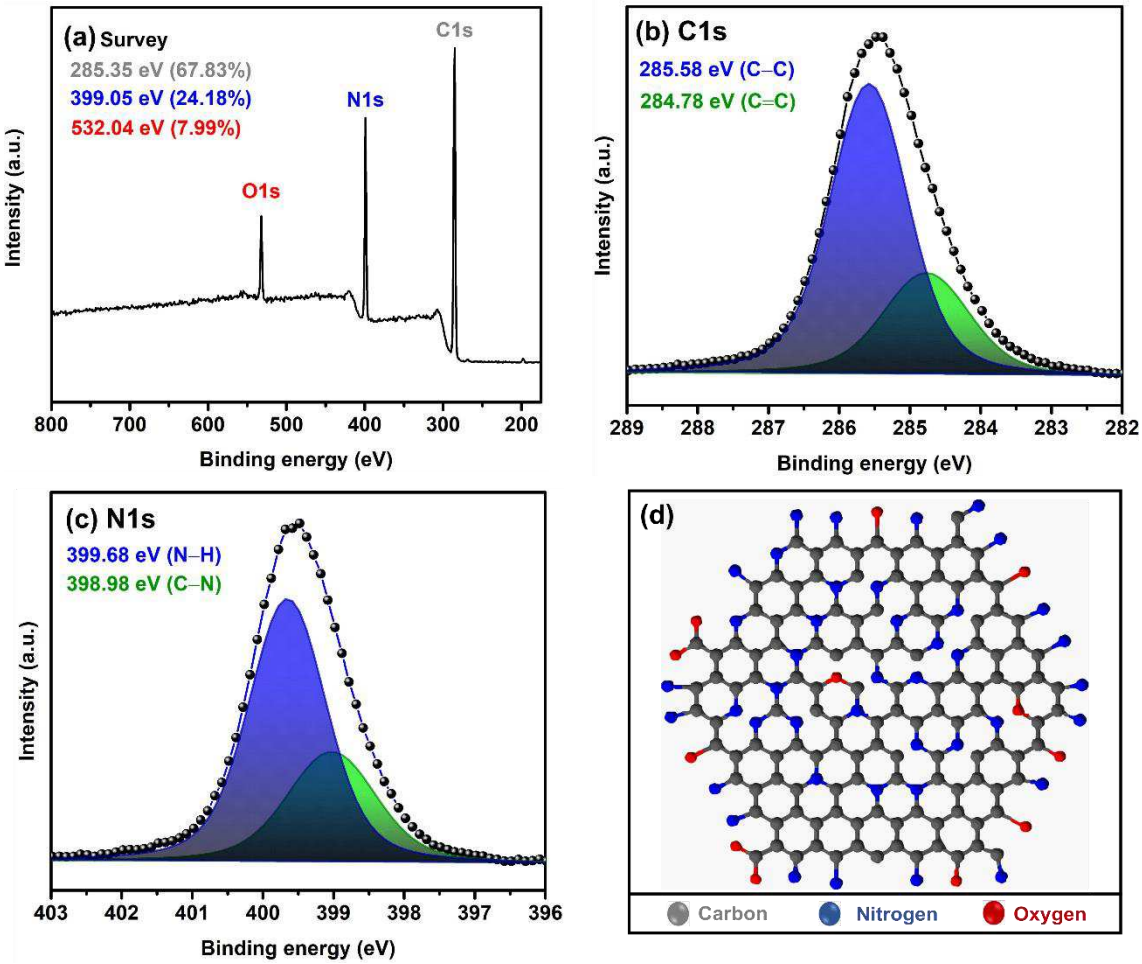

Source: (OLIVEIRA *et al*, 2023)

The N-CD-Ch optical properties were examined using UV-Vis absorption and fluorescence spectroscopy. Figure 6 (a) shows the UV-Vis absorption and emission spectra of N-CD-Ch. The absorption band around 219 nm is related to the transitions π-π^* of the C=C bonds of the aromatic π system and the band at 345 nm can be attributed to the C=O bonds of

carbonyl groups (HAMMI *et al.*, 2021). The fluorescence emission of the N-CD-Ch was observed at 465 nm, under excitation of 340 nm. Under visible light, the suspension of CQDs showed a transparent color, while under UV light (exc. 365 nm) a blue color was observed, as shown in the inset of Figure 6 (a). According to the literature, carbogenic cores form excitons, which can transit through energy traps on the surface of the CQDs and then return to the ground state, emitting blue light (ARUMUGAM *et al.*, 2020). Additionally, the fluorescence QY of N-CD-Ch was calculated to be 7.7 %, which is in good agreement with said literature (FANG; ZHUO; ZHU, 2019; JI, X. *et al.*, 2021; WANG, C. *et al.*, 2020).

In Figure 6 (b) an excitation-independent fluorescence behavior for N-CD-Ch from 330 to 380 nm is observed. This result converges with the one obtained by Raman spectroscopy, since surface defects present in the carbogenic core can be uniformly distributed, ensuring a fixed emission around 465 nm. However, from 390 to 450 nm, a significant shift occurs due to the presence of different particle size values and surface states for N-CD-Ch (CARNEIRO *et al.*, 2019). Taking into account emission intensities, an excitation wavelength of 340 nm was selected in the experiments of this work.

Fig. 6. (a) The UV-Vis absorption and fluorescence spectra of N-CD-Ch. Inset: photograph of N-CD-Ch water suspension under visible light (left) and UV light (right); **(b)** Fluorescence spectra of N-CD-Ch sample under different excitation wavelengths.

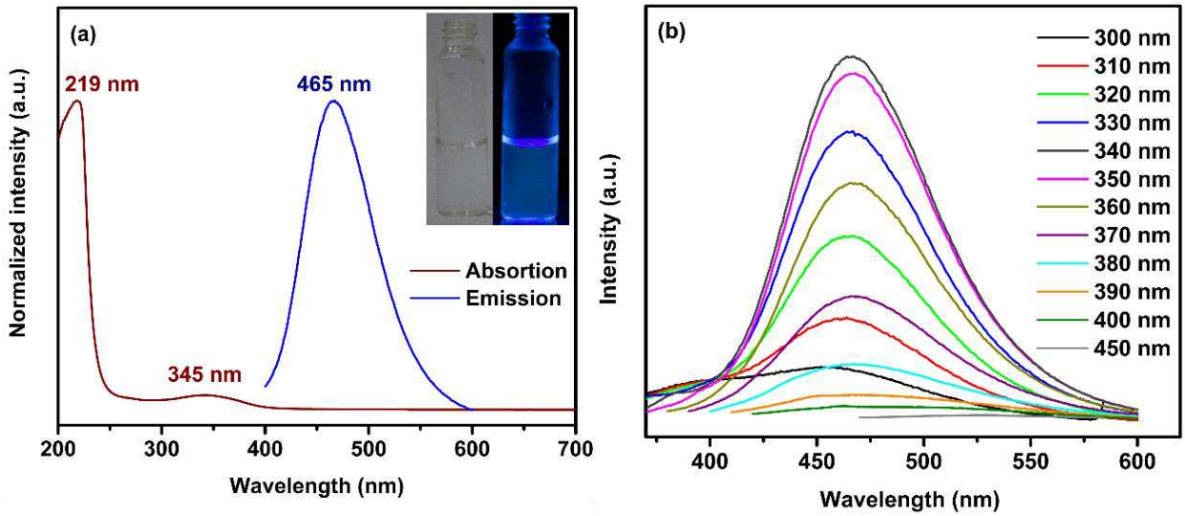

Source: (OLIVEIRA *et al*, 2023)

3.3.2 Sensing tests

Firstly, some parameters were investigated to explore the potential of N-CD-Ch in the Co^{2+} sensing. The fluorescence intensity as a function of time was investigated, which remained practically unchanged as shown in Figure 7. It is clear from the results that the fluorescence intensity does not significantly change after 40 minutes of preparing the colloidal suspension. Moreover, over extended periods, the fluorescence intensity and profile of the photoluminescence spectrum remain stable, providing evidence for their photostability.

Fig. 7. Photostability experiment for 40 min.

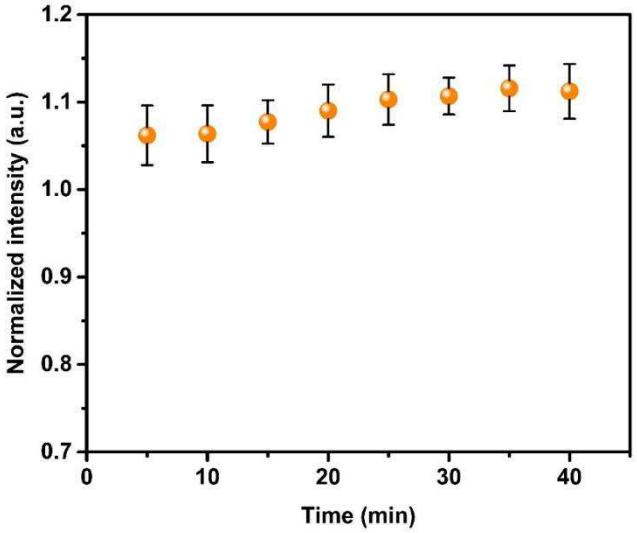

Source: (OLIVEIRA *et al*, 2023)

Figure 8 (a) shows another parameter investigated, the fluorescence spectra of N-CD-Ch at different concentrations. It is possible to observe that the fluorescence intensity is directly proportional to the concentration of N-CD-Ch, as can be seen in Figure 8 (a) (inset), where a good linear correlation ($y = 49774.3x + 1253.8$) was obtained with a squared correlation coefficient (R^2) of 0.9988. The self-quenching process caused by the aggregation of nanoparticles was not observed within the concentration range. Thereby, the concentration of 0.25 mg mL^{-1} was chosen for further experiments, since it represents a median concentration value. In addition, this concentration displays a high fluorescence intensity, which can provide a good response signal in the sensing platform.

Furthermore, the pH effect was carefully investigated, since the pH of the solution may affect the efficiency of sensing. As displayed in Figure 8 (b), an increase in the pH values enhances the N-CD-Ch fluorescence intensity. According to the literature, at low pH values,

nitrogen and carboxyl groups are protonated, decreasing the solubility of the nanoparticles and resulting in their aggregation (CARNEIRO *et al.*, 2021). However, considering blood plasma pH value, which is approximately 7.0, the pH of the real sample would not interfere in the sensing tests. Therefore, sensing tests were performed in the PBS buffer at pH 7.4.

Fig. 8. **(a)** Fluorescence spectra of N-CD-Ch at different concentrations. Inset: the linear relationship between fluorescence intensity and N-CD-Ch concentration at 465 nm; **(b)** pH-response fluorescence at 465 nm; **(c)** fluorescence intensity after the addition of different concentrations of Co^{2+}. In the range of 0 to 50 µmol L^{-1} the increment was 5 µmol L^{-1}, while in the range of 50 to 500 µmol L^{-1} the increment was 50 µmol L^{-1}. Inset: photograph of the aqueous solution of N-CD-Ch under UV light at different concentrations of Co^{2+}, ranging from 0 to 500 µmol L^{-1} with an increment of 50 from left to right; **(d)** UV-Vis absorption as a function of Co^{2+} concentration. Inset: photograph of the aqueous solution of N-CD-Ch from 0 (left) to 500 µmol L^{-1} of Co^{2+} (right) with an increment of 50. All average and standard deviation values were calculated based on triplicate experiments.

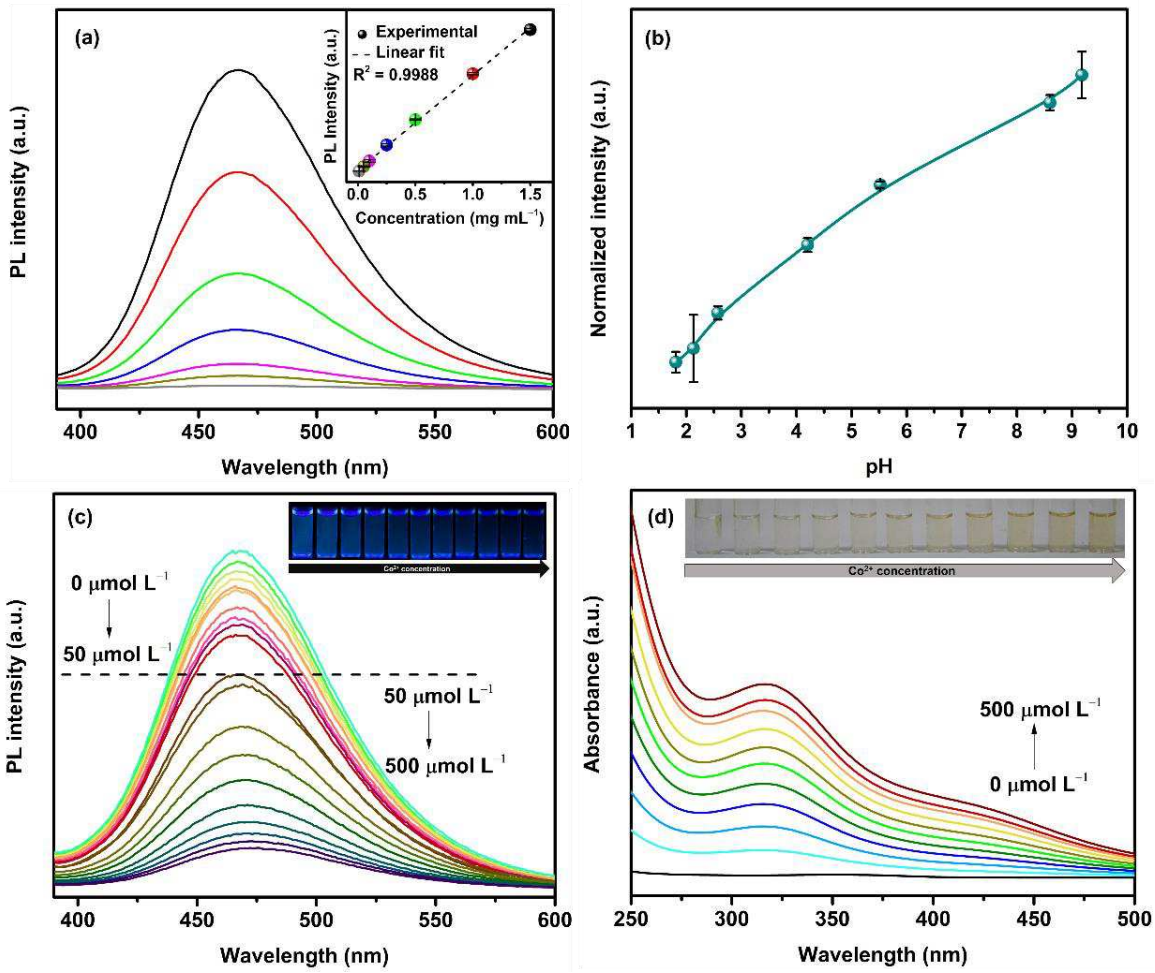

Source: (OLIVEIRA *et al*, 2023)

Under optimized conditions (excitation wavelength of 340 nm, N-CD-Ch concentration of 0.25 mg mL^{-1} and pH 7.4), the PL spectrum of N-CD-Ch around 465 nm decreased gradually with the increase of Co^{2+} concentration, as shown in Figure 8 (c). Furthermore, the inset of Figure 8 (c) shows a saturation trend of the fluorescence quenching when the analyte concentration reaches 500 µmol L^{-1}, where the fluorescence intensity in the blue region disappears. Several types of phenomena govern the fluorescence quenching of fluorophore species such as N-CD-Ch. In this work, the interaction mechanism of Co^{2+} ions with N-CD-Ch will be discussed in the next section, based on thermodynamic data.

According to Figure 8 (c), two concentration ranges were used and the lower concentration range (0-50 µmol L^{-1}) suggested that the present sensing strategy is highly sensitive towards the detection of Co^{2+} ions. Figure 9 shows I_0/I ratio values plotted as a function of the Co^{2+} concentration for *LOD* determination of the fluorescent nanoprobe, calculated using Equation 2, obtaining a value of 0.98 µmol L^{-1}, approximately 10^3x lower than that recommended by the WHO.

Experimentally, it was observed that the addition of Co^{2+} ions to N-CD-Ch solution changes the color from colorless to pale yellow, indicating another way to quantify Co^{2+} ions. Thus, in this work, a colorimetric sensor was also developed and investigated, and the results can be seen in Figure 8 (d). According to Figure 8 (d), the absorbance at 315 nm increases proportionally with the Co^{2+} concentration and the color of the solution changes from colorless to pale yellow, Figure 8 (d) (inset). Jing *et al*. (JING *et al.*, 2019) and Bano *et al*. (BANO *et al.*, 2019) suggest that this color changing is related to a complexation reaction, which can be confirmed through the displacement of the absorption band of CQDs after the addition of Co^{2+} ions.

In this work, this behavior was confirmed as the absorption band of N-CD-Ch shifted from 342 to 315 nm after addition of Co^{2+} ions. This suggests a change in the electronic structure of N-CD-Ch by the formation of the N-CD-Ch-Co complex (JING *et al.*, 2019), as displayed in Figure 10. The *LOD* of the colorimetric sensor was determined from the absorbance values at 315 nm, which were plotted as a function of the Co^{2+} concentration and a linear relationship was observed from 0 to 250 µmol L^{-1} (R^2 = 0.9970). The limit of detection (LOD) was calculated according to Equation 2, and the value found was 3.01 µmol L^{-1}. This value indicates a high sensibility of the sensing platform, since the LOD values of both methods (fluorescent and colorimetric sensor) are below the maximum Co^{2+} limit allowed by the World Health Organization (WHO) in drinking water (JAMES H. KIM, HERMAN J. GIBB, 2006). A comparison between data already reported in the literature with the results obtained in this work

can be seen in Table 1.

Fig. 9. The linear relationship between the normalized photoluminescence at 465 nm and Co^{2+} concentration. All average and standard deviation values were calculated based on triplicate experiments.

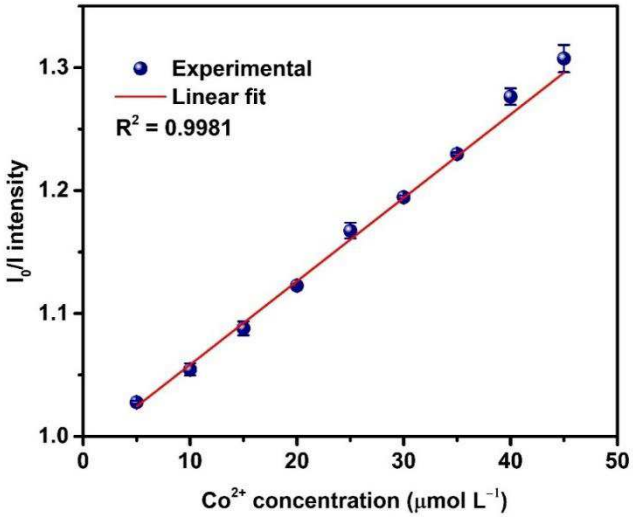

Source: (OLIVEIRA *et al*, 2023)

Fig. 10. Absorption spectra of N-CD-Ch (blue line) and N-CD-Ch with Co^{2+} ion (yellow line) in the concentration of 250 μmol L^{-1}.

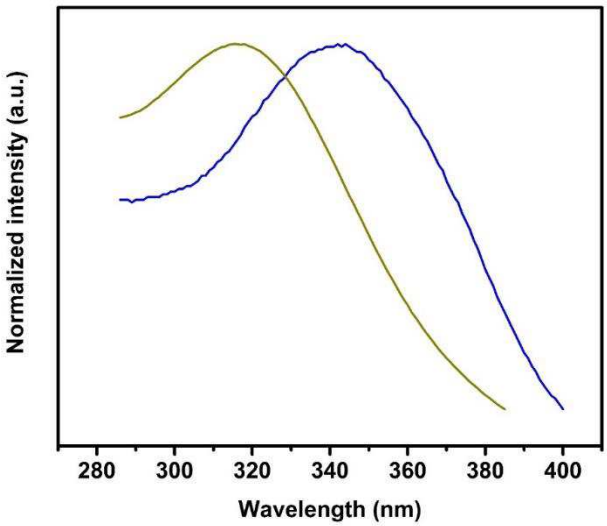

Source: (OLIVEIRA *et al*, 2023)

Table 1. Comparison of the proposed method with earlier reported literature for the detection of Co^{2+}.

Method	Probe	LOD (µmol L^{-1})	Linear range (µmol L^{-1})	Real sample	References
Absorbance	Coumarin skeleton (L)	7.09	0-90	Water (diferente sources)	(VASHISHT *et al.*, 2019)
Fluorescent	Nitrogen-carbon dots	0.25	1-60	Tap water	(JING *et al.*, 2019)
Fluorescent	Nitrogen-carbon dotsCarbon quantum dots	0.12	0.5-3	Vitamin-B12	(BANO *et al.*, 2019)
Fluorescent	Carbon dots	0.38	0-500	Tap water and river water	(HU *et al.*, 2020)
Fluorescent	Carbon quantum dots	0.00052	0.0005-2	Water samples, human urine and cells	(ZHAO, X. *et al.*, 2021)
Fluorescent	Polymer (PEI-MA)	0.27	0-200	-	(YANG, JIN *et al.*, 2022)
Fluorescent/Absorbance	Carbon quantum dots	0.98/3.01	0-50/0-250	Real blood plasma	**This work**

Source: (OLIVEIRA *et al*, 2023)

3.3.3 Thermodynamic and interaction mechanism

Titrations curves at 298.75, 308.15 and 318.15 K were performed to investigate the thermodynamics properties involved in the interaction Co^{2+} and sensing platform, as shown in Figure 11 (a)-(c). In all temperatures, at a fixed concentration of N-CD-Ch, the increase of the Co^{2+} concentration in the suspension results in the decrease of fluorescence intensity. However, this behavior is different for studied temperatures. Taking into account the Co^{2+} concentration of 200 µmol L^{-1}, it can be observed that at 298.75 and 308.15 K the I/I_0 intensity is close to 0.4, as can be seen in Figures 11 (a) and (b). This same point has an intensity close to 0.2 at 318.15 K, as shown in Figure 11c. This difference is clearly illustrated when the data are fitted to the Stern-Volmer equation, as displayed in Figure 11 (a)-(c) insets.

According to Table 2, it can be seen that the temperature is inversely proportional to the Stern-Volmer constant, and this behavior is characteristic of systems where the quenching mechanism is predominantly static (GHALI, 2010). Since K_{SV} is proportional to k_q, according to Equation 4, the increase in temperature infers the rate of the bimolecular reaction between N-CD-Ch and Co^{2+} ions, shifting the equilibrium towards the formation of the non-fluorescent complex N-CD-Ch-Co.

Fig. 11. Titration curves at **(a)** 298.75 K **(b)** 308.15 K and **(c)** 318.15 K. The inset shows the fit to Stern-Volmer Equation. All measurements were recorded at 465 nm of the emission spectrum. **(d)** Graph obtained from the Van't Hoff equation for determination of thermodynamic parameters. All average and standard deviation values were calculated based on triplicate experiments.

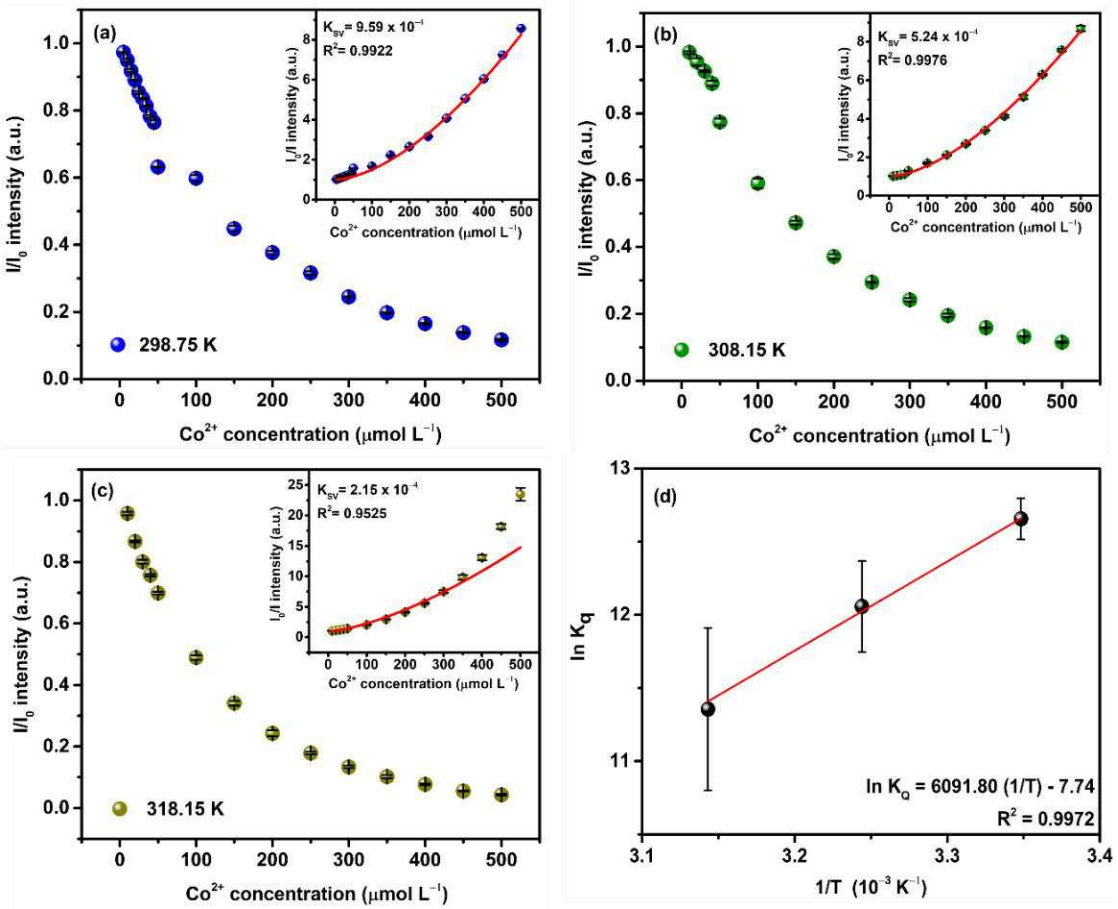

Source: (OLIVEIRA *et al*, 2023)

Figure 12 shows a schematic representation of the complexation mechanism between N-CD-Ch and Co^{2+} ions. Basically, the amine groups present on the surface of fluorescent nanoparticles act as multiple ligands, which coordinately bind to Co^{2+} metal ions, forming a non-fluorescent complex. Furthermore, the inner filter effect (IFE) is frequently observed in Co^{2+} sensing. IFE is generally an apparent quenching mechanism, since the absorber only filters the radiation emitted from a fluorophore species, causing a decrease in their fluorescence intensity (ZU *et al.*, 2017). The IFE mechanism can be confirmed by the superposition of the absorption spectrum of the absorber with the emission or excitation spectrum of the fluorophore (AL-HASHIMI; OMER; RAHMAN, 2020). In this work, the absorption spectrum of the Co^{2+} ion overlapped the N-CD-Ch emission spectrum, as can be

seen in Figure 13, suggesting the occurrence of the IFE mechanism.

Fig. 12. Schematic representation of the complexation mechanism between N-CD-Ch and Co^{2+} ions.

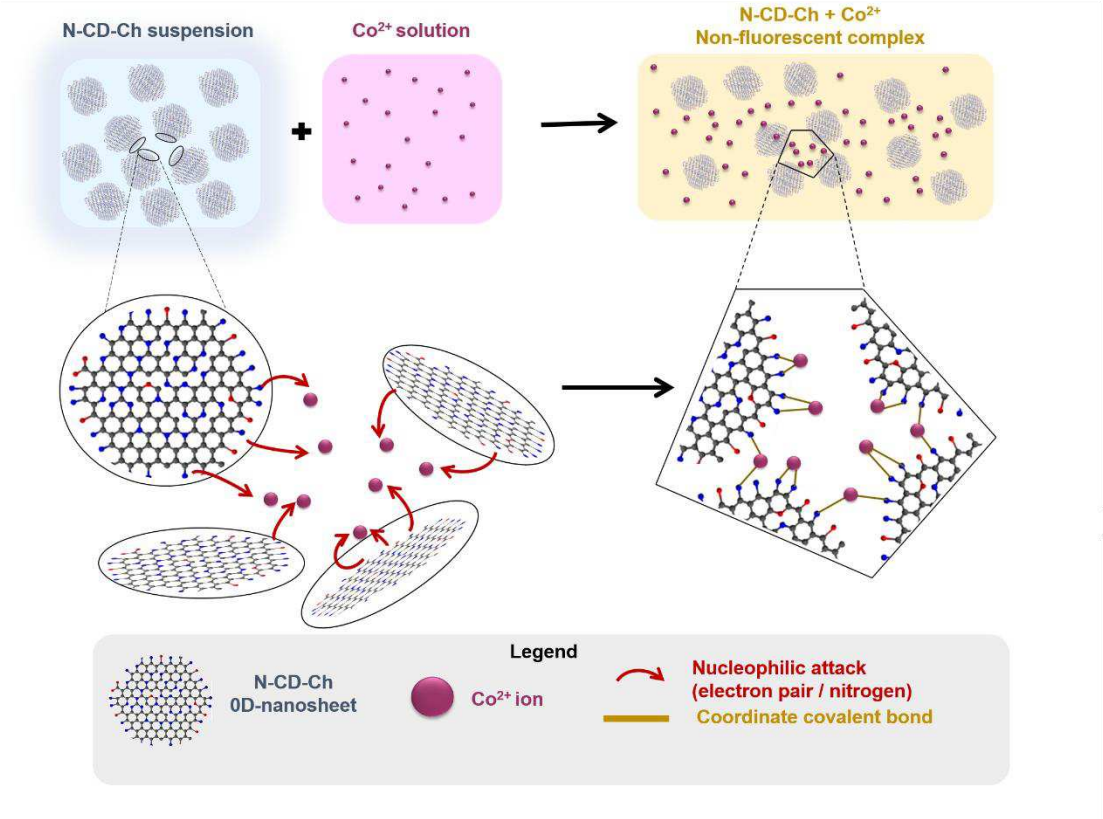

Source: (OLIVEIRA *et al*, 2023)

Fig. 13. Overlapping of absorbance of quencher (yellow dots) with excitation (red line) and emission spectra (blue line) of N-CD-Ch.

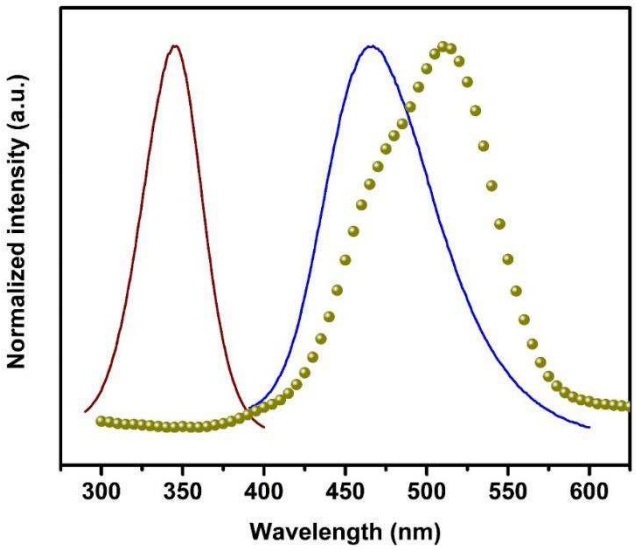

Source: (OLIVEIRA *et al*, 2023)

The fluorescence lifetime of N-CD-Ch was determined from FLIM measurements and found value of 2.93 ns was used in conjunction with Equation 4 to determine the k_q values at three different temperatures. Figure 11 (d) shows the Van't Hoff graph used to calculate the thermodynamics properties, following Equation 5. From the slope of the curve, as seen in Figure 11 (d), the ΔH value was determined, as well as the ΔS value from the curve intercept. The ΔG value was also estimated from Equation 6. The results are shown in Table 2. The negative value of ΔH ensures that the interaction of N-CD-Ch with Co^{2+} ions is an exothermic process, with the energy released by the system. Furthermore, the positive value of ΔS indicates a small increase in the total entropy of the system, related to the mixture of the fluorophore with the quencher. The negative value of ΔG for N-CD-Ch and Co^{2+} ions are complementary to ΔH and ΔS values, indicating that the interaction between N-CD-Ch and Co^{2+} ions occurs spontaneously. Thereby, in an exothermic process, a temperature increasing destabilizes the system, making the ΔG value more positive, as can be seen in Table 2.

Table 2. The Stern-Volmer constant, bimolecular rate constant and thermodynamic parameters as a function of the temperature.

Temperature (K)	K_{SV} **(10^{-4})**	K_q **(10^4)**	ΔG **(kJ mol^{-1})**	ΔH **(J mol^{-1})**	ΔS **(J mol^{-1} K^{-1})**
298.75	9.59 ± 1.25	32.7 ± 4.28	-31.5 ± 0.35		
308.15	5.24 ± 1.56	17.9 ± 5.33	-31.0 ± 0.79	-732 ± 38.8	0.93 ± 0.13
318.15	2.15 ± 1.62	7.34 ± 5.54	-29.6 ± 1.47		

Source: (OLIVEIRA *et al*, 2023)

3.3.4 Co^{2+} sensing in real samples and interferents investigation

After further evaluation through the mechanism of interaction between Co^{2+} ions and N-CD-Ch, it was proposed a Co^{2+} sensing of a real blood plasma sample according to the methodology reported by Maynar *et al* (MAYNAR, MARCOS *et al.*, 2018). Due to the presence of interfering organic materials, the sample was diluted 10^7-fold, and then doped with different concentrations of Co^{2+}, which ranged from 0 to 250 µmol L^{-1} (Figure 14). The I/I_0 ratio was plotted as a function of Co^{2+} ions concentration and, as expected, the fluorescence emission was

inversely proportional to the Co^{2+} concentration, as shown in Figure 15 (a). Based on this behavior, a linear fit was plotted over the range of 100 to 250 µmol L^{-1} (R^2 = 0.9799) for the plot of I_0/I versus Co^{2+} concentration, as shown in Figure 16. A blind test was used to determine recovery using as reference the concentrations of 100 and 200 µmol L^{-1} of Co^{2+} in the real sample. The recovery obtained was 100.92% for the concentration of 100 µmol L^{-1} and 92.23% for 200 µmol L^{-1} with relative standard deviation (RSD) values of 0.90% and 0.42%, respectively. These results are in agreement with other works reported in the literature (BANO *et al.*, 2019; JING *et al.*, 2019), and are indicative of the applicability of this nanoprobe in the detection of Co^{2+} in blood plasma.

Fig. 14. (a) Real blood plasma sample; **(b)** decomposition of the organic matrix at 88 °C with the addition of HNO_3 and H_2O_2; **(c)** treated and diluted real sample; **(d)** addition of different concentration of Co^{2+} ions to the real sample.

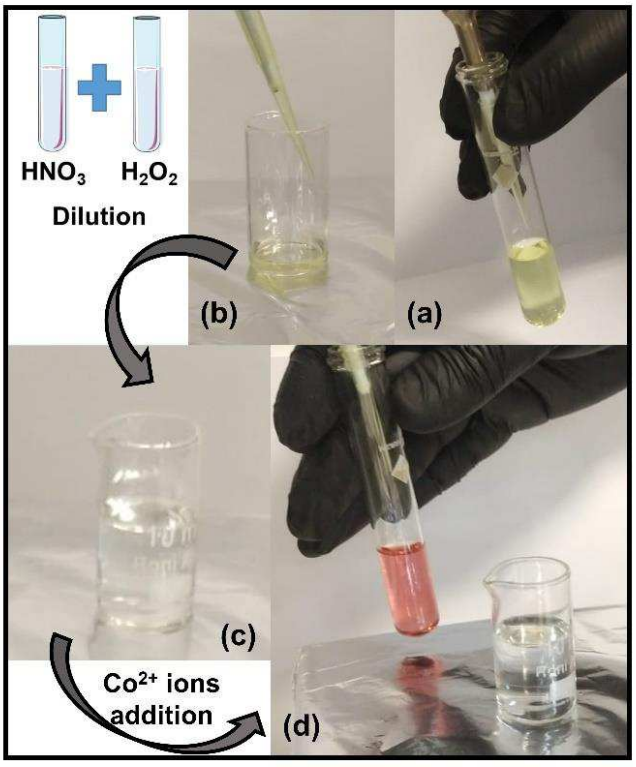

Source: (OLIVEIRA *et al*, 2023)

Fig. 15. (a) Titration curve of Co^{2+} in the real sample of human blood in PBS buffer pH 7.4. **(b)** Fluorescence response of the N-CD-Ch aqueous solution in the presence of different ions with Co^{2+} (brown bars) and without Co^{2+} (blue bars). **(c)** Canonical score plot obtained from the LDA after PCA of real sample titration. **(d)** Canonical score plot obtained from the LDA after PCA of different ions with Co^{2+}. **(e)** Color comparison of N-CD-Ch solution after addition of different ions at 250 µmol L^{-1}. Average and standard deviation values of (a) and (b) were calculated based on three replicates, while (c) and (d) classifications were obtained based on six replicates and 95% confidence level.

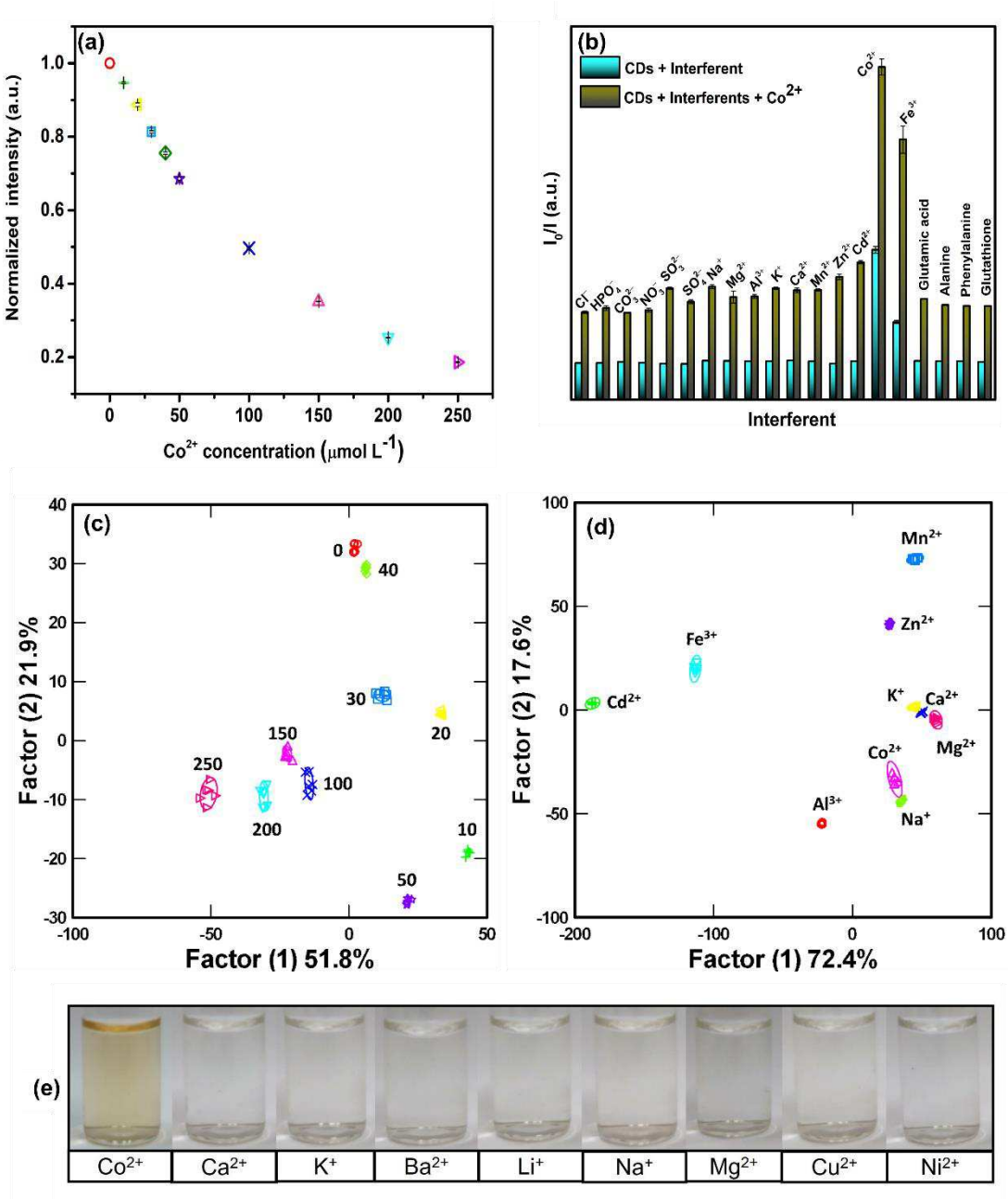

Source: (OLIVEIRA *et al*, 2023)

Fig. 16. The linear relationship between fluorescence at 465 nm and Co^{2+} concentration present in the real sample. All average and standard deviation values were calculated based on triplicate experiments.

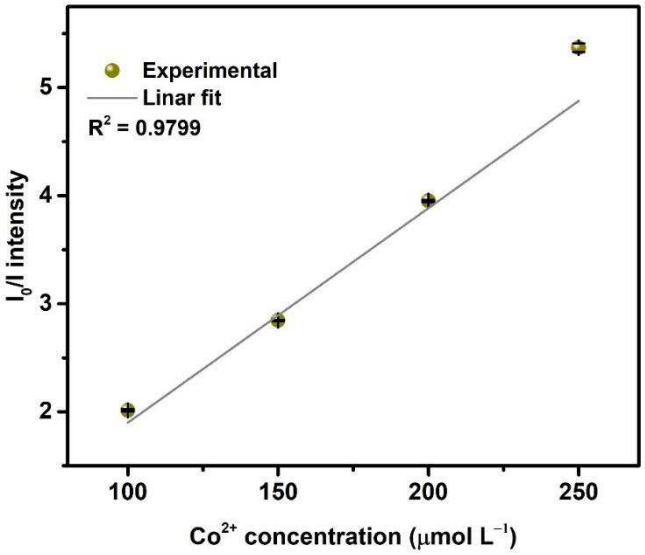

Source: (OLIVEIRA *et al*, 2023)

Indeed, the success in the detection of Co^{2+} ions is dependent on a selective platform. Therefore, different interferents were also investigated as possible fluorescence quenchers in the absence (blue bars) and presence of Co^{2+} ions (brown bars), as shown in Figure 15 (b). Different interferents in the concentration of 250 μmol L^{-1} were added to the CDs dispersion and it was possible to observe that Co^{2+} and Fe^{3+} ions are excellent fluorescence quenchers of N-CD-Ch. However, Co^{2+} ions have greater quenching power than Fe^{3+} ions, as shown in Figure 15 (b). This specificity is probably due to a non-fluorescent complex formed between Co^{2+} and N-CD-Ch, since the change of color is observed only in the presence of Co^{2+} ions in the dispersion, as shown in Figure 15 (e).

To obtain different ways to quantify the Co^{2+} ion, multivariate analyses were used to detect Co^{2+} ions in a real blood plasma sample. More specifically, the PCA chemometric tool was used to reduce the size of the large amount of data generated from the I/I_0 ratio of 6 replicates of 10 different concentrations, considering the entire fluorescence spectrum. The PCA tool has grouped the data and generated a new dataset, called principal components (PCs), which consist of a robust and reduced representation of the original dataset. The LDA is used to model the differentiation of fluorescence response and classify patterns formed in the PCs. Its classification is based on Mahalanobis distance, where the higher the distance between the groups, the smaller the data overlap (LE *et al.*, 2017).

Figure 15 (c) displays the success in detecting different concentration values of Co^{2+} in a real blood plasma sample, using a 95% confidence limit. This graph was plotted based only on two canonical factors (51.8 and 21.9%), generated from the LDA of the PCs. These canonical factors together have 73.7% of the variance of all data, making it feasible to use the two-dimensional graph. Finally, it was observed that the multivariate analysis method was also able to discriminate the interferents, as illustrated in Figure 15 (d). Clearly, the Na^{+}, Mg^{2+}, Al^{3+}, K^{+}, Ca^{2+}, Mn^{2+} e Cd^{2+} ions have a response signal very close to each other (blue bars in Figure 15 (b)), making it difficult to differentiate these ions *via* fluorescent method. Similar behavior was observed for Mg^{2+} and Al^{3+}, and Ca^{2+} and Mn^{2+} ion pairs (brown bars in Figure 15 (b)), which showed very close fluorescent responses in the presence of the Co^{2+} ion. However, by aid of PCA and further using the LDA, it was possible to successfully differentiate each ion, as shown in Figures 15 (d). These results indicate that, in addition to detecting Co^{2+} using different methods, the sensing platform developed in this work is presented as a potential to detect several ions and can be used in future sensing strategies.

3.4 Conclusions

In this work, we have presented a Co^{2+} ion multi-sensing platform based on carbon quantum dots. The spectroscopic and structural characterizations allowed a better understanding of the interaction of N-CD-Ch with Co^{2+} ions. A fluorescent nanoprobe was successfully developed for the selective and sensitive detection of the analyte, based on the static quenching mechanism and IFE. The supposed formation of a yellowish complex formed from the interaction of N-CD-Ch with Co^{2+} ions is supported by spectroscopic characterizations that suggest a change in the electronic structure of the N-CD-Ch after the addition of Co^{2+} in solution. The yellowish complex was used as a response signal for the development of an optimal sensitivity colorimetric Co^{2+} sensor. The sensing platform has become multifaceted with the use of PCA and LDA chemometric algorithms, which were able to distinguish the analyte from other interfering ions. Finally, the sensing platform proved to be robust and efficient, concerning Co^{2+} ions sensing, and also capable of quantifying Co^{2+} in a real blood plasma sample. Thus, we expected that the nanoprobe based on N-CD-Ch could be used in the sensitive and selective quantification of Co^{2+} ions, especially contributing to WADA establishing a standard method for detection of Co^{2+} ions in blood samples from athletes.

CHAPTER IV

4 CARBON QUANTUM DOTS WITH ULTRA-HIGH QUANTUM YIELD FOR VERSATILE TURN-ON SENSOR OF GLUTEN AND CYANIDE IONS

Abstract

In this work, we reported the synthesis of carbon quantum dots (CQDs) with high fluorescent quantum yield (90.7%). These nanoparticles were applied in a turn-off/turn-on sensor able to detect cyanide ions. In this sensing strategy, Fe^{3+} ions were added to the aqueous suspension of CQDs to quench the fluorescence of the system, which was recovered from the presence of cyanide ions. Furthermore, a sensor array was developed using the LDA chemometric tool, to classify different species present in cookie formulations, including gluten. The turn-off/turn-on sensor proved to be sensitive and effective for detecting cyanide ions, with a detection limit of 3.77 ppm. This high sensibility and selectivity allowed quantifying the analyte in a real sample of tap water.

Keywords: Carbon Quantum Dots; Quantum yield; Cyanide; Fluorescent sensing.

4.1 Introduction

Carbon Quantum Dots (CQDs) are small carbon nanoparticles containing different functional groups on the surface, with high stable chemical and which are excellent candidates for fluorescent nanoprobes (BENLI *et al.*, 2023; DAS; SANKAR MONDAL; PAUL, 2023; JOHN *et al.*, 2023). In addition to these properties, these nanoparticles exhibit high biocompatibility, low cytotoxicity, good water solubility, and high productivity at a low cost (PALACIO-VERGARA *et al.*, 2023; ZOGHI *et al.*, 2023). However, CQDs generally have a low quantum yield (QY), when compared to inorganic quantum dots, which limits their practical applications (KANSAY *et al.*, 2023). To increase the QY, doping with heteroatoms (boron, nitrogen, sulfur and phosphorus) and surface functionalization are strategies identified as effective to enable different applications (ANTHONY; PANDURANGAN; ABBAS, 2023; LIN, L. *et al.*, 2022; PADMAPRIYA *et al.*, 2023). For example, Tan *et al* synthesized CQDs with QY as high as 92.1% by one-step hydrothermal treatment of citric acid and o-phenylenediamine (TAN; YANG; WAN, 2021). The authors observed that the functionalization of the nanoparticles facilitates their application in the field of sensors, especially in the development of fluorescent probes.

In this regard, CQDs have been extensively applied for sensing of biomolecules (ABDULKHALEQ *et al.*, 2023; THULASINATHAN *et al.*, 2023), metal ions (ALI *et al.*, 2023; LIN, S. *et al.*, 2023), anions such as nitrite (YANG, Y. *et al.*, 2023) and cyanide (CN^-) (DONG *et al.*, 2013) and even gluten (KARAMDOUST; MILANI-HOSSEINI; FARIDBOD, 2023). One of the possibilities of sensing these species is from changes in the intensity of the fluorescence spectra of the CQDs. In this perspective, a turn-off/turn-on sensor can be developed from the quenching of the fluorescence intensity of the CQDs, with a posterior enhancing (EL-MALLA *et al.*, 2022). On the other hand, a second alternative is to apply the optical signals from fluorescence spectra in a sensor array, providing a versatile method to discriminate multi-target solutions, in complex matrix such as food (CRUZ *et al.*, 2021). Moreover, in order to maximize the discrimination, chemometrics tools, such as linear discriminant analysis (LDA) may be applied for construction of fingerprints or patterns (DAI *et al.*, 2021). Our group has in recent years developed sensing platforms employing CQDs to identify classes of substances such as metal ions (OLIVEIRA *et al.*, 2023), pesticides (CARNEIRO *et al.*, 2019) and food additives (CARNEIRO *et al.*, 2021). Given this concern with the food safety, we advanced our methodology developed in previous works for explore the full potential of CQDs as alternative way of CN^- anions detection.

CN^- is one of the most toxic ions that can be found in food. It can complex with the ferric ions present in the cytochrome oxidase enzyme, leading to hypoxia in the body, which can be fatal to the consumer who ingests food or water contaminated with this species (DONG *et al.*, 2013). CN^- ion could be lethal for human in concentrations as low as 1.5 mg kg^{-1} of body weight. Therefore, according with World Health Organization, the amount maximum acceptable in drinking water must not exceed the concentration of 1.9 μmol L^{-1}, whereas the US environmental protection agency sets a limit of 7.8 μmol L^{-1} (PUNDI *et al.*, 2021; YILMAZ *et al.*, 2022). In addition, some food such as cassava naturally contain cyanogenic glycosides and can also release toxic cyanide ion when they are manufactured (ZHONG *et al.*, 2021). Traditional methods, including chromatography (MADMON *et al.*, 2021) and electrochemical techniques (VIRBICKAS *et al.*, 2021), have been used for detecting CN^-. However, in the last years, selectivity/sensitivity, portability, ease of use, and detection without using expensive instruments are advantages sought in analytical methods aimed at sensing species found in food. CQDs with ultra-high QY have such characteristics and their use as optical sensors provide a viable alternative to quantify CN^- in industrial scale.

Given the exposed, our present study reports a synthesis of CQDs from citric acid and ethylenediamine that resulted in nanoparticles with a QY of 90.7% and therefore were labeled as CD-90. This nanomaterial was purified and structurally characterized to further investigate its interaction with CN^- ions. Our proposal consisted in the development of a turn-off/turn-on sensing platform based on quenching fluorescence of CQDs by Fe^{3+} ions and subsequent enhancing with CN^- ions. Despite the high selectivity of the sensor to Fe^{3+} ions, we proposed in a parallel experiment the development of a platform to detect possible molecules present in excess in cookie formulations. Thus, the LDA algorithm discriminated the proposed analytes (folic acid, Fe^{3+}, glucose, gluten and sodium bicarbonate) in the real sample with 100% accuracy. It is important to point out that such substances can occasionally be used in formulations in abusive amounts, causing damage to the consumer's health, justifying the relevance of their detection.

4.2 Experimental section

4.2.1 Material and reagents

Hydrochloric acid (HCl, 36.5-38.0%) was purchased from Synth. Sodium hydroxide (NaOH, 98.0%) was purchased from Dinamica. Quinine sulfate

($(C_{20}H_{24}N_2O_2)_2{\cdot}H_2SO_4{\cdot}2H_2O$, 99.0-101.0%), sulfuric acid (H_2SO_4, 95.5%) sodium sulfate anhydrous (Na_2SO_4, 99.0-101.0%), anhydrous glucose ($C_6H_{12}O_6$, 99.5%), citric acid ($C_6H_8O_7$, 99.5%), ethylenediamine ($C_2H_4(NH_2)_2$, 98%), iron (III) chloride ($FeCl_3.6H_2O$, 98%), sodium bicarbonate ($NaHCO_3$, 99.5%), folic acid ($C_{19}H_{19}N_7O_6$, 98%) were purchased from Vetec. Potassium cyanide (KCN, 97.0%) was purchased from Merck. Gluten was purchased commercially from the manufacturer C2 Alimentos ®. All chemicals were of analytical reagent grade without previous treatment and purchased in Brazil. Distilled water (0.087 MΩ cm) was used during the experiments. A cellulose membrane Spectra/Por®6 dialysis membrane of 1 kDa MWCO was used for dialysis.

4.2.2 Synthesis of CQDs

First, 1.0 g of citric acid was solubilized in 4.0 mL of distilled water. Then, 1.0 mL of ethylenediamine and other 5.0 mL of distilled water were added, totaling 10 mL of solution. This mixture was transferred to a 50 mL Teflon-lined autoclave and heated up to 200 °C for 3 h, according to conventional hydrothermal method (KOU *et al.*, 2023; ZHANG, JIANBIN *et al.*, 2022). After coolling to room temperature (25 ± 2 °C), the autoclave was opened and the colloidal suspension was purified by dialysis at room temperature in two cycles (12 h/cycle). Finally, a suspension 1.09 mg g^{-1} was freeze-dryed for structural characterizations. The remaining CQDs solutions were stored at 4 °C for further sensing experiments.

4.2.3 Instrumentation and characterization of CQDs

The absorption spectra were recorded in the spectrophotometer UV-Vis Shimadzu UV-2600. The fluorescence spectra were obtained in the Shimadzu RF-6000 spectrofluorophotometer. The Fourier transform infrared (FTIR) spectrum was recorded by using a scanning range of 400 to 4000 cm^{-1}. The Raman spectrum was recorded in a range of 500 to 2500 cm^{-1}, using a Horiba Raman spectrometer. The spectral excitation was performed using a laser line of 785 nm, with adjustable filters and adequate powers of 10.7 and 151 μW with 10 accumulations of 50 s.

X-ray photoelectron spectroscopy (XPS) was performed using a ThermoFisher Scientific model K-alpha+, using monochrome radiation from Al-kα with pass energy of 200 eV and 50 eV for the survey and high-resolution scanning spectra, respectively. The spot size was 400 μm. The pressure in the analysis chamber was approximately 10^{-7} Pa. Peak fitting was

done using the program provided by the equipment manufacturer (Avantage), with mixed Gaussian/Lorentzian curves and background subtraction using the Smart algorithm.

Atomic force microscopy (AFM) images were obtained using an Asphalt Research microscope of MFP-3D AFM type. Laser Scanning Confocal Microscopy (LSCM) was performed to obtain the confocal images. A confocal microscope (Zeiss - LSM 780) coupled to an Axio Examiner.Z1 (Carls Zeiss) with 20x objective (EC Plan-Neofluar – NA 0.5) and internal Zeiss detector was used. To investigate the fluorescence life-time decay, a Fluorescence Life-Time Imaging Microscopy (FLIM) was applied. The analysis was carried out in a dried film mounted with an air immersion objective and a rate of 10^4-10^5 counts/s. To acquire life-time decay, we used a Becker and Hickl set with a resolution of 200 ps. A pulsed 405 nm laser was used with 80MHz repetition rate.

4.2.4 Sensing experiments

Initially, the main parameters that affect the emission intensity of CQDs were analyzed, in order to optimize the experimental conditions. Thus, fluorescence intensity was investigated as a function of CD-90 concentration (0.010 - 50 μg mL^{-1}) and pH (3.2 - 9.5). Posteriorly, the effect of the fluorescence signal was tested in the presence of species present in cookie formulations, in order to evaluate the selectivity of the sensing strategy. In view of these results, it was possible to develop a sensor array based on chemometric tools. Basically, folic acid, Fe^{3+} ions, gluten, glucose and $NaHCO_3$ at a concentration of 25 ppm were added to the dispersion of CQDs (1.0 μg mL^{-1}). The data were normalized and used to construct a data matrix, which was processed in a supervised pattern recognition method. Thus, an array sensor was developed using Linear Discriminant Analysis (LDA), making it possible to recognize the different investigated species.

Furthermore, a turn-off/turn-on cyanide ion sensing strategy was also developed. Briefly, CD-90 (1.0 μg mL^{-1}) and Fe^{3+} ions (25 ppm) were transferred to a quartz cuvette and aliquots of KCN stock solution (concentrations from 7.6 to 76 ppm) were added. The emission spectra were recorded after 2.0 min of incubation at 350 nm excitation and the PL intensity at 440 nm was used for CN^- quantification. Measurements were performed in triplicate. Posteriorly, a calibration curve was constructed by CN^- titration and the detection limit of the sensing strategy could be determined using equation 2. Finally, tests with real samples were carried out with tap water and then, different concentrations of KCN solutions were spiked for

the recovery tests.

4.3 Results and discussion

4.3.1 Characterization of CD-90

Initially, the morphology of CD-90 was analyzed by Atomic Force Microscopy (AFM) operating in a tapping mode configuration. Clearly, nanoparticles with quasi-spherical morphology can be observed in the AFM topography image in Figure 17 (a). In the topographical height profile (inset), the scanning in the line red region identified particles sizes around 1.5-2.0 nm, which it is similar to other studies with N-doped CQDs precursor (BU *et al.*, 2019; DEY *et al.*, 2014; WANG, HAO *et al.*, 2016).

Fig. 17. AFM results of CD-90: **(a)** topography image and AFM section height profile of the particles (inset); **(b)** phase image. The AFM scanning was performed over a 4 µm x 4 µm region.

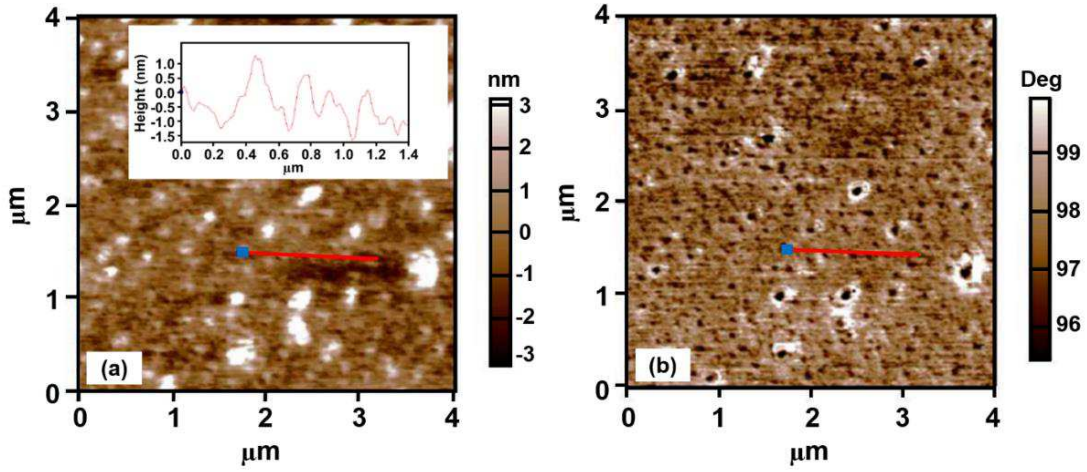

Source: Author.

In addition, a core-shell nanostructure was identified through the AFM phase image presented in Figure 17 (b). To complement the information about the morphology and fluorescent properties of the nanomaterial obtained, LSCM images were recorded and are displays in Figure 18. It is possible to observe fluorescence in the blue, green and red, regions when the CD-90 was excited at 405, 488 and 561 nm, as shown in Figure 18 (a), 18 (b) and 18 (c), respectively. The merge of the recorded images was applied as shown in Figure 18 (d). The scale of the confocal images is visualized in 30 µm, so the aggregates of CD-90 are evidenced. Clearly, the existence of spherical aggregates is confirmed by this technique in good agreement

with AFM results.

Fig. 18. Confocal microscopy analysis of CD-90 dried film with emission at: **(a)** 405nm; **(b)** 488nm; **(c)** 561 nm and **(d)** the merge of the channels.

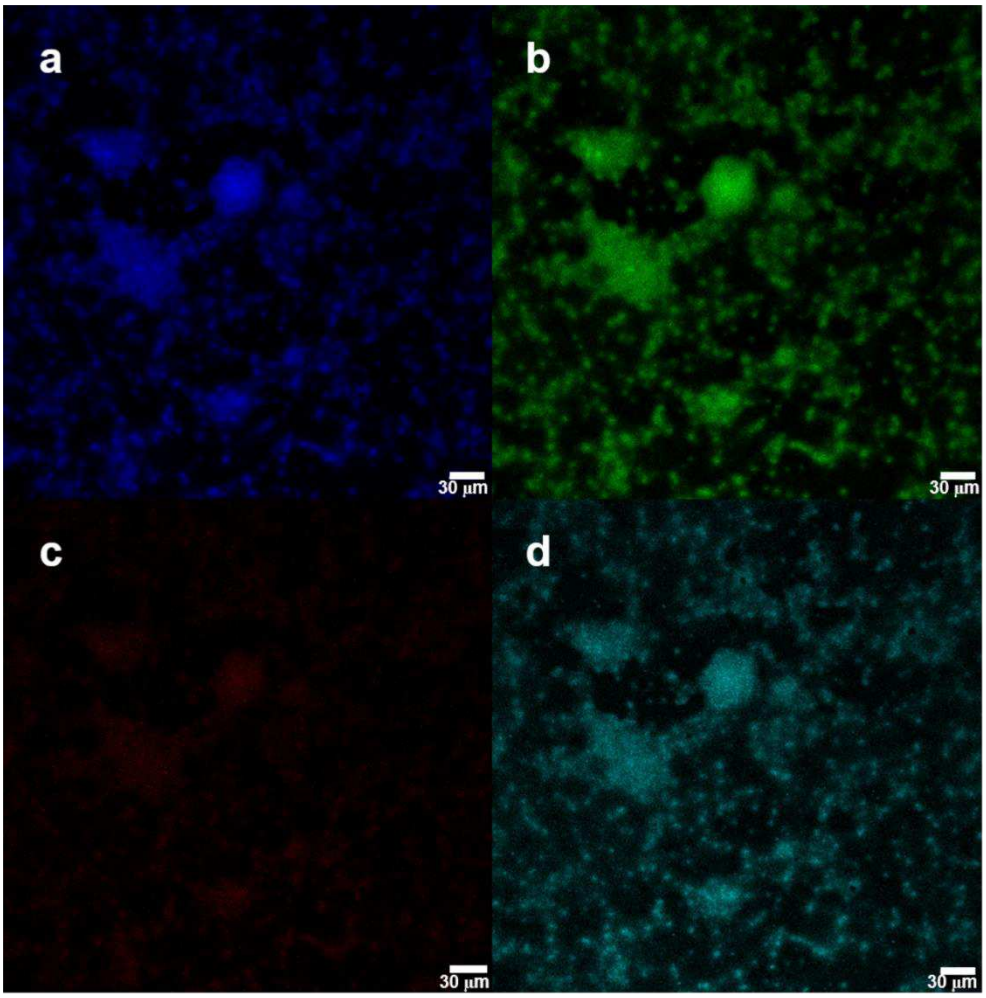

Source: Author.

Information regarding the functional groups present in CD-90 sample was obtained by FTIR. The spectrum is presented in Figure 19, which shows bands in the region between 3400 and 2800 cm^{-1} corresponding to stretching vibration of –O–H (hydroxyl) or –N–H (amine), contributing to the hydrophilic nature of nanoparticles (FU; GAO; ZHI, 2019). The band located at 1564 cm^{-1} also can be attributed to the angular deformation of –N–H, while bands at 1657 and 1485 cm^{-1} are related to stretching vibration of –C=O and –C–N, respectively (ZHAO, L. *et al.*, 2019). Further, the band located at 1392 cm^{-1} is related to the –C=C stretching existing in the core of the nanoparticles (KURDEKAR *et al.*, 2016). The presence of –C–H bonds from aromatic rings is confirmed by the bands ranging from 800 to 600 cm^{-1} (DA COSTA *et al.*,

2018). Additionally, the spectra of the physical mixture of precursors were also analyzed and clearly, it was observed differences between these spectra and CD-90 spectrum. The appearance of the bands at 1657 and 1485 cm^{-1} in the spectrum of the CD-90 sample shows that the chemical reaction was performed and new chemical bonds –C=O and –C–N appeared in the structure of the nanoparticles.

Fig. 19. FTIR spectra of CD-90 and their precursors (mix of citric acid and ethylenediamine).

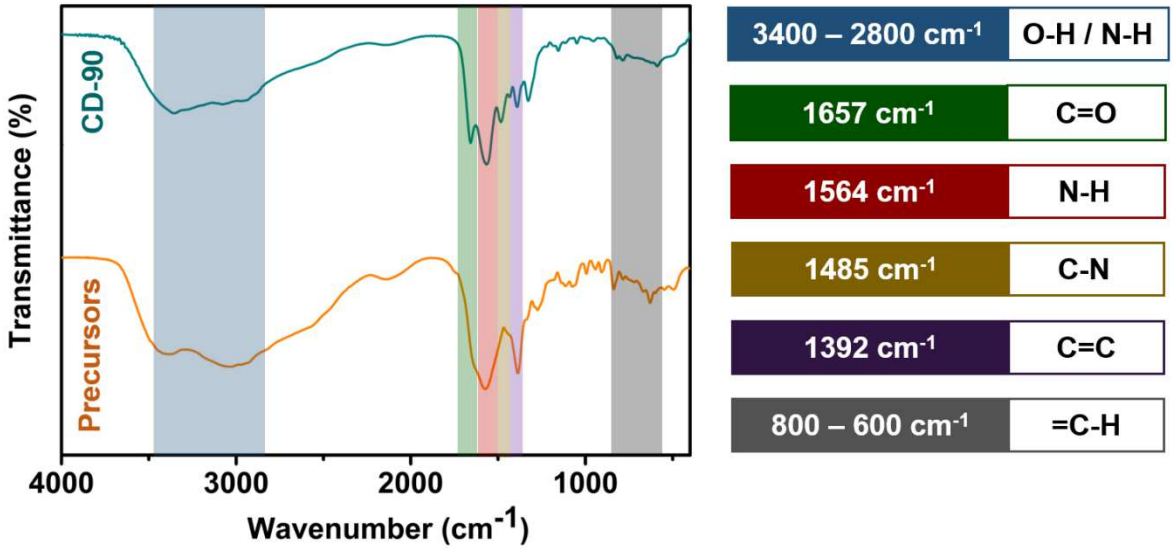

Source: Author.

XPS measurements allowed to analyze the composition and structure of the CD-90. Figure 20 (a) presents the full survey spectrum, which revealed three apparent binding peaks at 284.7, 398.0 and 529.8 eV, corresponding to the signals originated from C1s, N1s and O1s, respectively. The calculated atomic percentage of C, N and O are 66.45, 14.56 and 18.99%, respectively. As shown in Figure 20 (b), the deconvolution spectrum of C1s revealed six peaks at 283.4, 283.9, 284.7, 286.2, 288.0 and 289.8 eV, corresponding to the C-H, C-N-C, C=C/C-C, C=N, C=O, O=C-OH groups, respectively (DENG, Y. *et al.*, 2013; GE *et al.*, 2017; GONG *et al.*, 2015; STEFANAKIS *et al.*, 2014; YANG, F.; ZHOU; DUAN, 2021). The signal at 291.4 eV is related the π-π* transition on carbon lattices with sp^2 hybridization (PERMATASARI *et al.*, 2016). Moreover, the high-resolution XPS spectrum of N1s (Figure 20 (c)) also exhibited four prominent peaks at 398.6, 400.3, 402.7 and 404.4 eV, revealing the presence of the pyridinic (N-H), pyrrolic (N=C), graphitic (C_3-N) and oxidized pyridine nitrogen, respectively (DEHVARI *et al.*, 2019; PARK, Y. R. *et al.*, 2017; YANG, F.; ZHOU; DUAN, 2021; YU *et al.*, 2016; ZOU *et al.*, 2022). The inset in Figure 20 (c) illustrates the expected distribution of the different types of nitrogen present in some portions of the CD-90 layers. The broad high-

resolution XPS spectrum of O1s, as seen in Figure 20 (d), is split into three peaks centered at 527.2, 531.0 and 533.6 eV, corresponding to adsorbed oxygen, O-H and C=O bonds, respectively (DAGER *et al.*, 2019; ZOU *et al.*, 2022).

Fig. 20. (a) XPS survey; high-resolution spectra: **(b)** C1s; **(c)** N1s and description of N rings present in carbon lattice (inset); **(d)** O1s.

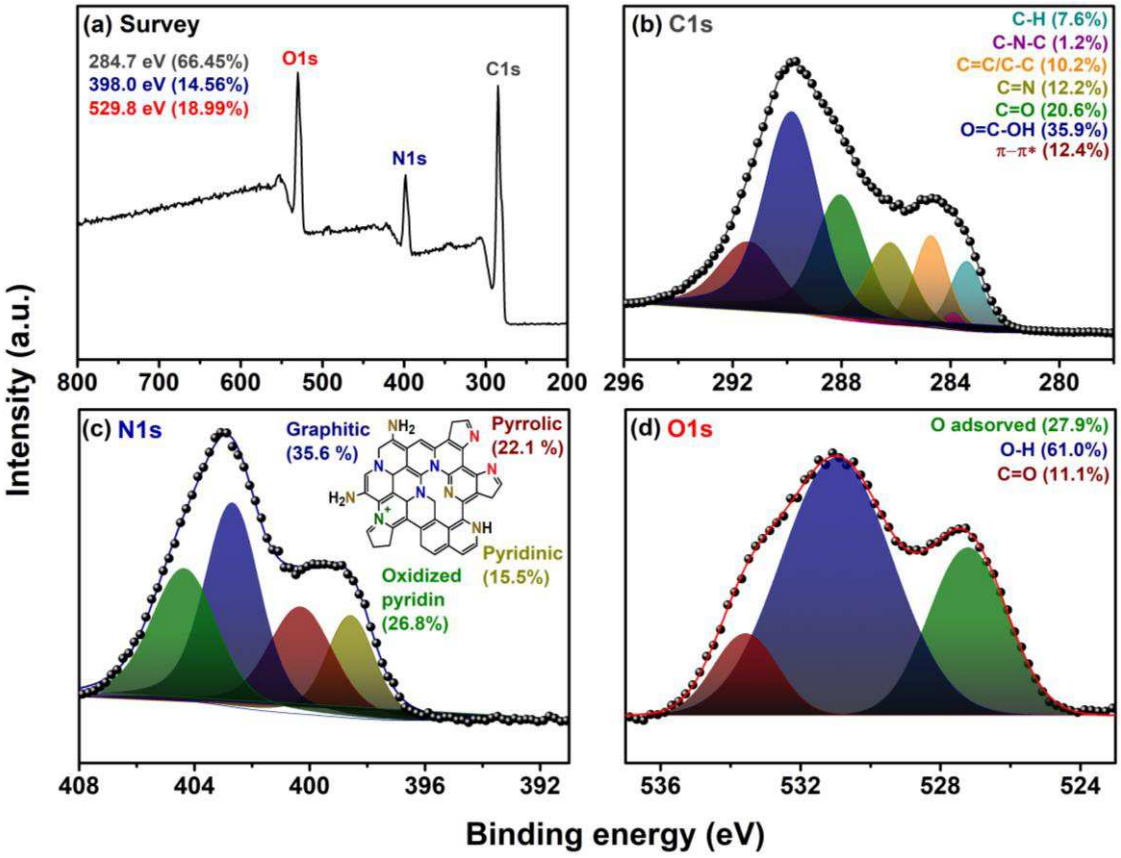

Source: Author.

The optical properties of the CD-90 were investigated through UV-visible absorption and photoluminescence spectroscopy. Figure 21 (a) shows the UV-Vis, excitation and emission spectra of the synthesized sample. A characteristic band in UV-Vis spectrum is observed near 239 nm, related to the π- π* transition, whereas the band at 347 nm is attributed to the n- π* transitions (WU, P. *et al.*, 2017). The first signal is related to the transitions π - π* corresponding to sp^2-type carbon bonds (VAZ *et al.*, 2017) and the other band is associated with n - π* transition of –C=O, C–N, or –C–OH bonds which may be related to carboxyl (–COOH) or amine ($–NH_2$) groups on the surface of nanoparticles, respectively (TADESSE *et al.*, 2018). The excitation spectrum obtained by monitoring the blue emission at 440 nm is consistent with the absorption spectrum. Furthermore, under 350 nm excitation, the CD-90 presents an

emission at 440 nm.

Fig. 21. Results of spectroscopic characterizations: **(a)** UV-Vis, excitation and emission spectra of CD-90; **(b)** Photoluminescence spectra with different excitation wavelengths (300 to 400 nm) of CD-90. Inset: CD-90 under UV lamp.

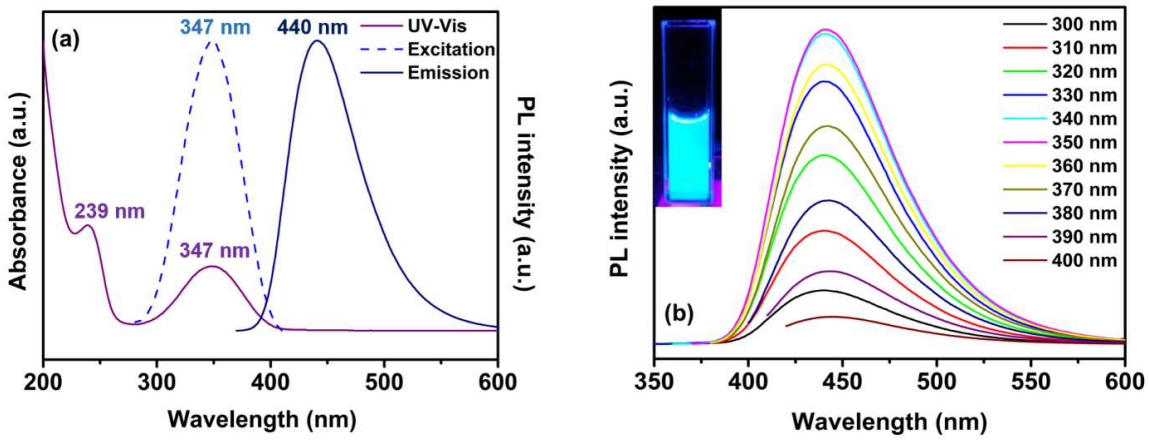

Source: Author.

To deeper explore the optical properties of the as-prepared CQDs, we carried out a detailed PL study by changing excitation wavelengths ranging from 300 to 400 nm. CD-90 showed an independent excitation behavior, as seen in Figure 21 (b), with maximum excitation wavelength at 350 nm. According to earlier research (DUAN *et al.*, 2023; LIAO, X. *et al.*, 2023; SHARMA; CHOWDHURY, 2023), this excitation-independent property is explained by a narrow size distribution of the particles and a less number of defects on their surface (MONDAL; GHORAI; SAHA, 2018). Thereby, in order to optimize the sensing experiments, it was observed that at 350 nm the highest emission intensity was achieved, which it was chosen as the excitation wavelength for all further experiments. Moreover, in agreement with the emission spectra, this sample has a high blue fluorescence under a 365 nm UV lamp irradiation (Figure 21 (b), inset). The QY value obtained for CD-90 was surprisingly high (90.7%), allowing this sample to be identified as having an ultra-high QY, as well as the CQDs obtained by Jangi and Akhond (HORMOZI JANGI; AKHOND, 2021). This excellent result allowed a wide range of applications for the CD-90 and under optimized conditions, a new sensing platform was developed.

4.3.2 Optimization of experimental conditions for sensing of CN^-

Before developing a sensing platform, the conditions under which CD-90 has the best fluorescent responses were investigated. Figure 22 (a) shows the effect of concentration on CD-90 photoluminescence. It is possible to observe that the maximum emission was obtained at 440 nm, considering the concentration range studied. Furthermore, the increase in concentration intensified the emission of CD-90 at 440 nm, which increased linearly, as shown in Figure 22 (b). Based on these results, the concentration of 1.0 μg mL^{-1} was selected for the other experiments, since it presents a emission intensity as high as 14850 a.u. The ultra-high QY of CD-90 ensures this high emission intensity at low concentrations and allows these nanoparticles to be used as excellent nanoprobes.

Another parameter investigated was the pH. According to Figure 22 (c) under strongly acidic conditions, the emission intensity of CD-90 is unfavorable and this can be attributed to the protonation of its surface groups (ZHAO, S. *et al.*, 2022). In fact, in an acidic environment, nanoparticles tend to aggregate and the phenomenon of self-quenching of fluorescence must occur (OLIVEIRA *et al.*, 2023). Therefore, the detection system developed in this work was carried out under neutral pH.

Finally, with the experimental conditions optimized, the fluorescence intensity of CD-90 in the presence of species commonly used in the formulation of cookies was investigated. The results obtained can be seen in Figure 22 (d), which indicates the strong fluorescence quenching caused by Fe^{3+} ions. This result is in line with what the literature predicts (CHANG *et al.*, 2021; WANG, B. *et al.*, 2022). According to Xu *et al* the Fe^{3+} ions quench the emission of CDs through a mechanism called inner filter effect (IFE), which occurs when the absorption spectrum of the quencher overlaps with the excitation or emission spectrum of the fluorophore (XU *et al.*, 2023). In this work, this effect was confirmed and can be seen in Figure 23. However, the quenching caused by Fe^{3+} ions is not the main focus of this work, but this will be used as a probe for the construction of a turn-off/turn-on CN^- ions sensor, which will be presented later.

Fig. 22. Fluorescence-response evaluation of CD-90 at different experimental conditions: (a) concentration effect of CD-90 on fluorescence; **(b)** PL intensity as a function of concentration; **(c)** effect of pH in the CD-90 fluorescence intensity; **(d)** fluorescence intensity in the presence of species presents in cookies formulations at concentration of 25 ppm. All average and standard deviation values were calculated based on triplicate experiments.

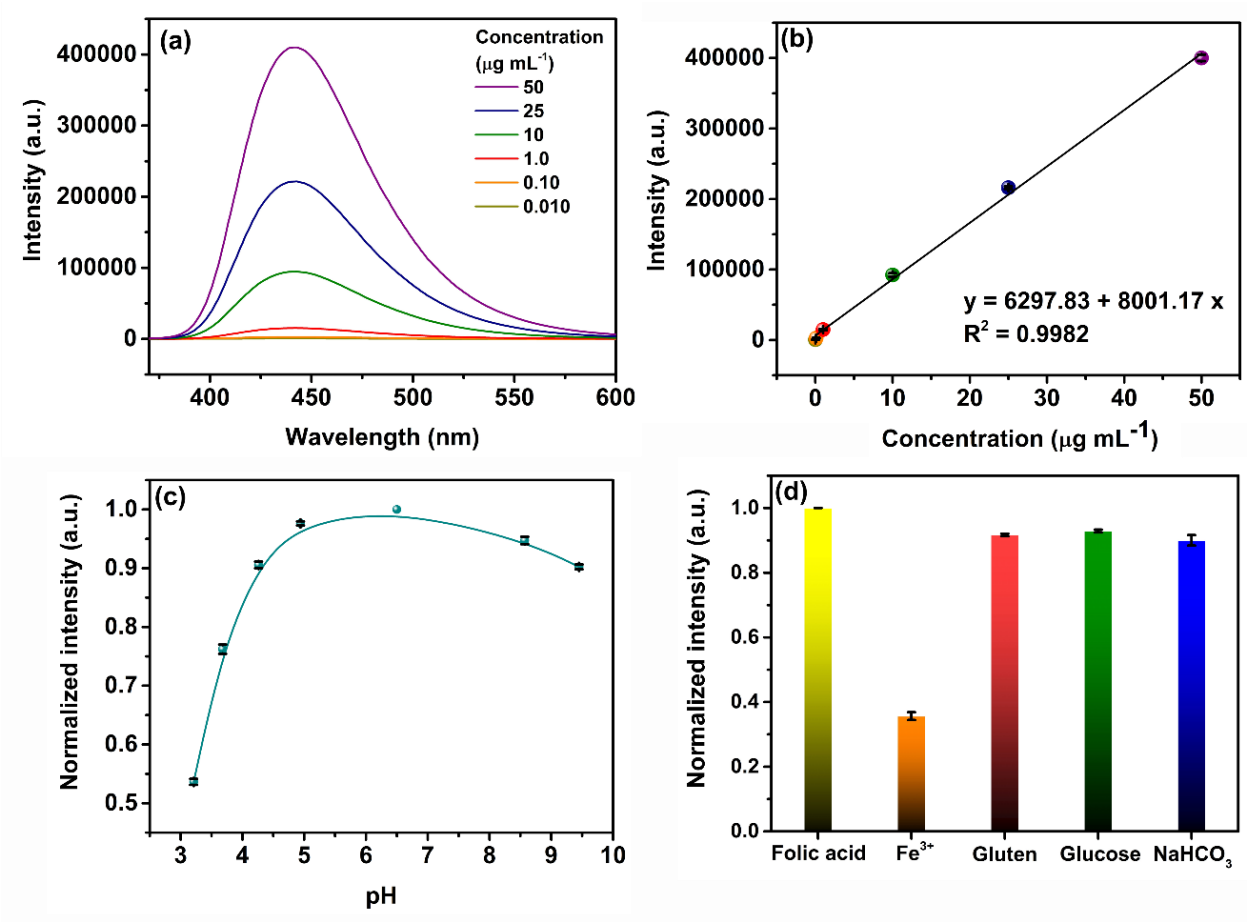

Source: Author.

Fig. 23. UV-Vis absorption spectrum (Abs Fe^{3+}) and excitation spectrum of CD-90 for evaluation of spectral overlap and confirmation of IFE.

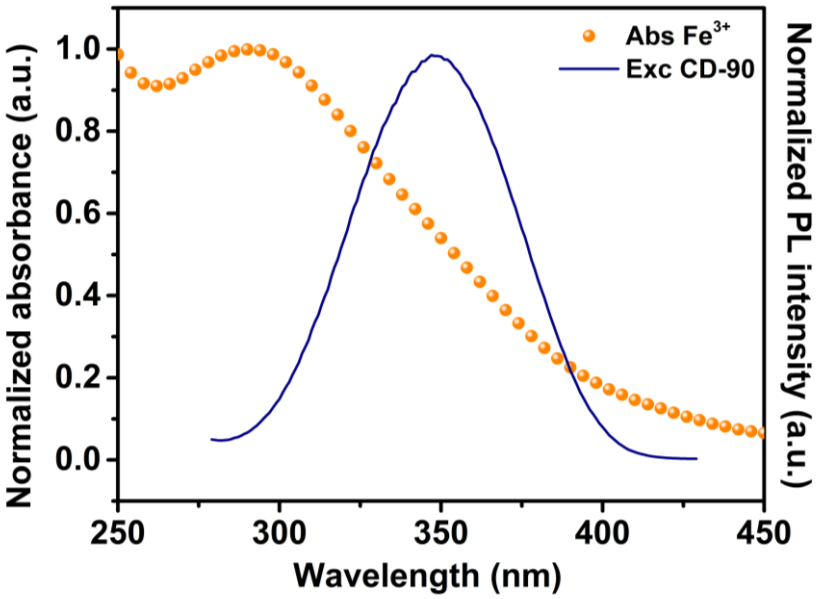

Source: Author.

4.3.3 Development of sensor array for gluten detection and turn-off/turn-on sensing for CN^- detection

The results displayed in Figure 22 (d) are based on a univariate analysis of data processing, where only the fluorescence intensity at 440 nm is considered. However, if a multivariate analysis data is performed and the entire emission spectrum is considered, the result can be surprisingly positive. Figure 24 shows the results obtained from a multivariate analysis of the emission spectra of the main species found in cookie formulations. Specifically, LDA chemometric tool was employed in this study. In this type of investigation, the entire fluorescence spectrum (230 points) is evaluated instead of a single point and a large data matrix is generated (5 species x 6 replicates x 230 points). LDA is a supervised pattern recognition technique and is capable of classifying distinct groups of samples, which have characteristic fingerprints generated from the data matrix (PRENDERGAST; SMITH, 2022). Based on this, a sensor array was developed in this work and the folic acid, Fe^{3+} ions, $NaHCO_3$, glucose and gluten species were successfully discriminated, as shown in Figure 24 (a). These results are promising and indicate that CD-90 can be used to detect gluten, which is often present in bread, cakes and cookies, but is extremely dangerous for people with celiac disease. LDA assigns classes to data based on the Mahalanobis distance, where the greater the distance between the

groups, the greater the probability of a correct classification (CAO *et al.*, 2023). Thus, the performance of the sensor array on a real cookie sample was investigated and the result can be seen in Figure 24 (b). In fact, the sensor array proposed in this study showed potential for practical applications in real samples. The investigated species were distinctly grouped, indicating success in data classification using LDA.

Fig. 24. 3D-Canonical score plot for the fluorescence patterns obtained from LDA: **(a)** analytical standards; **(b)** real sample of cookies. The species were detected at concentration of 25 ppm in CD-90 suspension under neutral pH. All measurements were based on experiments with six replicates.

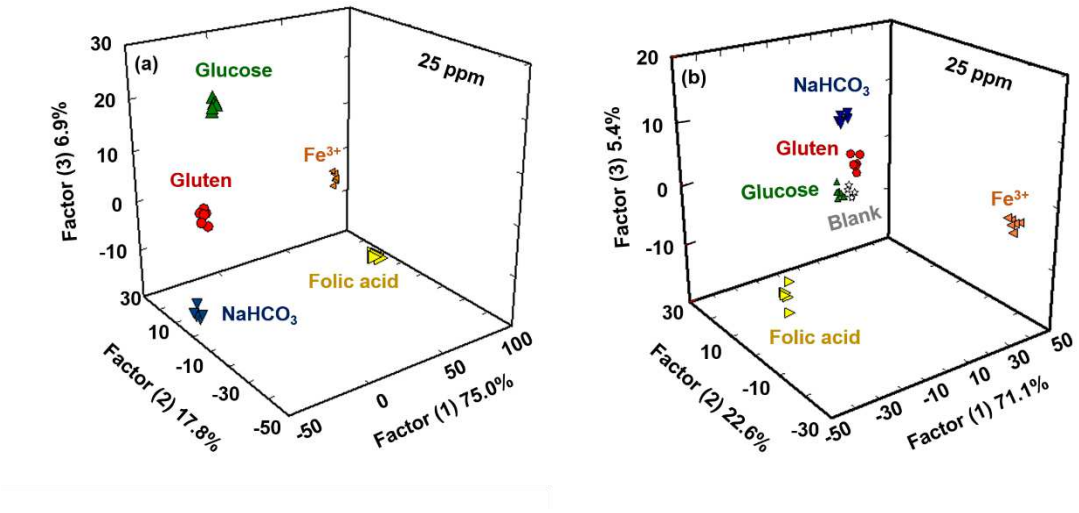

Source: Author.

In addition, the CD-90 was also used in the development of a turn-off/turn-on sensor for CN^- detection. For this, the fluorescence intensity of CD-90 was quenched with the addition of Fe^{3+} ions and later recovered by the addition of CN^- ions. According to Figure 25 (a), increasing the concentration of Fe^{3+} ions significantly decreased the fluorescence intensity of CD-90 and this is more evident in Figure 25 (b), which shows the decrease in fluorescence intensity normalized at 440 nm. It is possible to observe that at high concentrations the points deviate from linearity, suggesting that static and dynamic mechanisms act in the chemical interactions that govern the CD-90 fluorescence quenching process (CARNEIRO *et al.*, 2021).

Fig. 25. Sensing tests for the detection of Fe^{3+}/CN^-: **(a)** turn-off sensing with fluorescence quenching of the CD-90 fluorescence spectrum; **(b)** variation in fluorescence intensity with Fe^{3+} concentration at wavelength 440 nm; **(c)** turn-on sensing with fluorescence recovery of the CD-90 fluorescence spectrum; **(d)** variation in fluorescence intensity with CN^- concentration at wavelength 440 nm. All average and standard deviation values were calculated based on triplicate experiments.

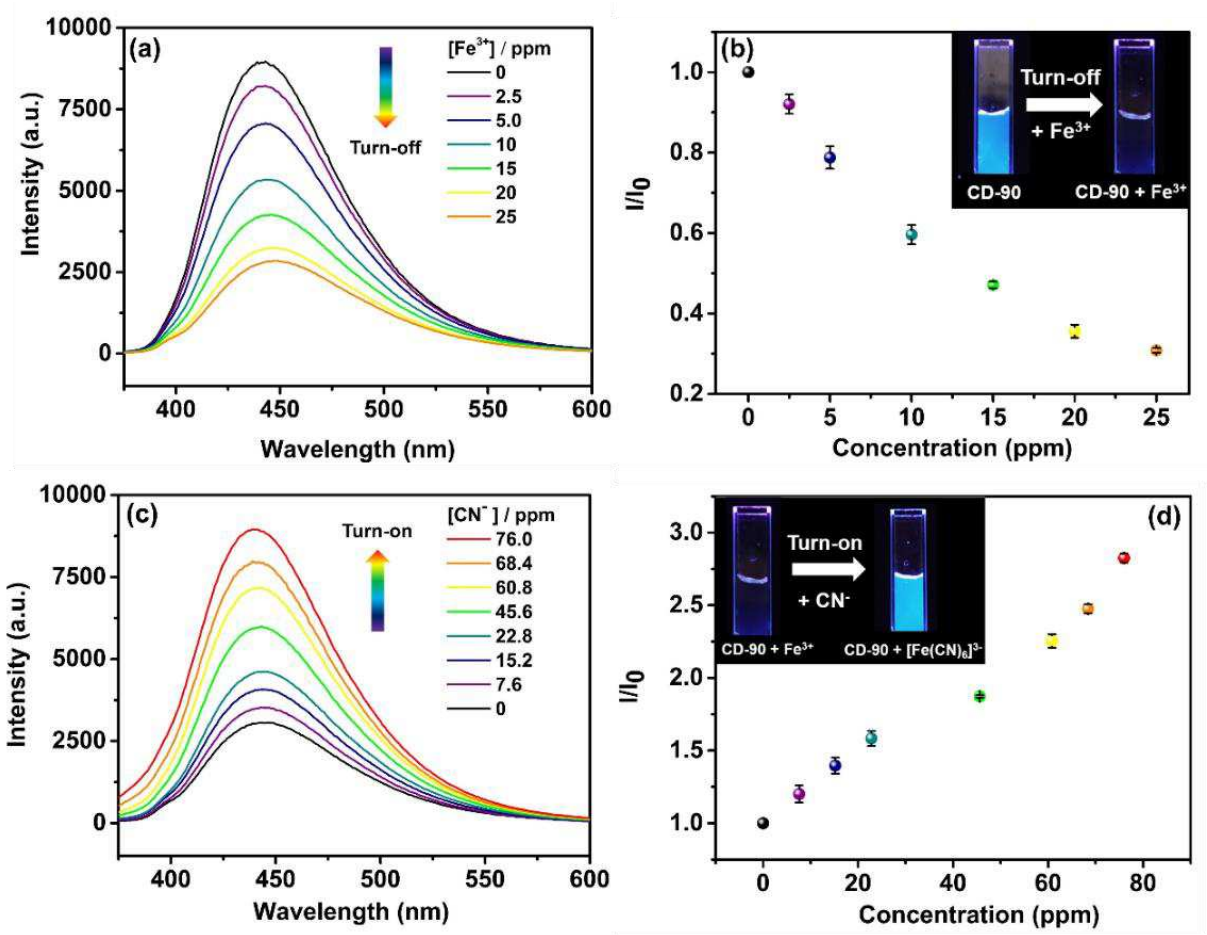

Source: Author.

The inset in Figure 25 (b) shows the fluorescence emission of CD-90 under UV light and also shows the quenching caused by the addition of 25 ppm Fe^{3+} ions. The Figure 25 (c) shows the restoration of CD-90 fluorescence obtained from the complexation of the Fe^{3+} ions with CN^- ions, according to the equation 7:

$$Fe^{3+} + 6CN^- \rightleftharpoons [Fe(CN)_6]^{3-} \quad \textbf{(7)}$$

$$k = \frac{[[Fe(CN)_6]^{3-}]}{[Fe^{3+}][CN^-]^6}$$

where k is the formation constant of the complex, $[[Fe(CN)_6]^{3-}]$ is the complex

concentration and $[Fe^{3+}]$ and $[CN^-]$ are the concentrations of the ions Fe^{3+} and CN^-, respectively.

It is possible to observe that the emission intensity increases with the increase of the CN^- concentration since the complexation equilibrium is favored, shifting the balance towards the formation of products, as shown in equation 7. Thus, a turn-off/turn-on sensor for the detection of CN^- was developed, based on the competitive coordination mechanism (XU, O. *et al.*, 2023). In Figure 25 (d) these data are more clearly demonstrated and the inset shows the recovery of CD-90 fluorescence under UV light. The data seen in Figure 25 (b) and Figure 25 (d) were linearly adjusted to construct calibration curves for quenching and recovery of the CD-90 fluorescence, of which the equations can be consulted in Table 3. The LOD of the CN^- sensor was calculated using the equation 2 and the value found was 3.77 ppm, which is comparable to the literature, as shown in Table 4.

Table 3. Linear adjustment for quenched and recovery of CD-90 fluorescence.

Turn-off	Turn-on
Fe^{3+}	CN^-
$y = -0.00778x + 0.95292$	$y = 0.02174x + 1.02049$
$R^2 = 0.9610$	$R^2 = 0.9800$

Source: Author.

Table 4. Comparison of the proposed method with earlier reported literature for the detection of CN^-.

Method	**Probe**	**LOD (ppm)**	**Real sample**	**References**
Colorimetric	Recognition solution	0.27	Textile industry effluents	(RAI *et al.*, 2021)
Fluorescent	Azine derivative (L1)	0.00377	-	(DEVENDHIRAN *et al.*, 2021)
Fluorescent	CPPO-AuNCs CL	0.00133	Tap and lake waters	(LI, L. *et al.*, 2022)
Fluorescent	LysNP-AuNCs	39.07	Tap water	(TSENG *et al.*, 2022)
Fluorescent	ZnS quantum dots	0.0188	Tap and ground	(SHAMSIPUR; RAJABI, 2014)
Fluorescent	GQDs	0.00033	Tap water	(ACHADU; NYOKONG, 2019)
Fluorescent	Carbon dots	0.3256	Tap water and human serum	(ZHANG, JIA; DONG; YU, 2015)
Fluorescent	CQDs	3.77	Tap water	**This work**

Source: Author.

Finally, the practicality of the sensing strategy developed in this work was validated from the analysis of real samples of tap water. The results can be seen Table 5 and indicate that the turn-off/turn-on sensor has potential for practical applications in CN^- ion detection systems.

Table 5. Determination results of CN^- ions in real sample of tap water under optimal conditions (N=3).

Sample	Added (ppm)	Found (ppm)	Recovery (%)	RSD (%)
Tap water	7.62	6.59	86.4	28.3
	45.6	43.2	94.8	7.34

Source: Author.

4.4 Conclusion

This paper suggests a useful sensing method for detection of potential toxic agents in food, such as gluten and cyanide ion. Applying CQDs with ultrahigh QY, we were able to develop an efficient strategy to ensure food security, based on the quantification of the proposed analytes. The fluorescent nanoprobe presented emission intensity quenched by Fe^{3+} ions through an internal filter effect. The insertion of cyanide ions recovers the luminescence of the CQDs from a competitive coordination mechanism, allowing the development of a turn-off/turn-on sensor. Moreover, the sensor array illustrated the great potential for distinguish species present in cookie formultations, including gluten, an allergen responsible for serious damage to the consumer health. The developed sensor array could successfully discriminate the species with 100% accuracy, based on classification matrix. Up to this report, we conclude that a simple and efficient gluten and cyanide ion detection method has been successfully developed, including being used in practical applications for the quantification of the analyte in real samples.

CHAPTER V

5 GENERAL CONCLUSIONS

Nanotechnology is increasingly present in everyday applications and the exploration of nanomaterials such as CQDs brings many benefits to humanity. In this thesis, results are presented that demonstrate the application of CQDs in the field of sensing. Specifically, the results obtained in Chapter III point to a multiple way of sensing Co^{2+} ions that guaranteed the fulfillment of specific objectives a), b), c), d) and e), since:

- ✓ CQDs were successfully synthesized from a hydrothermal route and were characterized morphologically, structurally and optically. The CQDs presented a quasi-spherical shape with a particle size of 4.51 nm and a surface rich in nitrogen and oxygen, which generate different surface states, making the CQDs fluorescent;
- ✓ Under optimized experimental conditions (excitation wavelength 340 nm, concentration of 0.25 mg mL^{-1} and pH 7.4), the CQDs had their fluorescence quenched by Co^{2+} ions, making it possible to find a linear relationship between emission intensity and concentration of the analyte;
- ✓ The interaction of Co^{2+} ions with CQDs formed a yellowish complex, which proportionally increased its absorbance at 315 nm when the analyte concentration increased;
- ✓ The use of PCA and LDA generated characteristic fingerprints for each concentration of Co^{2+} ions and interfering ions that were added to the CQDs, making it possible to successfully discriminate each concentration and the analyte of interest;
- ✓ CQDs successfully quantified Co^{2+} ions in a real sample of blood plasma, obtaining a recovery of 100.92 % with an RSD of 0.9 % for the reference concentration of 100 $\mu mol\ L^{-1}$;

Furthermore, the results presented in Chapter IV show that CQDs are also powerful tools in the quantification of CN^- ions and, fulfilling specific objectives f), g), h) and i), we can conclude that:

- ✓ CQDs with ultra-high quantum yield of 90.7% were successfully obtained from ethylenediamine and citric acid;

- ✓ A CD-90/Fe^{3+} nanoprobe was successfully developed for the sensitive detection of CN^- and a linear relationship could be found for the fluorescence recovery of CQDs after analyte addition;
- ✓ LDA was able to successfully discriminate folic acid, Fe^{3+} ions, $NaHCO_3$, glucose and gluten species, since no group overlap was observed;
- ✓ CQDs successfully quantified CN^- ions in a real sample of tap water, obtaining a recovery of 94.8 % with an RSD of 7.34 % for the reference concentration of 53.2 ppm.

Finally, as a general conclusion, we can infer that the use of CQDs in sensing platforms has shown to be promising and versatile. CQDs can contribute to WADA in establishing a standard method for quantifying Co^{2+} ions, as well as being used as a powerful food safety tool, being capable of quantifying CN^- ions in real samples. Thus, with this work, we hope to contribute to the literature on carbon nanoparticles, more specifically by applying nanomaterials in chemical sensing.

PUBLISHED WORKS AND PARTICIPATION IN EVENTS

Journal of Photochemistry & Photobiology, A: Chemistry 411 (2021) 113198

Contents lists available at ScienceDirect

Journal of Photochemistry & Photobiology, A: Chemistry

journal homepage: www.elsevier.com/locate/jphotochem

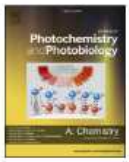

Highly sensitive sensing of food additives based on fluorescent carbon quantum dots

S.V. Carneiro [a], M.H.B. Holanda [b], H.O. Cunha [a], J.J.P. Oliveira [a], S.M.A. Pontes [a], A.A.C. Cruz [a], L.M.U.D. Fechine [a], T.A. Moura [c], A.R. Paschoal [c], R.A. Zambelli [b], R.M. Freire [d,e], P.B. A. Fechine [a,*]

[a] Grupo de Química de Materiais Avançados (GQMat), Departamento de Química Analítica e Físico-Química, Universidade Federal do Ceará – UFC, Campus do Pici, CP 12100, CEP 60451-970, Fortaleza, CE, Brasil
[b] Laboratório de Biomateriais Alimentícios (LBMA), Departamento de Engenharia de Alimentos, Universidade Federal do Ceará – UFC, Campus do Pici, CP 12100, CEP 60451-970, Fortaleza, CE, Brasil
[c] Departamento de Física, Universidade Federal do Ceará – UFC, Campus do Pici, CP 12100, CEP 60451-970, Fortaleza, CE, Brasil
[d] Institute of Applied Chemical Sciences, Universidad Autónoma de Chile, 8910060, Santiago, Chile
[e] Center for the Development of Nanoscience and Nanotechnology (CEDENNA), 9170124, Santiago, Chile

ARTICLE INFO

Keywords:
Carbon quantum dots
Fluorescence
Sensing platform
Linear discriminant analysis
Food additives
Pickled olives

ABSTRACT

A robust fluorescence-based sensing strategy was designed considering relevance of analyzing chemical additives in industrialized food. In this study, a sensing approach was developed using fluorescent carbon quantum dots (CQDs) as a chemometric tool. CQDs were synthesized by a simple one-step hydrothermal route using the American natural seed *Caelsalpinia pulcherrima*, and further characterized regarding their chemical structure. Five food additives were identified, citric acid, lactic acid, ascorbic acid, sodium benzoate and potassium sorbate, which showed a highly sensitive response with a limit of detection (LOD) as low as 252 ng mL^{-1}. The sensing platform was designed using the supervised method for recognizing patterns of linear discriminant analysis (LDA), where we could identify different concentrations of additives, after optimization of experimental parameters. Furthermore, the sensing strategy successfully identified all tested additives in a pickled olives sample with 95 % of confidence, where 100 % of combinations were correctly identified based on classification matrix. Overall, the obtained results evidence the accuracy and potential of CQDs-based fluorescence sensing in the identification of food additives.

Certificado
DE PARTICIPAÇÃO

Brazilian Biophysical Society

Certificamos que o trabalho intitulado

PONTOS QUÂNTICOS DE CARBONO OBTIDOS DE FONTE NATURAL E SUA APLICAÇÃO PARA O SENSORIAMENTO DE ADITIVOS ALIMENTARES

S. V. Carneiro1; H. O. Cunha1; M. H. B. Holanda2; J. J. P. Oliveira1; S. M. A. Pontes1; A. A. C. Cruz1; L. M. U. D. Fechine1; R. A. Zambelli2; R. M. Freire1 e P. B.A. Fechine1 1Grupo de Química de Materiais Avançados (GQMat), Departamento de Química Analítica e Físico-Química, 2Laboratório de Biomateriais Alimentícios (LBMA), Departamento de Engenharia de Alimentos, Universidade Federal do Ceará, Fortaleza, CE

Foi apresentado na forma de e-poster, durante a realização do **VI Congresso regional da Sociedade Brasileira de Biofísica (SBBf)**, no período de 22 a 25 de março de 2021.

Nano-Structures & Nano-Objects 32 (2022) 100917

Contents lists available at ScienceDirect

Nano-Structures & Nano-Objects

journal homepage: www.elsevier.com/locate/nanoso

One-pot Solvothermal Synthesis of Full-color Carbon Quantum Dots for Application in Light Emitting Diodes

Sheyliane Maria Adriano Pontes [a], Vivian Stephanie Ferreira Rodrigues [a], Samuel Veloso Carneiro [a], José Joelson Pires Oliveira [a], Thiago Alves Moura [b], Alexandre Rocha Paschoal [b], Renato Altobelli Antunes [c], Davi Rabelo de Oliveira [d], Jéssica Ribeiro Oliveira [d], Lillian Maria Uchoa Dutra Fechine [a], Selma Elaine Mazzetto [d], Pierre Basílio Almeida Fechine [a], Claudenilson da Silva Clemente [d,*]

[a] Group of Chemistry of Advanced Materials (GQMat), Department of Analytical Chemistry and Physical-Chemistry, Pici Campus, Federal University of Ceara, Fortaleza - Ce, Zip Code 60451-970, Brazil
[b] Department of Physics, Pici Campus, Federal University of Ceara, Fortaleza - Ce, Zip Code 60440-900, Brazil
[c] Center for Engineering, Modeling and Applied Social Sciences, Federal University of ABC, Santo André – SP, Zip Code 09210580, Brazil
[d] Laboratory of Products and Process Technology (LPT), Department of Organic and Inorganic Chemistry, Pici Campus, Federal University of Ceara, Fortaleza - Ce, Zip Code 60440-900, Brazil

ARTICLE INFO

Article history:
Received 22 February 2022
Received in revised form 5 July 2022
Accepted 17 September 2022

Keywords:
Carbon quantum dots
Photoluminescence
Nanocomposite
Optoelectronic devices
White light emitting diode

ABSTRACT

Full-color Carbon Quantum Dots (FCQDs) have intrinsic characteristics as components for White Light Emitting Diode (WLED) technology, but are not yet applied in the current lighting industry. In this work, FCQDs were prepared by optimizing the synthetic route in order to obtain a simple and one-step solvothermal carbonization of citric acid and urea in dimethylformamide. The synthesis at 166 °C for 11 h and 24 min (FCQD2) was selected from spectroscopy in the ultraviolet–visible (UV–Vis) region and its fluorescence indicated emission over almost the entire visible region of the electromagnetic spectrum with a 380 nm excitation source and a concentration of 0.22 mg mL^{-1}. The morphological, structural and optical properties were evaluated and they showed that nanoparticles with dimensions between 2 and 10 nm consisted mainly of carbon atoms with functional groups on the surface. FCQD2 was incorporated in a polymeric matrix (PVA) and the coordinates of the Color Rendering Index (CRI) showed better color quality than a commercial WLED. It appears that FCQD2, with an easy synthesis and being ecofriendly, has potential for incorporation in a solid matrix, as well as application in WLEDs for the improvement of optoelectronic devices, replacing inorganic quantum dots.

ACS APPLIED MATERIALS & INTERFACES

www.acsami.org Research Article

Doped Carbon Quantum Dots/PVA Nanocomposite as a Platform to Sense Nitrite Ions in Meat

Samuel Veloso Carneiro, José Joelson Pires Oliveira, Vivian Stephanie Ferreira Rodrigues, Lillian Maria Uchoa Dutra Fechine, Renato Altobelli Antunes, Manoel Lourenço Alves Neto, Thiago Alves de Moura, Carlos Lenz César, Hernandes Faustino de Carvalho, Alexandre Rocha Paschoal, Rafael Melo Freire, and Pierre Basílio Almeida Fechine*

Cite This: *ACS Appl. Mater. Interfaces* 2022, 14, 43597–43611 Read Online

ACCESS | Metrics & More | Article Recommendations | Supporting Information

ABSTRACT: A sensor device based on doped-carbon quantum dots is proposed herein for detection of nitrite in meat products by fluorescence quenching. For the sensing platform, carbon quantum dots doped with boron and functionalized with nitrogen (B,N-Cdot) were synthesized with an excellent 44.3% quantum yield via a one-step hydrothermal route using citric acid, boric acid, and branched polyethylenimine as carbon, boron, and nitrogen sources, respectively. After investigation of their chemical structure and fluorescent properties, the B,N-Cdot at aqueous suspensions showed high selectivity for NO_2^- in a linear range from 20 to 50 mmol L^{-1} under optimum conditions at pH 7.4 and a 340 nm excitation. Furthermore, the prepared B,N-Cdots successfully detected NO_2^- in a real meat sample with recovery of 91.4−104% within the analyzed range. In this manner, a B,N-Cdot/PVA nanocomposite film with blue emission under excitation at 360 nm was prepared, and a first assay detection of NO_2^- in meat products was tested using a smartphone application. The potential application of the newly developed sensing device containing a highly fluorescent probe should aid in the development of a rapid and inexpensive strategy for NO_2^- detection.

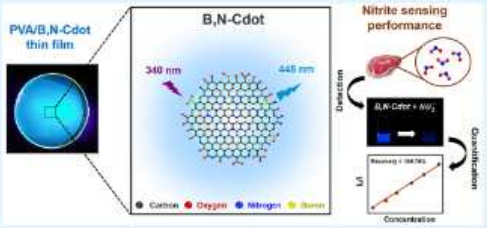

KEYWORDS: *carbon quantum dots, sensor device, nanocomposite, fluorescent sensing, nitrite, meat*

ELSEVIER

Encyclopedia of Sensors and Biosensors

Volume 2, 2023, Pages 542-559

Sensing Materials: Optical Sensing Based on Carbon Quantum Dots

A.A.C. Cruz [a], S.V. Carneiro [a], S.M.A. Pontes [a], J.J.P. Oliveira [a], J.P.O. Lima [a], V.M. Costa [a], L.M.U.D. Fechine [a], C.S. Clemente [b], R.M. Freire [c d], P.B.A. Fechine [a]

Show more

https://doi.org/10.1016/B978-0-12-822548-6.00025-X Get rights and content

Abstract

Fluorescent carbon quantum dots (CQDs) are carbon nanoparticles with excellent optical properties, which have found wide use in sensing platforms. In this chapter, we describe the recent advancement of CQDs and optical sensors, principally focusing in syntheses methods, luminescence-dependence of size and chemical composition, and applications in sensor arrays by chemometric techniques. In addition, we also present a discussion considering the remaining challenges and future trends in the development of fluorescents sensors.

Materials Today Nano 22 (2023) 100345

Contents lists available at ScienceDirect

Materials Today Nano

journal homepage: https://www.evise.com/profile/#/MTNANO/login

Recent advances in nanostructured materials: A look at the applications in optical chemical sensing

S.V. Carneiro [a], J.J.P. Oliveira [a], V.S.F. Rodrigues [a], J.P.O. Lima [a], J.H.O. do Nascimento [b], R. Santos-Oliveira [c, d], L.M.U.D. Fechine [a], R.M. Freire [e], P.B.A. Fechine [a, *]

[a] Advanced Materials Chemistry Group (GQMat), Department of Analytical Chemistry and Physical Chemistry, Federal University of Ceara – UFC, Campus do Pici, CP 12100, CEP 60451-970 Fortaleza, CE, Brazil
[b] Innovation in Micro and Nanotechnologies Group (GPIMN), Department of Textile Engineering, Federal University of Rio Grande do Norte – UFRN, Center of Technology, Campus Universitário Lagoa Nova, CEP 59078-970, Natal, RN, Brazil
[c] Brazilian Nuclear Energy Commission, Nuclear Engineering Institute, Rio de Janeiro, 21941906, Brazil
[d] Universidade Unigranrio, Laboratory of Advanced Science, Duque de Caxias – RJ, 25071-202, Brazil
[e] Laboratory of Pesticide Residues and Environment, Instituto de Investigaciones Agropecuarias, INIA Centro Regional La Platina, Santiago 8820000, Chile

ARTICLE INFO

Article history:
Received 17 October 2022
Received in revised form
26 March 2023
Accepted 15 April 2023
Available online 20 April 2023

Keywords:
Optical chemical sensor
Fluorescence
Nanomaterials
Polymeric films
Sensor array
Plasmonic nanoparticles
Limit of detection
Dimensionality
Synthesis of nanoparticles

ABSTRACT

Recently, optical chemical sensors have been used to simplify traditional methods of chemical analyses. Indeed, sensing strategies based on the photoluminescence properties of nanomaterials need to be well-understood, since there are several nanomaterials with different features regarding their applicability in the optical sensor field. This review summarizes the main 0D, 1D and 2D nanomaterials used in sensing devices, with a special look in their optical properties and different methods of synthesis, as well as a briefing overview related to their colloidal stability, chemical structure and kinetic and thermodynamic parameters. In addition, the analytical performances of different optical sensing strategies are also highlighted, in which pattern recognition algorithms and the development of polymeric-based films are tools used to contribute for the application of new optical chemical sensors with exceptional sensibility and selectivity. Furthermore, this review would give some insights into advances development of optical chemical sensors, using nanomaterials of different dimensionalities.

Dyes and Pigments 215 (2023) 111253

Contents lists available at ScienceDirect

Dyes and Pigments

journal homepage: www.elsevier.com/locate/dyepig

Determination of Co^{2+} ions in blood samples: A multi-way sensing based on NH_2-rich carbon quantum dots

J.J.P. Oliveira [a, b], S.V. Carneiro [b], A.A.C. Cruz [b], L.M.U.D. Fechine [b], S. Michea [c], R.A. Antunes [d], M.L.A. Neto [e, f], T.A. Moura [e], C.L. César [e, f], H.F. Carvalho [f, g], A.R. Paschoal [e], G.S. Lopes [h], R. M. Freire [i], P.B.A. Fechine [b, *]

[a] Graduate Program in Materials Science and Engineering, Department of Metallurgical and Materials Engineering, Federal University of Ceará - UFC, Campus do Pici, Building 729, Fortaleza, 60.440-554, Brazil
[b] Advanced Materials Chemistry Group (GQMat), Department of Analytical Chemistry and Physical Chemistry, Federal University of Ceará – UFC, Campus do Pici, CP 12100, CEP 60451-970, Fortaleza, CE, Brazil
[c] Applied Research Physics Group, Institute of Applied Chemical Sciences, Faculty of Engineering, Universidad Autónoma de Chile, Santiago, Chile
[d] Center for Engineering, Modeling and Applied Social Sciences, Federal University of ABC, CEP: 09210-580, Santo André, SP, Brazil
[e] Department of Physics, Federal University of Ceará – UFC, Campus do Pici, CP 12100, CEP 60451-970, Fortaleza, CE, Brazil
[f] National Institute of Photonics Applied to Cell Biology, State University of Campinas, IFGW - Unicamp Cid. Universitária, 13083863, Campinas, SP, Brazil
[g] State University of Campinas, Institute of Biology, Department of Cell Biology, Department of Cell Biology - IB - CP. 6109 UNICAMP Cid. Universitária, 13083863, Campinas, SP, Brazil
[h] Laboratory of Applied Chemistry (LEQA)- Department of Analytical Chemistry and Physical-Chemistry, Federal University of Ceará– UFC, Campus do Pici, CP 12100, CEP 60451-970, Fortaleza, CE, Brazil
[i] Laboratory of Pesticide Residues and Environment, Instituto de Investigaciones Agropecuarias, INIA Centro Regional La Platina, Santiago, 8820000, Chile

ARTICLE INFO

Keywords:
Carbon quantum dots
Cobalt sensing
Colorimetric sensor
Chemometric tools

ABSTRACT

Multiple forms of detecting Co^{2+} are reported in this work to quantify these ions in real blood plasma samples. Carbon Quantum Dots (CQDs) were used as a fluorescent nanoprobe. The CQDs were obtained from a bottom-up approach using a hydrothermal method and choline chloride and branched poly(ethyleneimine) as precursor molecules. Several spectroscopic and structural characterizations were performed. The efficient fluorescence quenching of CQDs related to the Co^{2+} ion was used for the detection of the analyte, generating a sensing strategy with a limit of detection (LOD) of 0.98 μmol L^{-1}. Furthermore, the interaction between the Co^{2+} ion with the CQDs resulted in the color change of the solution from colorless to pale yellow. Thus, a colorimetric Co^{2+} sensor was also developed, since there was an absorption band at 315 nm attributed to the formation of the complex CQD + Co^{2+}. The colorimetric method showed an excellent sensitivity to Co^{2+}, with a LOD of 3.01 μmol L^{-1}. In addition, Principal Component Analysis (PCA) together with Linear Discriminant Analysis (LDA) were used successfully to distinguish different concentrations of Co^{2+} and different interfering ions present in the solution. Finally, a real sample of blood plasma was properly treated and doped with different concentrations of Co^{2+}, which was successfully quantified via fluorescent method. Therefore, the CQDs obtained in this work are a powerful and versatile Co^{2+} detection tool.

REFERENCES

ABDULKHALEQ, A. M. A. *et al.* Development of highly selective novel fluorescence turn-on probe based on carbon dots for sensing peroxynitrite (ONOO−) in vitro and in vivo. **Dyes and Pigments**, v. 217, p. 111404, 1 set. 2023.

ACHADU, O. J.; NYOKONG, T. Fluorescence "turn-ON" nanosensor for cyanide ion using supramolecular hybrid of graphene quantum dots and cobalt pyrene-derivatized phthalocyanine. **Dyes and Pigments**, v. 160, p. 328–335, 1 jan. 2019.

AHMED ABDEL HAMID, M. *et al.* Microwave prepared nitrogen and sulfur co-doped carbon quantum dots for rapid determination of ascorbic acid through a turn off–on strategy. **Spectrochimica Acta Part A: Molecular and Biomolecular Spectroscopy**, v. 293, p. 122440, 15 maio 2023.

AL-HASHIMI, B.; OMER, K. M.; RAHMAN, H. S. Inner filter effect (IFE) as a simple and selective sensing platform for detection of tetracycline using milk-based nitrogen-doped carbon nanodots as fluorescence probe. **Arabian Journal of Chemistry**, v. 13, n. 4, p. 5151–5159, 1 abr. 2020.

ALAMGIR, S. *et al.* Colorimetric and spectroscopic cobalt(II) sensing by a simple Schiff base. **Polyhedron**, v. 187, p. 114681, 1 set. 2020.

ALI, M. S. *et al.* Fluorescent N-doped carbon quantum dots: A selective detection of Fe3+ and understanding its mechanism. **Chemical Physics Letters**, v. 825, p. 140574, 16 ago. 2023.

ALORABI, A. Q. A new colorimetric chemosensor based on 1,3,4-oxadiazole derivative for the high selectivity and sensitivity of Fe3+ ion detection. **Journal of Molecular Structure**, p. 132019, 27 nov. 2021.

ANTHONY, A. M.; PANDURANGAN, P.; ABBAS, S. Ligand engineering with heterocyclic aromatic thiol doped carbon quantum dots. **Carbon**, v. 211, p. 118086, 25 jun. 2023.

ARIAS VELASCO, V. *et al.* Context and prospects of carbon quantum dots applied to environmental solutions. **Environmental Nanotechnology, Monitoring & Management**, v. 20, p. 100884, 1 dez. 2023.

ARUMUGAM, S. S. *et al.* Facile preparation of fluorescent carbon quantum dots from denatured sour milk and its multifunctional applications in the fluorometric determination of gold ions, in vitro bioimaging and fluorescent polymer film. **Journal of Photochemistry and Photobiology A: Chemistry**, v. 401, p. 112788, 1 out. 2020.

AZIZI, M. *et al.* Carbon quantum dot based nanocarrier labeled with anti-PDL1 antibody as a promising theranostic candidate for the triple negative breast cancer treatment. **Materials Chemistry and Physics**, v. 315, p. 128981, 1 mar. 2024.

BANO, D. *et al.* Synthesis of highly fluorescent nitrogen-rich carbon quantum dots and their application for the turn-off detection of cobalt (II). **Optical Materials,** v. 92, p. 311–318, 1 jun. 2019.

BAO, H. *et al.* Luminescence of carbon quantum dots and their application in biochemistry. **Heliyon**, v. 9, n. 10, p. e20317, 1 out. 2023.

BASRI, K. N. *et al.* Chemometrics analysis for the detection of dental caries via UV absorption spectroscopy. **Spectrochimica Acta Part A: Molecular and Biomolecular Spectroscopy**, v. 266, p. 120464, 5 fev. 2022.

BENLI, E. E. *et al.* Sensitive fluorometric determination of picric acid and antioxidant stabilizers in propellant compositions using amine-rich nitrogen-doped carbon quantum dots. **Talanta Open**, v. 8, p. 100245, 1 dez. 2023.

BU, L. *et al.* One-step synthesis of N-doped carbon dots, and their applications in curcumin sensing, fluorescent inks, and super-resolution nanoscopy. **Microchimica Acta**, v. 186, n. 10, p. 1–12, out. 2019.

BULAT, T. *et al.* Employing carbon quantum dots to combat cytomegalovirus. **Materials Chemistry and Physics**, v. 311, p. 128495, 1 jan. 2024.

CAO, Z. *et al.* Spectral classification by generative adversarial linear discriminant analysis. **Analytica Chimica Acta**, v. 1261, 2023.

CARNEIRO, S. V. *et al.* Highly sensitive sensing of food additives based on fluorescent carbon quantum dots. **Journal of Photochemistry and Photobiology A: Chemistry**, v. 411, p. 113198, 15 abr. 2021.

CARNEIRO, S. V. *et al.* Recent advances in nanostructured materials: A look at the applications in optical chemical sensing. **Materials Today Nano**, v. 22, p. 100345, 1 jun. 2023.

CARNEIRO, S. V. *et al.* Sensing strategy based on Carbon Quantum Dots obtained from riboflavin for the identification of pesticides. **Sensors and Actuators, B: Chemical**, v. 301, p. 127149, 12 dez. 2019.

CHANG, D. *et al.* Iron ion sensing and in vitro and in vivo imaging based on bright blue-fluorescent carbon dots. **Spectrochimica Acta Part A: Molecular and Biomolecular Spectroscopy**, v. 260, p. 119964, 5 nov. 2021.

CHEN, H. *et al.* Construction of optical dual-mode sensing platform based on green emissive carbon quantum dots for effective detection of ClO- and cellular imaging. **Spectrochimica Acta Part A: Molecular and Biomolecular Spectroscopy**, v. 309, p. 123733, 15 mar. 2024.

CRUZ, A. A. C. *et al.* Optical Sensing Strategy Based on Carbon Quantum Dots. **Reference Module in Biomedical Sciences**, 1 jan. 2021.

CUARTERO, M. Electrochemical sensors for in-situ measurement of ions in seawater. **Sensors and Actuators B: Chemical**, p. 129635, 9 fev. 2021.

DA COSTA, R. S. *et al.* An Alternative Route to Obtain Carbon Quantum Dots from Photoluminescent Materials in Peat. **Materials**, v. 11, n. 9, ago. 2018.

DAGER, A. *et al.* Synthesis and characterization of Mono-disperse Carbon Quantum Dots from Fennel Seeds: Photoluminescence analysis using Machine Learning. **Scientific Reports**, v. 9, n. 1, p. 1–10, 2019.

DAI, H. *et al.* Four-channel fluorescent sensor array based on various functionalized CdTe quantum dots for the discrimination of Chinese baijiu. **Spectrochimica Acta Part A: Molecular and Biomolecular Spectroscopy**, v. 252, p. 119513, maio 2021.

DAS, S.; SANKAR MONDAL, U.; PAUL, S. Highly fluorescent metal doped carbon quantum dots prepared from hen feather demonstrating pH-dependent dual sensing of 4-nitrophenol and Hg2+ ion. **Applied Surface Science**, v. 638, p. 157998, 30 nov. 2023.

DEHVARI, K. *et al.* Sonochemical-assisted green synthesis of nitrogen-doped carbon dots from crab shell as targeted nanoprobes for cell imaging. **Journal of the Taiwan Institute of Chemical Engineers**, v. 95, p. 495–503, fev. 2019.

DENG, J. *et al.* Electrochemical Synthesis of Carbon Nanodots Directly from Alcohols. **Chemistry – A European Journal**, v. 20, n. 17, p. 4993–4999, 22 abr. 2014.

DENG, Y. *et al.* Long lifetime pure organic phosphorescence based on water soluble carbon dots. **Chemical Communications**, v. 49, n. 51, p. 5751, maio 2013.

DEVENDHIRAN, T. *et al.* Synthesis and physical studies of coumarin-based chemosensor for cyanide ions. **Inorganic Chemistry Communications**, v. 134, p. 108951, 1 dez. 2021.

DEVI, M. *et al.* Fluorescent graphitic carbon nitride and graphene oxide quantum dots as efficient nanozymes: Colorimetric detection of fluoride ion in water by graphitic carbon nitride quantum dots. **Journal of Environmental Chemical Engineering**, v. 9, n. 1, p. 104803, 1 fev. 2021.

DEY, S. *et al.* New methods of synthesis and varied properties of carbon quantum dots with high nitrogen content. **Journal of Materials Research**, v. 29, n. 3, p. 383–391, fev. 2014.

DHANDAPANI, E. *et al.* Highly green fluorescent carbon quantum dots synthesis via hydrothermal method from fish scale. **Materials Today: Proceedings**, 20 maio 2021.

DING, H. *et al.* Solvent-Controlled Synthesis of Highly Luminescent Carbon Dots with a Wide Color Gamut and Narrowed Emission Peak Widths. **Small**, v. 14, n. 22, p. 1800612, 29 maio 2018.

DONG, Y. *et al.* "Turn-on" fluorescent detection of cyanide based on polyamine-functionalized carbon quantum dots. **RSC Advances**, v. 4, n. 8, p. 3701–3705, dez. 2013.

DSOUZA, S. D. *et al.* The importance of surface states in N-doped carbon quantum dots. **Carbon**, v. 183, p. 1–11, 15 out. 2021.

DUAN, X.-H. *et al.* Accurate ethanol determination in Chinese Baijiu based on red-emitted carbon quantum dots (CQDs) and a simple pH correction. **Food Chemistry**, v. 428, p. 136733, 1 dez. 2023.

EL-MALLA, S. F. *et al.* Rapid microwave synthesis of N,S-doped carbon quantum dots as a novel turn off-on sensor for label-free determination of copper and etidronate disodium. **Analytica Chimica Acta**, v. 1197, p. 339491, mar. 2022.

EMAM, H. E. Carbon quantum dots derived from polysaccharides: Chemistry and potential applications. **Carbohydrate Polymers**, v. 324, p. 121503, 15 jan. 2024.

FANG, J.; ZHUO, S.; ZHU, C. Fluorescent sensing platform for the detection of p-nitrophenol based on Cu-doped carbon dots. **Optical Materials**, v. 97, p. 109396, 1 nov. 2019.

FECHINE (org.), *et al*. Avanços no desenvolvimento de nanomateriais. Fortaleza: Imprensa Universitária UFC, 2020. E-book (303p.) ISBN: 978-65-991493-7-5.

FU, Y.; GAO, G.; ZHI, J. Electrochemical synthesis of multicolor fluorescent N-doped graphene quantum dots as a ferric ion sensor and their application in bioimaging. **Journal of Materials Chemistry B**, v. 7, n. 9, p. 1494–1502, fev. 2019.

GALAY, E. P.; DOROGIN, R. V.; TEMERDASHEV, A. Z. Quantification of cobalt and nickel in urine using inductively coupled plasma atomic emission spectroscopy. **Heliyon**, v. 7, n. 1, p. e06046, 1 jan. 2021.

GALSTYAN, V. "Quantum dots: Perspectives in next-generation chemical gas sensors" – A review. **Analytica Chimica Acta**. [S.l.]: Elsevier B.V. , 4 jan. 2021

GE, L. *et al.* Photoluminescence of carbon dots and their applications in Hela cell imaging and Fe3+ ion detection. **Journal of Materials Science**, v. 52, n. 17, p. 9979–9989, set. 2017.

GEANĂ, E. I.; ARTEM, V.; APETREI, C. Discrimination and classification of wines based on polypyrrole modified screen-printed carbon electrodes coupled with multivariate data analysis. **Journal of Food Composition and Analysis**, v. 96, p. 103704, 1 mar. 2021.

GEHLEN, M. H. The centenary of the Stern-Volmer equation of fluorescence quenching: From the single line plot to the SV quenching map. **Journal of Photochemistry and Photobiology C: Photochemistry Reviews**, v. 42, p. 100338, 1 mar. 2020.

GHALI, M. Static quenching of bovine serum albumin conjugated with small size CdS nanocrystalline quantum dots. **Journal of Luminescence**, v. 130, n. 7, p. 1254–1257, 1 jul. 2010.

GIDWANI, B. *et al.* Quantum dots: Prospectives, toxicity, advances and applications. **Journal of Drug Delivery Science and Technology**. [S.l.]: Editions de Sante. , 1 fev. 2021

GONG, X. *et al.* Facile synthesis of nitrogen-doped carbon dots for Fe3+ sensing and cellular imaging. **Analytica Chimica Acta**, v. 861, p. 74–84, fev. 2015.

GUO, R. *et al.* Functionalized Carbon Dots for Advanced Batteries. **Energy Storage Materials**, v. 37, p. 8–39, 1 jan. 2021.

HAMMI, N. *et al.* Nanostructured metal oxide@carbon dots through sequential chitosan templating and carbonisation route. **Carbohydrate Polymer Technologies and Applications**,

v. 2, p. 100043, 25 dez. 2021.

HORMOZI JANGI, S. R.; AKHOND, M. Ultrasensitive label-free enantioselective quantification of d-/l-leucine enantiomers with a novel detection mechanism using an ultra-small high-quantum yield N-doped CDs prepared by a novel highly fast solvent-free method. **Sensors and Actuators B: Chemical**, v. 339, p. 129901, jul. 2021.

HU, G. *et al.* Carbon dots derived from flax straw for highly sensitive and selective detections of cobalt, chromium, and ascorbic acid. **Journal of Colloid and Interface Science**, v. 579, 2020.

JAMES H. KIM, HERMAN J. GIBB, P. D. H. Concise international chemical assessment document 69:cobalt and inorganic cobalt compounds. **World Health Organization**, p. 1–93, 2006.

JANG, G.-S. *et al.* An exploration of 3-methoxypropionitrile chemical sensor based on layered hexagonal NiCo2O4 nanoplates as electrode material. **Ceramics International**, 15 fev. 2021.

JAYAN, S. S. *et al.* Facile synthesis of carbon dots using tender coconut water for the fluorescence detection of heavy metal ions. **Materials Today: Proceedings**, 26 dez. 2020.

JI, X. *et al.* Green synthesis of weissella-derived fluorescence carbon dots for microbial staining, cell imaging and dual sensing of vitamin B12 and hexavalent chromium. **Dyes and Pigments**, v. 184, p. 108818, 1 jan. 2021.

JI, Z. *et al.* Hierarchical flower-like architecture of nickel phosphide anchored with nitrogen-doped carbon quantum dots and cobalt oxide for advanced hybrid supercapacitors. **Journal of Colloid and Interface Science**, 15 nov. 2021.

JIANG, H. *et al.* New strategy for synthesis and functionalization of carbon nanoparticles. **Langmuir**, v. 26, n. 3, p. 1991–1995, 2 fev. 2010.

JING, N. *et al.* Nitrogen-doped carbon dots synthesized from acrylic acid and ethylenediamine for simple and selective determination of cobalt ions in aqueous media. **Journal of Luminescence**, v. 206, p. 169–175, 1 fev. 2019.

JOHN, B. K. *et al.* Bioresource-derived multifunctional carbon quantum dots as a fluorescence and electrochemical sensing platform for picric acid and noncytotoxic food storage application. **Journal of Industrial and Engineering Chemistry**, v. 126, p. 546–556, 25 out. 2023.

JOSEPH, A.; THOMAS, S. Energy, exergy and corrosion analysis of direct absorption solar collector employed with ultra-high stable carbon quantum dot nanofluid. **Renewable Energy**, v. 181, p. 725–737, 1 jan. 2022.

KANSAY, V. *et al.* Sustainable synthesis and characterization of fluorescent nanoprobe based on unintentional heteroatom doped-carbon quantum dots for bioimaging of human neuroblastoma cancer cells and living organisms. **Journal of Photochemistry and Photobiology A: Chemistry**, v. 443, p. 114879, 1 set. 2023.

KARAGIANNI, A. *et al.* Application of carbon-based quantum dots in photodynamic therapy.

Carbon, v. 203, p. 273–310, 25 jan. 2023.

KARAMDOUST, S.; MILANI-HOSSEINI, M. R.; FARIDBOD, F. Simple detection of gluten in wheat-containing food samples of celiac diets with a novel fluorescent nanosensor made of folic acid-based carbon dots through molecularly imprinted technique. **Food Chemistry**, v. 410, p. 135383, 1 jun. 2023.

KASINATHAN, K. *et al.* Green synthesis of multicolour fluorescence carbon quantum dots from sugarcane waste: Investigation of mercury (II) ion sensing, and bio-imaging applications. **Applied Surface Science**, v. 601, p. 154266, 1 nov. 2022.

KHAN, S. *et al.* A review on nanotechnology: Properties, applications, and mechanistic insights of cellular uptake mechanisms. **Journal of Molecular Liquids**, v. 348, p. 118008, 15 fev. 2022.

KOU, X. *et al.* Construction of carbon dots having aggregation-induced emission and intramolecular charge transfer properties. **Dyes and Pigments**, p. 111092, 11 jan. 2023.

KUMAR, J. V.; RHIM, J.-W. Fluorescent carbon quantum dots for food contaminants detection applications. **Journal of Environmental Chemical Engineering**, p. 111999, 22 jan. 2024.

KURDEKAR, A. *et al.* Comparative performance evaluation of carbon dot-based paper immunoassay on Whatman filter paper and nitrocellulose paper in the detection of HIV infection. **Microfluidics and Nanofluidics**, v. 20, n. 7, jul. 2016.

LATIEF, U. *et al.* A facile green synthesis of functionalized carbon quantum dots as fluorescent probes for a highly selective and sensitive detection of Fe3+ ions. **Spectrochimica Acta Part A: Molecular and Biomolecular Spectroscopy**, v. 262, p. 120132, 5 dez. 2021.

LE, N. D. B. *et al.* Cancer Cell Discrimination Using Host-Guest “doubled” Arrays. **Journal of the American Chemical Society**, v. 139, n. 23, p. 8008–8012, 14 jun. 2017.

LI, L. *et al.* A robust gold nanocluster-peroxyoxalate chemiluminescence system for highly sensitive detection of cyanide in environmental water. **Sensors and Actuators B: Chemical**, v. 353, p. 131038, 15 fev. 2022.

LI, N. *et al.* One-step synthesis of N, P Co-doped orange carbon quantum dots with novel optical properties for bio-imaging. **Optical Materials**, v. 111, p. 110618, 1 jan. 2021.

LI, XIANGYOU *et al.* Preparation of carbon quantum dots with tunable photoluminescence by rapid laser passivation in ordinary organic solvents. **Chemical Communications**, v. 47, n. 3, p. 932–934, 21 dez. 2010.

LI, XUE *et al.* Novel prussian blue@Carbon-dots hybrid thin film: The impact of carbon-dots on material structure and electrochromic performance. **Electrochimica Acta**, v. 355, p. 136659, 20 set. 2020.

LIAO, S. *et al.* A reusable P, N-doped carbon quantum dot fluorescent sensor for cobalt ion. **Sensors and Actuators, B: Chemical**, v. 260, p. 156–164, 1 maio 2018.

LIAO, X. *et al.* Yellow fluorescent carbon quantum dots for Ag+/GSH detection and

differentiation between normal and cancer cells. **Materials Today Communications**, v. 35, p. 106383, 1 jun. 2023.

LIN, L. *et al.* Continuous microflow synthesis of fluorescent phosphorus and nitrogen co-doped carbon quantum dots. **Chemical Engineering Research and Design**, v. 178, p. 395–404, 1 fev. 2022.

LIN, S. *et al.* Sustainable synthesis of lignin-derived carbon dots with visible pH response for Fe3+ detection and bioimaging. **Spectrochimica Acta Part A: Molecular and Biomolecular Spectroscopy**, v. 302, p. 123111, 5 dez. 2023.

LIU, W. *et al.* Preparation of nitrogen-doped carbon dots with a high fluorescence quantum yield for the highly sensitive detection of Cu2+ ions, drawing anti-counterfeit patterns and imaging live cells. **New Carbon Materials**, v. 34, n. 4, p. 390–402, 1 ago. 2019.

LUO, J. *et al.* Hydrothermal synthesis of bright blue-emitting carbon dots for bioimaging and fluorescent determination of baicalein. **Optical Materials**, v. 113, p. 110796, 1 mar. 2021.

MADMON, M. *et al.* Simple and fast determination of free cyanide in drinking water by liquid chromatography electrospray ionization tandem mass spectrometry following “in vial” derivatization. **International Journal of Mass Spectrometry**, v. 463, p. 116553, maio 2021.

MAYNAR, M. *et al.* Influence of a 6-month physical training program on serum and urinary concentrations of trace metals in middle distance elite runners. **Journal of the International Society of Sports Nutrition**, v. 16, n. 1, p. 53, 14 nov. 2019.

MAYNAR, MARCOS *et al.* Serum concentration of cobalt, molybdenum and zinc in aerobic, anaerobic and aerobic-anaerobic sportsmen. **Journal of the International Society of Sports Nutrition**, v. 15, n. 1, p. 1–8, 13 jun. 2018.

MOKHINE, S. *et al.* Selective and sensitive determination of Folic acid amidst interfering metal ions and biomolecules using N- doped carbon quantum dots (N-CQDs). **Nano-Structures & Nano-Objects**, v. 37, p. 101085, 1 fev. 2024.

MOLAEI, M. J. Turmeric-derived gadolinium-doped carbon quantum dots for multifunctional fluorescence imaging and MRI contrast agent. **Journal of Luminescence**, v. 257, p. 119692, 1 maio 2023.

MONDAL, T. K.; GHORAI, U. K.; SAHA, S. K. Dual-Emissive Carbon Quantum Dot-Tb Nanocomposite as a Fluorescent Indicator for a Highly Selective Visual Detection of Hg(II) in Water. **ACS Omega**, v. 3, n. 9, p. 11439–11446, set. 2018.

MU, X. *et al.* Sensitive Ratiometric Fluorescence Probe Based on Chitosan Carbon Dots and Calcein for Alkaline Phosphatase Detection and Bioimaging in Cancer Cells. **Analytica Chimica Acta**, p. 339163, 11 out. 2021.

NAIR, A. *et al.* Natural carbon-based quantum dots and their applications in drug delivery: A review. **Biomedicine and Pharmacotherapy**. [S.l.]: Elsevier Masson s.r.l. , 1 dez. 2020.

NAJLAOUI, D. *et al.* Development of a selective and highly sensitive optical chemical sensor

for determination of sulfaguanidine based on a novel mixed isopolymolybdates. **Optik**, p. 166507, 12 fev. 2021.

NAZRI, N. A. A. *et al.* Carbon quantum dots for optical sensor applications: A review. **Optics & Laser Technology**, v. 139, p. 106928, 1 jul. 2021.

NGUYEN, D. C. T. *et al.* Incorporation of carbon quantum dots with PEDOT:PSS for high-performance inverted organic solar cells. **Synthetic Metals**, v. 298, p. 117430, 1 set. 2023.

OLIVEIRA, J. J. P. *et al.* Determination of Co2+ ions in blood samples: A multi-way sensing based on NH2-rich carbon quantum dots. **Dyes and Pigments**, v. 215, p. 111253, 1 jul. 2023.

ONAT, E. *et al.* Highly active hydrogen production from hydrolysis of potassium borohydride by caffeine carbon quantum dot-supported cobalt catalyst in ethanol solvent by hydrothermal treatment. **International Journal of Hydrogen Energy**, v. 51, p. 362–375, 2 jan. 2024.

OZMEN, P.; DEMIR, Z.; KARAGOZ, B. An Easy Way to Prepare Reusable Rhodamine-Based Chemosensor for Selective Detection of Cu2+ and Hg2+ Ions. **European Polymer Journal**, p. 110922, 2 dez. 2021.

PADMAPRIYA, A. *et al.* Electrochemical sensor based on N,P–doped carbon quantum dots derived from the banana flower bract (Musa acuminata) biomass extract for selective and picomolar detection of dopamine. **Journal of Electroanalytical Chemistry**, v. 943, p. 117609, 15 ago. 2023.

PALACIO-VERGARA, M. *et al.* Biomass solvothermal treatment methodologies to obtain carbon quantum dots: A systematic review. **Talanta Open**, v. 8, p. 100244, 1 dez. 2023.

PARK, S. J.; YANG, H. K.; MOON, B. K. Correlated color temperature alteration with changing the position of carbon dot film for warm WLEDs. **Dyes and Pigments,** v. 186, p. 109063, 1 fev. 2021.

PARK, Y. R. *et al.* Quantum-Dot Light-Emitting Diodes with Nitrogen-Doped Carbon Nanodot Hole Transport and Electronic Energy Transfer Layer. **Scientific Reports**, v. 7, n. 1, p. 1–13, abr. 2017.

PATIL, A. M. *et al.* Recent progress of MXene synthesis, properties, microelectrode fabrication techniques for microsupercapacitors and microbatteries energy storage devices and integration: A comprehensive review. **Coordination Chemistry Reviews**, v. 517, p. 216020, 15 out. 2024.

PERMATASARI, F. A. *et al.* Role of C–N Configurations in the Photoluminescence of Graphene Quantum Dots Synthesized by a Hydrothermal Route. **Scientific Reports**, v. 6, n. 1, p. 1–8, fev. 2016.

PERUMAL, S. *et al.* Sustainable synthesis of multifunctional carbon dots using biomass and their applications: A mini-review. **Journal of Environmental Chemical Engineering**, v. 9, n. 4, p. 105802, 1 ago. 2021.

POURMADADI, M. *et al.* Properties and application of carbon quantum dots (CQDs) in biosensors for disease detection: A comprehensive review. **Journal of Drug Delivery Science**

and Technology, v. 80, p. 104156, 1 fev. 2023.

PRENDERGAST, L. A.; SMITH, J. A. Influence functions for linear discriminant analysis: Sensitivity analysis and efficient influence diagnostics. **Journal of Multivariate Analysis**, v. 190, p. 104993, 1 jul. 2022.

PU, Z. *et al.* Synthesis of diethylenetriamine-modified carbon quantum dots for dual sensing Fe3+ and Co2+and its application. **Optical Materials**, v. 146, p. 114598, 1 dez. 2023.

PUNDI, A. *et al.* Naked-eye colorimetric and turn-on fluorescent Schiff base sensor for cyanide and aluminum (III) detection in food samples and cell imaging applications. **Spectrochimica Acta Part A: Molecular and Biomolecular Spectroscopy**, v. 262, p. 120139, dez. 2021.

RAI, P. *et al.* A rapid and sensitive colorimetric method for the detection of cyanide ions in aqueous samples. **Environmental Technology & Innovation**, v. 24, p. 101973, 1 nov. 2021.

RAIKWAR, V. R. Synthesis and study of carbon quantum dots (CQDs) for enhancement of luminescence intensity of CQD@LaPO4:Eu3+ nanocomposite. **Materials Chemistry and Physics**, v. 275, p. 125277, 1 jan. 2022.

SAADH, M. J. *et al.* Emerging pathways in environmentally friendly synthesis of carbon-based quantum dots for exploring antibacterial resistance. **Inorganic Chemistry Communications**, v. 161, p. 112012, 1 mar. 2024.

SALJOUGHI, H.; KHAKBAZ, F.; MAHANI, M. Synthesis of folic acid conjugated photoluminescent carbon quantum dots with ultrahigh quantum yield for targeted cancer cell fluorescence imaging. **Photodiagnosis and Photodynamic Therapy**, v. 30, p. 101687, 1 jun. 2020.

SHAMSIPUR, M.; RAJABI, H. R. Pure zinc sulfide quantum dot as highly selective luminescent probe for determination of hazardous cyanide ion. **Materials Science and Engineering: C**, v. 36, n. 1, p. 139–145, 1 mar. 2014.

SHAO, C. *et al.* Dithiothreitol-capped red emitting copper nanoclusters as highly effective fluorescent nanoprobe for cobalt (II) ions sensing. **Microchemical Journal**, v. 163, p. 105922, 1 abr. 2021.

SHARMA, S.; CHOWDHURY, P. Fluorescence signal from carbon quantum dots synthesized from natural resources. **Materials Today: Proceedings**, 10 jun. 2023.

SKALNY, A. V. *et al.* Cobalt in athletes: hypoxia and doping - new crossroads. **Journal of Applied Biomedicine**, v. 17, n. 1, p. 28–28, 19 mar. 2019.

SONG, X. *et al.* Development of magnetism-reinforced in-tube solid phase microextraction combined with HPLC for the sensitive quantification of cobalt(II) and nickel(II) in environmental waters. **Microchemical Journal**, v. 159, p. 105370, 1 dez. 2020.

SPESSATO, L. *et al.* Tuning photodegradation performance using carbon quantum dots and niobium pentoxide. **Journal of Materials Science & Technology**, 1 fev. 2024.

STEFANAKIS, D. *et al.* Synthesis of fluorescent carbon dots by a microwave heating process: structural characterization and cell imaging applications. **Journal of Nanoparticle Research**, v. 16, n. 10, p. 1–10, set. 2014.

SU, H. *et al.* Cetuximab-conjugated iodine doped carbon dots as a dual fluorescent/CT probe for targeted imaging of lung cancer cells. *Colloids and Surfaces B: Biointerfaces*, v. 170, 2018.
SUN, L. *et al.* Nitrogen and sulfur Co-doped carbon dots as selective and visual sensors for monitoring cobalt ions. **Optical Materials**, v. 112, p. 110787, 1 fev. 2021.

SURENDRAN, P. *et al.* Synthesis of fluorescent carbon quantum dots from Manihot esculenta waste peels for nonlinear optical and biological applications. **Chemical Physics Impact**, v. 8, p. 100515, 1 jun. 2024.

TADESSE, A. *et al.* Synthesis of nitrogen doped carbon quantum dots/magnetite nanocomposites for efficient removal of methyl blue dye pollutant from contaminated water. **RSC Advances**, v. 8, n. 16, p. 8528–8536, fev. 2018.

TAN, A.; YANG, G.; WAN, X. Ultra-high quantum yield nitrogen-doped carbon quantum dots and their versatile application in fluorescence sensing, bioimaging and anti-counterfeiting. **Spectrochimica Acta Part A: Molecular and Biomolecular Spectroscopy**, v. 253, p. 119583, maio 2021.

THULASINATHAN, B. *et al.* DNA-functionalized carbon quantum dots for electrochemical detection of pyocyanin: A quorum sensing molecule in Pseudomonas aeruginosa. **Biosensors and Bioelectronics**, v. 227, p. 115156, 1 maio 2023.

TSENG, W. BIN *et al.* Synthesis of gold nanoclusters-loaded lysozyme nanoparticles for ratiometric fluorescent detection of cyanide in tap water, cyanogenic glycoside-containing plants, and soils. **Environmental Research**, v. 207, p. 112144, 1 maio 2022.

VASHISHT, D. *et al.* Colorimetric chemosensor based on coumarin skeleton for selective naked eye detection of cobalt (II) ion in near aqueous medium. **Sensors and Actuators B: Chemical**, v. 280, p. 219–226, 1 fev. 2019.

VASHISHT, D. *et al.* Solvothermal assisted phosphate functionalized graphitic carbon nitride quantum dots for optical sensing of Fe ions and its thermodynamic aspects. **Spectrochimica Acta - Part A: Molecular and Biomolecular Spectroscopy**, v. 228, p. 117773, 5 mar. 2020.

VAZ, R. *et al.* High luminescent carbon dots as an eco-friendly fluorescence sensor for Cr(VI) determination in water and soil samples. **Journal of Photochemistry and Photobiology A: Chemistry**, v. 346, p. 502–511, set. 2017.

VIRBICKAS, P. *et al.* Determination of cyanide concentration by chronoamperometry, cyclic voltammetry and fast Fourier transform electrochemical impedance spectroscopy. **Journal of Electroanalytical Chemistry**, v. 895, p. 115449, ago. 2021.

WANG, B. *et al.* Dual-mode detection sensor based on nitrogen-doped carbon dots from pine needles for the determination of Fe3+ and folic acid. **Spectrochimica Acta Part A: Molecular and Biomolecular Spectroscopy**, p. 121891, 17 set. 2022.

WANG, C. *et al.* Emissive carbon dots derived from natural liquid fuels and its biological sensing for copper ions. **Talanta**, v. 208, p. 120375, 1 fev. 2020.

WANG, HANG *et al.* Tumor diagnosis using carbon-based quantum dots: Detection based on the hallmarks of cancer. **Bioactive Materials**, v. 33, p. 174–222, 1 mar. 2024.

WANG, HAO *et al.* Nitrogen-doped carbon dots for "green" quantum dot solar cells. **Nanoscale Research Letters**, v. 11, n. 1, p. 1–6, jan. 2016.

WANG, Z. *et al.* Ratiometric fluorescent sensors for sequential on-off-on determination of riboflavin, Ag+ and l-cysteine based on NPCl-doped carbon quantum dots. **Analytica Chimica Acta**, v. 1144, p. 1–13, 1 fev. 2021.

WU, F. *et al.* Facile synthesis of N-rich carbon quantum dots from porphyrins as efficient probes for bioimaging and biosensing in living cells. **International Journal of Nanomedicine**, v. 12, 2017.

WU, F. *et al.* Near-infrared emissive lanthanide hybridized carbon quantum dots for bioimaging applications. **Journal of Materials Chemistry B**, v. 4, n. 38, 2016.

WU, P. *et al.* Hydrothermal synthesis of nitrogen-doped carbon quantum dots from microcrystalline cellulose for the detection of Fe3+ ions in an acidic environment. **RSC Advances**, v. 7, n. 70, p. 44144–44153, 11 set. 2017.

XU, G.-T. *et al.* Smartphone assisted fluorescent sensor for Fe3+ and ascorbic acid determination based on off-on carbon dots probe. **Chinese Journal of Analytical Chemistry**, v. 51, n. 1, p. 100206, 1 jan. 2023.

XU, O. *et al.* Novel Zn/Co–N co-doped carbon quantum dot-based "on-off-on" fluorescent sensor for Fe(III) and ascorbic acid. **Talanta Open**, v. 7, p. 100162, 1 ago. 2023.

XU, X. *et al.* Electrophoretic analysis and purification of fluorescent single-walled carbon nanotube fragments. *Journal of the American Chemical Society*, v. 126, n. 40, p. 12736–12737, 2004.

YANG, F.; ZHOU, P.; DUAN, C. Solid-phase synthesis of red dual-emissive nitrogen-doped carbon dots for the detection of Cu2+ and glutathione. **Microchemical Journal**, v. 169, p. 106534, out. 2021.

YANG, H. *et al.* Hydrophobic carbon dots with blue dispersed emission and red aggregation-induced emission. **Nature Communications**, v. 10, n. 1, p. 1–11, 1 dez. 2019.

YANG, JIN *et al.* Tailored polyethyleneimine-based fluorescent nanoparticles for functionalized applications in detection and adsorption of cobalt (II). **Dyes and Pigments**, v. 202, p. 110271, 1 jun. 2022.

YANG, JING *et al.* One-step hydrothermal synthesis of near-infrared emission carbon quantum dots as fluorescence aptamer sensor for cortisol sensing and imaging. **Talanta**, v. 260, p. 124637, 1 ago. 2023.

YANG, M. *et al.* Polyethyleneimine-functionalized carbon dots as a fluorescent probe for doxorubicin hydrochloride by an inner filter effect. **Optical Materials**, v. 112, p. 110743, 1 fev. 2021.

YANG, Y. *et al.* Highly sensitive and ratiometric detection of nitrite in food based on upconversion-carbon dots nanosensor. **Analytica Chimica Acta**, v. 1263, p. 341245, 4 jul. 2023.

YILMAZ, B. *et al.* A highly selective optical sensor for the detection of cyanide ions in aqueous solution and living cells. **Journal of Photochemistry and Photobiology A: Chemistry**, v. 424, p. 113651, fev. 2022.

YU, J. *et al.* Facilely synthesized N-doped carbon quantum dots with high fluorescent yield for sensing Fe3+. **New Journal of Chemistry**, v. 40, n. 3, p. 2083–2088, mar. 2016.

YUE, L. *et al.* Red-Emissive Ruthenium-Containing Carbon Dots for Bioimaging and Photodynamic Cancer Therapy. **ACS Applied Nano Materials**, v. 3, n. 1, 2020.

ZHANG, JIA; DONG, L.; YU, S. H. A selective sensor for cyanide ion (CN^-) based on the inner filter effect of metal nanoparticles with photoluminescent carbon dots as the fluorophore. **Science Bulletin**, v. 60, n. 8, p. 785–791, 9 abr. 2015.

ZHANG, JIANBIN *et al.* Green synthesis of carbon dots from elm seeds via hydrothermal method for Fe3+ detection and cell imaging. **Inorganic Chemistry Communications**, v. 144, p. 109837, 1 out. 2022.

ZHANG, L. Y. *et al.* Construction and photocatalysis of carbon quantum dots/layered mesoporous titanium dioxide (CQDs/LM-TiO2) composites. **Applied Surface Science**, v. 546, p. 149089, 30 abr. 2021.

ZHANG, S. R. *et al.* One-step synthesis of N, P-doped carbon quantum dots for selective and sensitive detection of Fe2+ and Fe3+ and scale inhibition. **Journal of Molecular Structure**, v. 1246, p. 131173, 15 dez. 2021.

ZHANG, W. *et al.* Carbon quantum dot fluorescent probes for food safety detection: Progress, opportunities and challenges. **Food Control**, v. 133, p. 108591, 1 mar. 2022.

ZHANG, W. J. *et al.* A ratiometric fluorescent and colorimetric dual-signal sensing platform based on N-doped carbon dots for selective and sensitive detection of copper(II) and pyrophosphate ion. **Sensors and Actuators, B: Chemical**, v. 283, p. 215–221, 15 mar. 2019.

ZHAO, C. *et al.* Green and microwave-assisted synthesis of carbon dots and application for visual detection of cobalt(II) ions and pH sensing. **Microchemical Journal**, v. 147, p. 183–190, 1 jun. 2019.

ZHAO, L. *et al.* Facile Synthesis of Nitrogen-Doped Carbon Quantum Dots with Chitosan for Fluorescent Detection of Fe3+. **Polymers**, v. 11, n. 11, p. 1731, out. 2019.

ZHAO, S. *et al.* Carbon dots combined with masking agent for high selectivity detection of Cr(VI) to overcome interference associated challenges. **Ecotoxicology and Environmental**

Safety, v. 244, p. 114069, 1 out. 2022.

ZHAO, X. *et al.* Facile synthesis of B,N-doped CQDs as versatile fluorescence probes for sensitive detection of cobalt ions in environmental water and biological samples. **Microchemical Journal**, v. 163, p. 105888, 1 abr. 2021.

ZHONG, Y. *et al.* Effect of ultrasonic pretreatment on eliminating cyanogenic glycosides and hydrogen cyanide in cassava. **Ultrasonics Sonochemistry**, v. 78, p. 105742, out. 2021.

ZHU, L. *et al.* A rotating paper-based microfluidic sensor array combining Michael acceptors and carbon quantum dots for discrimination of biothiols. **Chemical Engineering Journal**, v. 454, p. 140065, 15 fev. 2023.

ZOGHI, M. *et al.* Synthesis and characterization of chitosan/carbon quantum dots/Fe2O3 nanocomposite comprising curcumin for targeted drug delivery in breast cancer therapy. **International Journal of Biological Macromolecules**, p. 125788, 10 jul. 2023.

ZOU, C. *et al.* A paper-based visualization chip based on nitrogen-doped carbon quantum dots nanoprobe for Hg(II) detection. **Spectrochimica Acta Part A: Molecular and Biomolecular Spectroscopy**, v. 265, p. 120346, 15 jan. 2022.

ZU, F. *et al.* The quenching of the fluorescence of carbon dots: A review on mechanisms and applications. **Microchimica Acta**, v. 184, n. 7, p. 1899–1914, 2017.